2011

A comprehensive invariant subspace-based framework for power system small-signal stability analysis

Cheng Luo
Iowa State University

A comprehensive invariant subspace-based framework for power system small-signal stability analysis

by

Cheng Luo

A dissertation submitted to the graduate faculty

in partial fulfillment of the requirements for the degree of

DOCTOR OF PHILOSOPHY

Major: Electrical Engineering

Program of Study Committee:
Venkataramana Ajjarapu, Major Professor
Manimaran Govindarasu
James D. McCalley
Michael W. Smiley
Zhengdao Wang

Iowa State University

Ames, Iowa

2011

TABLE OF CONTENTS

LIST OF TABLES

LIST OF FIGURES

ACKNOWLEDGEMENTS

I would like to take this opportunity to express my thanks to those who helped me with various aspects of conducting research and the writing of this thesis. First and foremost, Dr. Ajjarapu for his guidance, support, and help throughout this research and my PhD study.

I would also like to thank my committee members for their efforts and contributions to this work: Dr. Manimaran Govindarasu, Dr. James D. McCalley, Dr. Michael W. Smiley, and Dr. Zhengdao Wang.

Finally, I wish to express my gratitude to my family. Especially, I want to thank my wife Zengxin Cheng for her love, understanding, support, and sharing the beautiful life with me.

CHAPTER 1. INTRODUCTION

This chapter describes the motivation of the research and the review of literature, presents a framework of the proposed methodology, and also gives the organization of the dissertation.

1.1 Background

In power system analysis, it is of interest to analyze the stability of the system for changing parameter values. Power system may experience qualitative change in the behavior for certain parameter values. This behavior can be predicted via bifurcation framework. The conventional numerical procedure for obtaining the bifurcation behavior would involve the following two phases: solving and tracing the equilibrium path, and identifying bifurcation points as well as the directions of new branches. The first phase includes solving a system of nonlinear equations by a predictor-corrector type of continuation method, whereas the second involves determining the bifurcation points. In power system *differential algebraic equations* (DAE) model, the change of equilibrium character with respect to bifurcation parameter is often effectively studied by analyzing changes of the eigenvalues of system state matrix in response to parameter variations. There are two common types of bifurcation points: *Hopf bifurcation* (HB) and *saddle-node bifurcation* (SNB). When HB occurs, the system Jacobian has a simple pair of purely imaginary eigenvalues, and there are no other eigenvalues on the imaginary axis and the right half of the complex plane. As the parameter changes, certain inequality conditions need to hold to ensure that this pair of critical eigenvalues cross the imaginary axis. At SNB point, the Jacobian has a simple zero eigenvalue, and there is no other eigenvalue on the imaginary axis. Usually, eigenvalue analysis is used, in which the potential critical eigenvalues are observed with respect to the parameter variation. This results in a piecewise

global small-disturbance stability analysis [1]. Fig. 1.1 shows the possible dynamic behaviors one can observe for changing parameter values. Some of the phenomena are more critical than others. It is useful if there is a systematic procedure to identify these phenomena, especially HB and SNB in power systems.

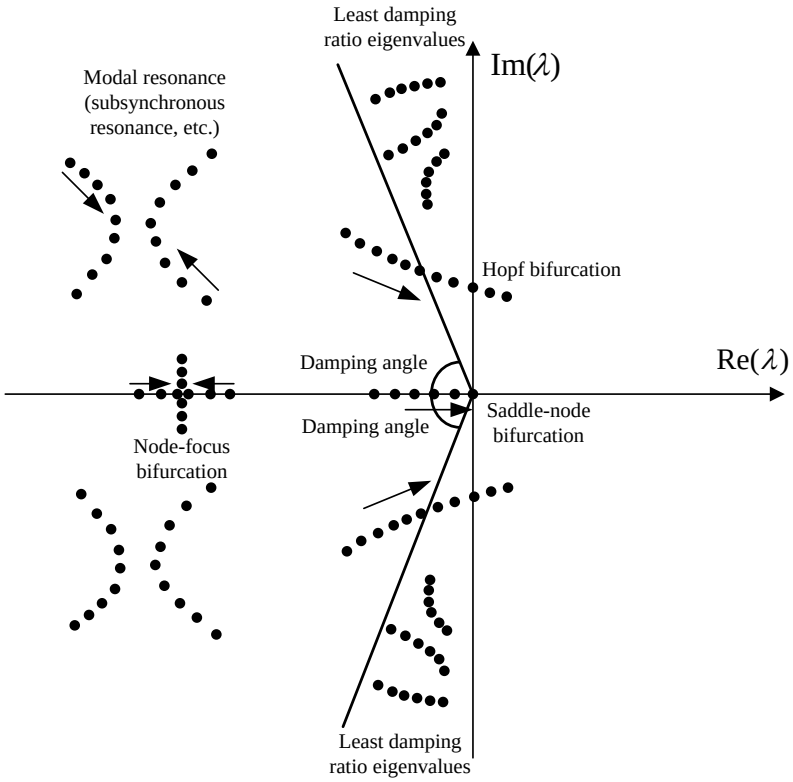

Figure 1.1 Different Dynamic Phenomena Related to Eigenvalues in Power Systems.

Power systems are steadily growing with ever larger installed generation capacity. Formerly separated systems are now interconnected. Modern power systems have evolved into systems with a very large size, stretching out over thousands of miles. Furthermore, in a market-driven environment with potential higher transmission system loading, greater variety of operating points, and huge power transfer over long distances, the system may be forced to operate closer to its stability limit. Increased electricity consumption in heavy load areas and environmental pressure on the transmission expansion also cause the system to operate under much more

stressed conditions than in the past. With the growth of interconnected power system, and especially the deregulation of the power market, the problems related to small-signal stability have become a critical issue for the power system security. Inter-area oscillation has been found to be a common problem in large power systems worldwide. Many electric systems have experienced poorly damped low-frequency inter-area oscillations as a result of system growth and interconnection. For example, there was an oscillatory disturbance in the Eastern Interconnection on June 12, 1992. The oscillatory instability is caused by Hopf bifurcation following the loss of transmission lines [2]. The incident took operators more than half an hour to take actions to suppress the oscillations. The power system outage that occurred in the Western Interconnection on August 10, 1996 is related to oscillatory stability, too. Recently, there was an oscillation incident in Central China Power Grid on October 29, 2005 which is caused by low-frequency oscillation.

A direct result of the electromechanical oscillation is the subsequent oscillations in other quantities such as the power flow on tie lines. Although the actual MW flow swings may be within the acceptable range, their effects may lead to oscillations in voltages which could have negative impact on the system performance. Furthermore, if not damped effectively, sustained oscillation can lead to fatigue of machine shafts, limit power transfer over tie lines, reduce the system stability margin, and cause serious control problems.

Damping also plays an important role in power system oscillatory stability since the damping ratio determines the decay rate of the oscillation. Fig. 1.2 shows the oscillations at the Malin–Round Mountain #1 500 kV transmission line in the WECC (*Western Electricity Coordinating Council*) system during the August 10, 1996 blackout [3]. It can be seen that the final breakup was caused by the growing unstable oscillation which started at about 725 seconds. This was due to decrease in system damping as a result of cascading events following the trip of a 500 kV line. It takes about seven minutes starting from the first line tripping till the whole system blackout. The entire WECC system were split into four islands with the loss of approximately 30 GW of load. More than seven million customers were affected by this catastrophic event [4]. The inter-area oscillations in the WECC system clearly identify

inadequate damping as the primary factor leading to system separation. The time scale of the blackout suggests that the potential oscillation problem may have been predictable if there is an approach to efficiently calculate the critical eigenvalues with least damping ratios. Such information is vital if operators are to maintain system security close to the system stability limit. On July 12, 1996, the same WECC system experienced voltage collapse that is related to saddle-node bifurcation.

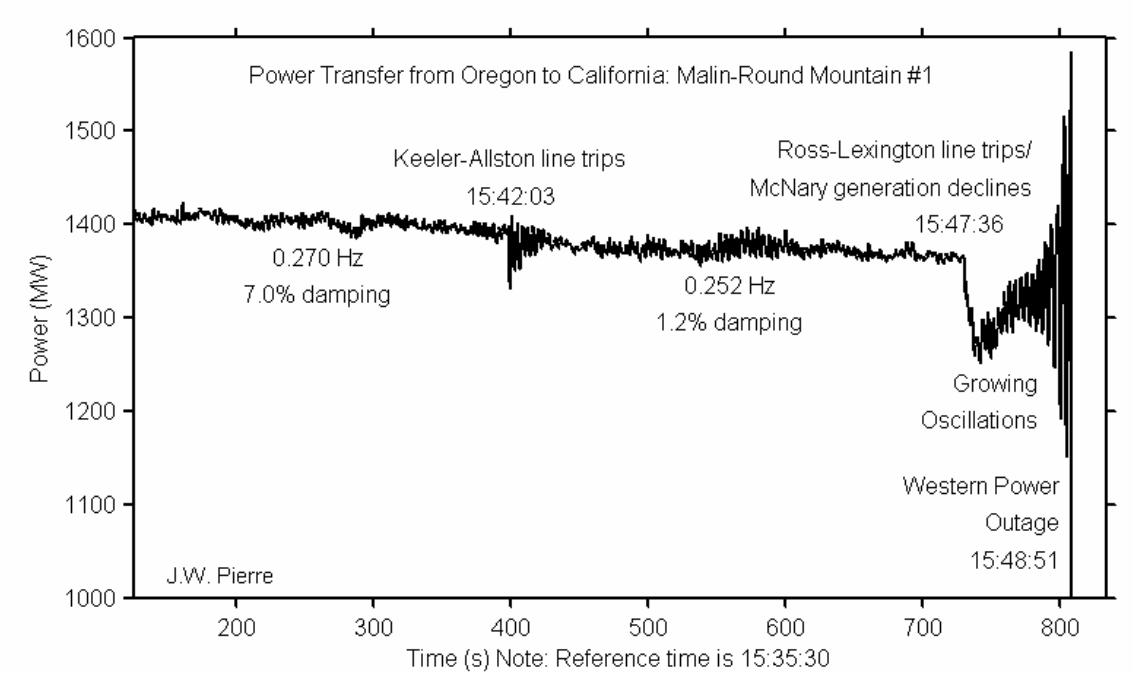

Figure 1.2 Oscillations on the WECC System Blackout, Aug 10, 1996 [3].

For power systems operating under the deregulated market environment, the onset of oscillation problem due to critical eigenvalues is one operational constraint which already limits bulk power transactions under some conditions. Better methods of analyzing the oscillations would lead to more accurate determination of these limits and the ability to operate the power system closer to the stability margin. An analytical tool to trace the movement of critical eigenvalues with respect to the changing system conditions will help analyze and investigate the cause of the problem. If an oscillation does occur, advice to the system operators or reliability coordinators on how to quickly suppress it would be very valuable. Furthermore, if

the oscillatory stability margin and the damping margin can be pre-determined for a specified scenario which might happen in the real time, it will provide operators the user guide in operating the power systems when dealing with the potential oscillation or damping problems.

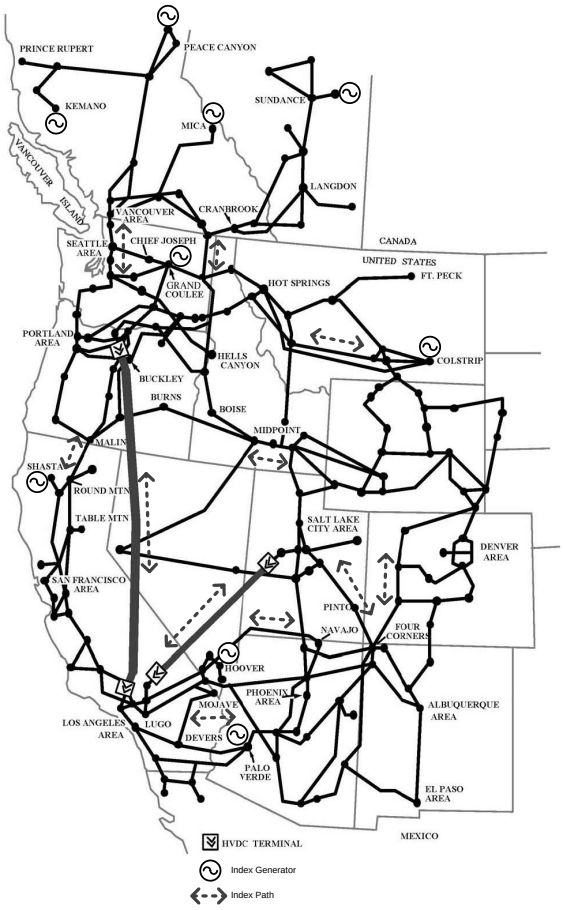

Figure 1.3 Dynamic Interactions in the WECC System [7].

The dynamics of the WECC system near 0.78 Hz has been an enigma for many years [5]. Abnormal behavior and strange results have always been linked to the possibility of a kind of resonance between interacting eigenvalue modes. It has been discovered that the oscillation is an inter-area mode due to the swing of the generators in the northwest and southwest against the generators in the center of the Western Interconnection [6]. Fig. 1.3 shows the index generators and paths for dynamic interactions in the system [7].

The WECC inter-area oscillation problem shows it is critical to investigate the mode (eigenvalue) interaction for dynamic power systems. Traditional approaches (such as the QR method)

have the shortcomings to deal with these problems since they are time consuming and only produce a set of discrete eigenvalues. Model reduction consists of replacing the original system with one of a much smaller dimension [8]. It requires a good understanding of the phenomenon in order to retain the system elements which are most relevant to it. How to efficiently identify mode interaction and modal resonance to provide more insight on the mechanism is an important research problem. Can we come up with a heuristic procedure to address the modal resonance and other dynamic phenomena in power systems?

For power system time-domain simulation, the trapezoidal method, which is an implicit method, is widely used in order to maintain the A-stability of the system [9]. Although the numerical stability is guaranteed for the implicit method, the computation is too costly and it restricts the practical application to large power system simulation. Can we do something to speed up the time-domain simulation?

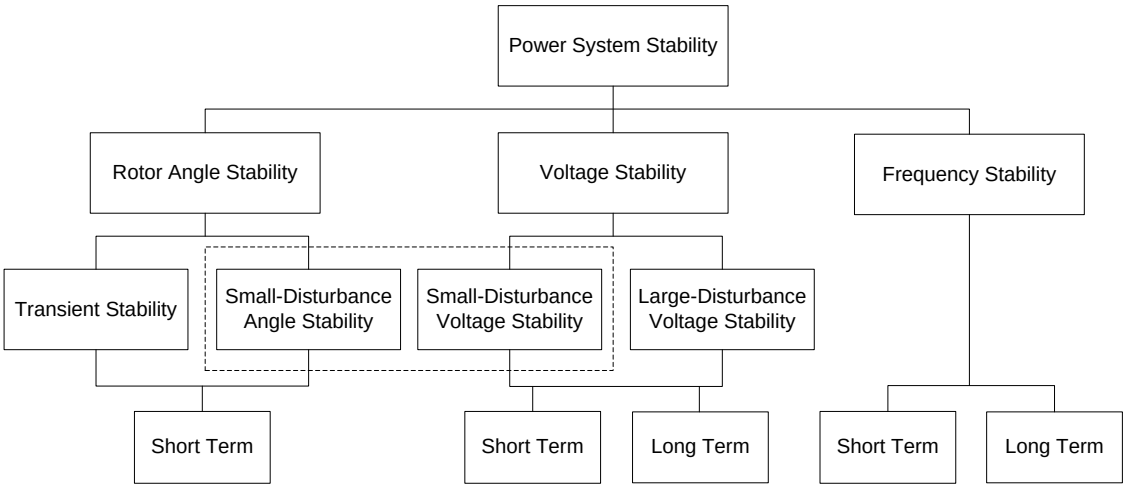

Figure 1.4 Classification of Power System Stability [10].

According to IEEE/CIGRE report [10], Fig. 1.4 shows the classification of power system stability according to different categories. As shown in the figure, the thesis will try to deal with the eigenvalue-related small-signal stability problems with the help of a novel mathematical approach. Small-disturbance or small-signal stability is concerned with the system response to small changes and is a fundamental requirement for the satisfactory operation of power

systems. The proposed definitions of different types of power system stability which will be addressed are summarized as follows [10]:

- *Small-disturbance (or small-signal) rotor angle stability* is the ability of the power system to maintain synchronism under small disturbances. In general, the disturbances are considered to be sufficiently small and hence can be analyzed by considering the system linearized at an equilibrium point represented by a steady state operating condition. Small-signal rotor angle stability problems may be either local or global in nature according to the scope of the oscillation and the oscillation frequency, and may be in the form of either undamped electromechanical oscillations or monotonic rotor acceleration leading to the loss of synchronism.

  - *Local mode oscillations* are oscillations involve a small part of the power system, and are usually associated with rotor angle oscillations of a single power plant against the rest of the power system. Since the inertia constant of generator's rotor mass is big, the frequency of local oscillation is approximately within the range of $1 \sim 2$ Hz.

  - *Inter-area mode oscillations* are caused by a group of generators in one area swinging against a group of generators in another area. It usually occurs among two or more close-coupled generators in a weak interconnection system. Therefore, the frequency of inter-area oscillation is lower than that of local oscillation, and is roughly in the range of $0.1 \sim 0.7$ Hz.

- *Small-disturbance voltage stability* refers to the system's ability to maintain steady voltages when subjected to small perturbations such as incremental changes in system load. Its analysis is normally based on the linearized system dynamic equations using modal analysis techniques.

Because the oscillations are a result of small perturbations, they are essentially linear in nature and can therefore be analyzed by using linear system techniques. In the thesis, a novel eigenvalue analysis method is proposed to analyze these stability problems associated

with eigenvalues. Small-signal stability analysis can provide valuable insight into the dynamic characteristics of any large system, and can assist in the design of controllers to mitigate inter-area or local oscillatory modes of concern.

Small-signal analysis reveals the details about the participation of generators either in groups or individually in the oscillations in terms of rotor angle, voltage, and frequency that develop for various operating conditions. The study of inter-area mode oscillations identifies specific clusters of generator locations that are responding coherently to the oscillations. By producing a set of these participating generators, the technique naturally suggests a number of candidate sites for the installation of *power system stabilizer* (PSS) or *phasor measurement unit* (PMU). Similar studies that focus on different ranges of frequency oscillations can reveal details into the individual generator that may oscillate against the rest of the power system due to the *subsynchronous resonance* (SSR) of the electrical network.

1.2 Review of Literature

1.2.1 Eigenvalue Computation in Power System Analysis

Eigenvalues play an important role in power system stability analysis. Eigenvalues can be used to determine the small-signal stability of the power systems. They are also good indicators for the bifurcation points such as saddle-node bifurcation and Hopf bifurcation. Eigenvalues and eigenvectors can be used to determine mode shapes, participation factors, controllability and observability of each mode. Eigenvalues with the largest real parts and eigenvalues with the least damping ratios are of great importance for power system applications. In power system analysis, eigenvalues are widely used to study system uncertainty, estimate stability boundary, and enhance system stability performance. Since eigenvalues are closely related to power system stability, eigenvalue computation is a very active area in the power system literature. Eigenvalue computation is a linear analysis technique based on the linearized model. Reference [11] describes the recent applications of linear analysis techniques to control system design, system identification, and large-scale system applications such as dynamic model reduction, etc.

Among all of the eigenvalue solver methods for general nonsymmetric matrices, the QR algorithm is widely used due to its robustness and high accuracy. But the QR algorithm is an algorithm for dense problems, it is inadequate for large systems, owing to the excessive computation time and memory requirements. The QR method is not efficient when the order of the state matrix is larger than 800. Round-off errors in power system matrices of order over 1000 also become significant, and a subset of eigenvalues in the QR eigensolution may be inaccurate. Therefore, significant effort has been expended to solve the problem by different means. Moreover, in most of the applications, there is no need to calculate the whole set of the eigenvalues like the QR algorithm does. Regarding the conventional eigenvalue computation methods, Golub and van der Vorst [12] summarize the main research developments in the computational methods for eigenvalue problems during the 20th century.

In general, the group of critical eigenvalues is usually a small subset in the whole spectrum. Most of the early research was on accelerating the computation of these eigenvalues especially for large systems. Several dominant sub-spectrum algorithms exist to serve this purpose such as the power method, the inverse power method, subspace iteration, and the Arnoldi method [12], etc. The efficiencies of dominant eigenvalue calculation methods are discussed and compared in [13] and [14]. The matrix transformation for the dominant eigenvalues is described in [15]. Among all of the dominant eigenvalue computation algorithms, the Arnoldi method is believed to be the most efficient approach. But the method is heavily influenced by the selection of the number of guard vectors. The only way to explore this is by numerical tests. It has been assumed that the dominant eigenvalue is the critical eigenvalue that will eventually cross the imaginary axis [16], but this may not always be the case especially when the current operating point is some distance away from the instability boundary. Moreover, it is pointed out in [17] that very close eigenvalues or eigenvalues with multiplicity may cause the algorithm to terminate prematurely.

Several other techniques have been developed that focus on evaluating a selected subset of eigenvalues. One such technique is the AESOPS program originally proposed in [18], where the acronym AESOPS stands for the *Analysis of Essentially Spontaneous Oscillations in Power*

Systems. Similar to the frequency response method, it uses frequency response to calculate eigenvalues associated only with rotor angle modes one at a time. The advantage is that it always converges to the dominant mode of interest. Unlike the modified Arnoldi method [19], AESOPS has the disadvantage of requiring repeated factorization of large matrices and slow convergence due to its heuristic nature. An improved AESOPS algorithm based on Newton-Raphson iteration was proposed in [20] to achieve fast convergence properties. The *selective modal analysis* (SMA) method proposed in [21] computes eigenvalues associated with selected modes of interest by using special techniques to identify variables that are relevant to the selected modes, and then constructing a reduced-order model that involves only the relevant variables. The PEALS (Program for Eigenvalue Analysis of Large Systems) described in [22] and developed by EPRI (Electric Power Research Institute) and Ontario Hydro has facilities for computing eigenvalues using the QR method, the AESOPS algorithm, and the modified Arnoldi method. The NEVA small disturbance analysis tool in NETOMAC software package developed by SIEMENS applies the inverse power method and Rayleigh quotient method. Cayley transform-based S matrix method proposed in [23] is very efficient in finding the unstable modes. STEPS (Sequential Two-state Eigenanalysis for Power Systems) program is introduced in [24] for computing the eigenvalues belonging to a small study zone. Reference [25] uses parallel processing-based Bi-iteration method to speed up the eigenvalue computation in small-signal stability assessment.

In [26], various indices based on eigenvalues and singular values are proposed to detect and predict oscillatory instabilities associated with Hopf bifurcation in power systems for online application. Dobson et al. [27, 28] and Padiyar et al. [29] have studied the resonance phenomena in power systems. Reference [27] investigates the inter-area power system oscillations in which the oscillatory modes interact near a strong resonance, resulting in instability of one of the modes. When a resonance occurs, the power system linearization has two complex conjugate pairs of eigenvalues that coincide in both frequency and damping. If the linearization is not diagonalizable at the resonance, the resonance is called a *strong resonance*. Otherwise, the resonance is called a *weak resonance*. Reference [27] further demonstrates that strong resonance

is a precursor to oscillatory stability. Reference [28] mathematically analyzes generic perturbations of two complex eigenvalues passing through a weak resonance where the modes are decoupled and the eigenvalues do not interact. In [29], the strong resonance is characterized by coincidence of both eigenvalues and eigenvectors, and weak resonance is characterized by coincidence of eigenvalues only. When the system is near a strong resonance, the eigenvalues and eigenvectors are very sensitive to parameter changes. A small parameter change might cause the eigenvalues to move quickly and turn through approximately 90 degrees in the complex plane [29], which brings difficulties for the conventional eigenvalue analysis.

In [30], invariant subspace method is used to compute a group of selected eigenvalues in power systems. The invariant subspace method allows eigenvalues that are difficult to study individually to be grouped into a subspace which can be handled quite efficiently. This is an iterative process whose convergence depends on the initial value used. The paper also compares the invariant subspace method with Newton's method for eigenvalue computation. In power system eigenvalue analysis, close eigenvalues computation is an issue to be dealt with since it is common for power systems to have close eigenvalues due to similar generator dynamic characteristics and many conventional methods will fail to converge in this case. For example, Newton's method will diverge since the matrix equation to be solved is ill-conditioned. But even when the corresponding eigenvectors are ill-conditioned, the invariant subspace associated with those close eigenvalues can be well determined. As a result, the invariant subspace-based method should work well in such case. However, further work is needed for the proposed method in [30]. First, it can only treat the explicit matrix for *ordinary differential equation* (ODE) systems, and is not able to deal with the implicit equations directly for the DAE systems. The sparsity of the Jacobian matrix will be lost during the matrix manipulation. Second, for different parameter values, the same process needs to be repeated. Is there a way to continuously track the movement of a number of specified eigenvalues with respect to system parameter without recalculating all of the eigenvalues? The thesis will propose an eigenvalue tracing method to facilitate the process.

Other existing methods, such as the modified Arnoldi method and simultaneous iteration

method, are applied in [19] which uses the properties of invariant subspace to compute a subset of eigenvalues and the corresponding eigenvectors of a matrix. It should be mentioned that the sparsity matrix techniques can be applied to the proposed methods for small-signal stability analysis. Reference [31] applies subspace iteration-based Jacobi-Davidson method to calculate the rightmost eigenvalues. Reference [32] further applies inexact two-sided Jacobi-Davidson method to compute the critical eigenvalues and corresponding eigenvector of power systems.

Instead of calculating all of the eigenvalues of the system state matrix, we can just calculate some critical eigenvalues which are close to the imaginary axis and update them with respect to system parameter change (load change, contingency, etc). Furthermore, it can also provide inexpensive capabilities for an improved, more reliable detection of bifurcations in power systems. The *continuation of invariant subspaces* (CIS) provides us a useful tool to reduce the system dimension and analyze the stability change as parameter varies [33, 34, 35, 36, 37, 38]. A generalized continuation method for the calculation of invariant subspace with any dimension is presented in [33]. It applies Newton's method to the associated Riccati equation and solves a Sylvester equation in each step. Similar method is used in [34] and [35].

Another scheme for the continuation of invariant subspaces is proposed in [36] and [37]. A continuation method for low-dimensional invariant subspaces of a parameterized family of large and sparse matrices is presented in [36]. The continuation method provides bases of the invariant subspaces depending smoothly on the parameter. From this information, the corresponding eigenvalues can be computed efficiently. The predictor and corrector steps are reduced to solve the bordered matrix equations of Sylvester type. A bordered version of the Bartels-Stewart algorithm is developed to solve these equations. To trace the invariant subspaces that contain all of the unstable and control modes, a combination of CIS and subspace iterations preconditioned by a projected Cayley transform is proposed in [37].

Reference [38] first applied CIS to the eigenvalue analysis in power system applications. In [38], a bordered version of the Bartels-Stewart algorithm is used to trace the critical eigenvalues of power system. The Cayley transform is used to map the rightmost eigenvalues to the eigenvalues with largest moduli, and the projected Arnoldi method is then applied to calculate

these eigenvalues. In [39], the derivative-based method is applied to power system oscillatory stability analysis. From the eigenvalue sensitivities information, an eigenvalue index is derived to identify the rate of change and the direction of the eigenvalues movement with respect to change in any parameter p of interest. But at parameter values where eigenvalue $\lambda_i(p)$ is a multiple eigenvalue, $\lambda_i(p)$ may not be differentiable, and it may be impossible to define a continuous right eigenvector. In the cases of multiple eigenvalues, or at the point of double real eigenvalues splitting into a pair of complex eigenvalues, the derivatives of the eigenvalues and eigenvectors vanish. In addition, when computing the derivatives numerically, a simple eigenvalue that is close to others may behave like a defective one [40]. The eigenvectors may be nearly linearly dependent, making some numerical schemes for the computation of derivatives badly behaved [41].

Many power system dynamic phenomena, such as strong resonance, et al., are related to the interaction of eigenvalues. The resonance in power system is basically caused by the interaction of different oscillatory modes, such as the coupling between the swing mode and the exciter mode as the *automatic voltage regulator* (AVR) parameters vary, or the modal coupling between the *subelectrical mode* (EM) and the *torsional mode* (TM) which results in a special power system phenomenon called SSR [42]. There are several techniques proposed to study the SSR phenomenon [42, 43, 45]. The most common approaches are eigenvalue analysis, frequency scanning, and numerical time-domain simulation. For eigenvalue analysis, it is computationally intensive. Although for large systems, there is selected eigenvalue calculation method available to calculate a specified set of eigenvalues [13], this method requires a skilled and experienced analyst in order to be effective [45]. Moreover, it is not very efficient to deal with the SSR problem since the EM and TMs do not have a common defined criterion and are difficult to be calculated separately by the conventional methods.

Eigenvalue sensitivity is a very useful concept in system analysis, ranking locations, and design of power system controller, such as series compensator [46], PSS [47], and HVDC (High-Voltage Direct Current) control [48], etc. Sensitivity analysis has been applied extensively to many power system stability and control problems. It is a valuable tool for the analysis,

planning, and operation of power systems. It includes but is not limited to the following: identification of the causes of stability problems and the weak lines; optimal tuning of control parameters; determination of the locations of compensating devices for stability enhancement such as capacitor compensation and FACTS (Flexible AC Transmission System) devices [49]. Various approaches have been proposed in the literature to calculate eigenvalue sensitivities [20, 26, 46, 47, 48, 50, 51, 52, 53, 54, 55]. The first-order eigenvalue sensitivity analyze has been proposed for voltage contingency ranking in [53] and voltage stability analysis in [56]. Reference [26] proposes an eigenvalue sensitivity-based index to predict and detect the oscillatory instabilities associated with the Hopf bifurcation in power systems. Reference [55] proposes the *sensitive pole algorithm* (SPA) to compute the eigenvalues most sensitive to parameter changes in large-scale power system matrices. References [57] and [58] apply eigenvalue sensitivity to calculate the feasibility boundary. Reference [57] proposes an iterative method to compute the Hopf bifurcation using eigenvalue sensitivity to get the zero real part for a certain oscillatory mode. Reference [58] proposes a similar iterative procedure to calculate the stability margin boundary. An effective method to calculate eigenvalues as well as eigenvalue sensitivities in a DAE system is required in order to efficiently identify the stability region. Reference [49] proposes a second-order eigenvalue sensitivity algorithm using only a particular dominant eigenvalue and the corresponding eigenvector. Probabilistic eigenvalue sensitivity was proposed and applied to PSS design in [47] and [59] to overcome the robustness problem of the conventional control design methods.

1.2.2 Application of Invariant Subspace-Based System Partition

Time-domain simulation is an important tool for power system dynamic analysis. It includes a step-by-step numerical integration of DAEs. Numerical integration methods can be classified into two categories: explicit methods and implicit methods. The explicit methods involve fixed-point iterations. They are computationally efficient but have numerical stability problem when dealing with stiff systems. The implicit methods involve solving nonlinear equations at each step. They are slow but stable. Implicit methods are commonly used for

running power system dynamic simulation. Numerous research effort has been made to improve the computational efficiency. In [60], the trapezoidal method is improved by reducing a large nonlinear system into two small systems to study the post fault power system dynamics for prediction use, and Newton's method is used to solve each small system.

Power system is a very stiff system, basically it is costly to analyze the system directly. Since the stiff part is only a small part compared with the dimension of whole system, we can build an invariant subspace with respect to the stiff part and decompose the system subsequently [9]. The original power system equations are decoupled into two parts that correspond to the stiff and non-stiff subspaces. For the stiff invariant subspace, the implicit method is applied to achieve the numerical stability. The explicit method is employed to handle the non-stiff invariant subspace for the mathematical efficiency. As a result, the new hybrid method is both numerically stable and computational efficient. This yields an invariant subspace-based decoupled method for power system time-domain simulation [9]. The decoupled method can be used for both small-signal stability analysis and transient stability analysis. For the decoupled method, one question needs to be solved is the calculation and update of invariant subspaces to split the stiff system. In [9], the invariant subspace is calculated by the Arnoldi method after spectral transformation. The eigenvalue computation is very expensive. Furthermore, as parameter changes, it will cause the system eigenvalues to change, so the invariant subspace needs to be repeatedly calculated and updated. The update of invariant subspace is costly too for the same reason. An efficient update of invariant subspace is proposed in the thesis based on the work by Shroff and Keller in [61].

1.2.3 Application of the Continuation Method

This section provides continuation method-related literature review since it plays a major part in the proposed methodology. The continuation method is a predictor-corrector method widely used in power systems to overcome singularity problem.

The best known application of the continuation method in power system is the *continuation power flow* (CPF). Reference [62] first proposed CPF to find the SNB point or critical point of

power system power flow equations for steady-state voltage stability analysis. The continuation method-based power flow calculation remains well-conditioned at and around the critical point, and can avoid the singularity problem for the traditional power flow methods (such as Newton's method, et al.). The basic idea is the introduction of one continuation parameter. The continuation process mainly includes two parts: the predictor and the corrector. Moreover, the tangent vector achieved from the predictor in CPF includes bus voltage angles ($d\delta_i$) and magnitudes (dV_i) in response to a different load change. The sensitivity information can be obtained from the tangent vector at each iteration, which can be used as voltage stability index to determine the weakness part of potential voltage stability problem in power systems.

Reference [63] is a further research result of the CPF paper [62]. It combines the continuation method and optimization scheme together to investigate the reactive power planning strategy when considering voltage collapse. In the paper, bus sensitivities and branch sensitivities are introduced and described in detail. The bus sensitivity indicates how weak a particular bus is near the critical point, which is the same as the voltage stability index proposed in [62]. The branch sensitivity is the derivative of the power loss in any line to the parameter. It indicates how important one particular branch is to the voltage stability. Similarly, generator reactive sensitivity is also proposed, which shows how the reactive power output of a generator is affected by the change of parameter.

Reference [64] applies the continuation method for direct equilibrium tracing to identify the voltage collapse. It simultaneously solves the system DAEs to obtain the equilibrium point, since all of the differential parts equal to zero at the steady state. Combined with a parameterized continuation technique, the methodology identifies the voltage collapse during the direct equilibrium tracing, without rebuilding the system dynamic Jacobian and checking its singularity. This significantly reduces the computational cost. With this approach, the PV buses and slack bus assumptions are no longer needed. Reference [65] presents *continuation-based quasi-steady-state* (CQSS) analysis to investigate the long-term voltage stability. *Quasi-steady-state* (QSS) simulation combined with continuation method can provide good convergence when the system approaches the bifurcation points. It can also readily identify the *singularity-induced*

bifurcation (SIB) in the long-term time scale.

The application of continuation method and other computational techniques in power system analysis (especially voltage stability assessment) has been summarized in [66].

1.3 Motivation

To deal with the above challenging problems, the thesis presents a novel comprehensive framework of invariant subspace-based methods for power system computation and analysis [67, 68, 69, 70, 71, 72, 73]. The *improved continuation of invariant subspace* (ICIS) is proposed which provides a mathematical tool for the stability analysis. The ICIS method allows us to trace the movement of any set of critical eigenvalues (rightmost eigenvalues, eigenvalues with least damping ratio, etc.) as parameter changes. The application of the ICIS method to identify various interacting dynamic phenomena will also be investigated. The successive eigenvalue sensitivities extracted from ICIS can be used for efficient identification of oscillatory stability margin and damping margin in power systems. A continuation method-based unified approach which combines the equilibrium point tracing and eigenvalue tracing is also proposed for critical eigenvalue tracing, bifurcation analysis, and voltage stability margin identification. The *recursive projection method* (RPM) [61, 74] can be used for efficient calculation and update of invariant subspace for the decoupled time-domain simulation [9]. The invariant subspace-based decoupled time-domain simulation method combines the implicit and explicit methods to realize the advantages of both methods [9]. Finally, we propose a comprehensive invariant subspace-based framework to systematically address various aspects that are related to power system steady state and dynamic phenomena as shown in Fig. 1.5.

This framework can be used to trace power system equilibrium points, to trace a set of critical eigenvalues of interest, and to trace time-domain trajectories. With this diagnostic tool, one can systematically identify various interacting power system dynamic phenomena of interest that include voltage collapse and oscillatory behavior, transient and QSS behavior among others. It provides a novel eigenvalue analysis tool for tracing of poorly damped modes and design of control systems to improve the damping, for the identification of oscillatory

stability margin and damping margin in security assessment.

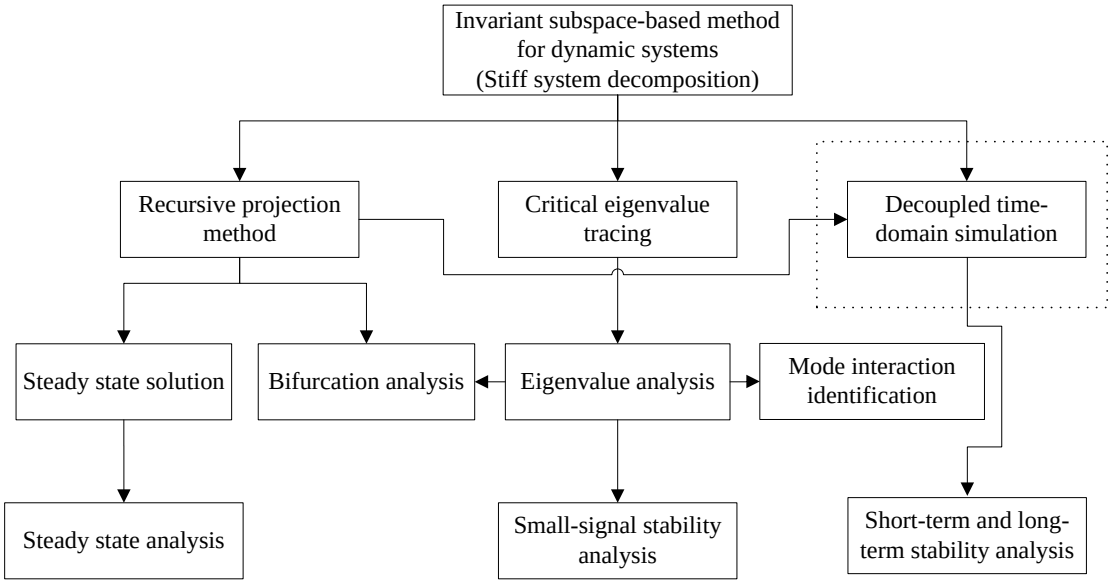

Figure 1.5 Invariant Subspace-Based Methods for Power System Computation and Analysis.

The summary of the invariant subspace-based methods for power system computation and analysis is shown in Fig. 1.5. Since power system is a very stiff system, basically it is costly to analyze the system directly. The invariant subspace-based methods are used to extract some part of the system that we are interested in and analyze specifically, or to decompose the system into two parts (the stiff and non-stiff parts) and treat them separately with different methods. As a result, we can either speed up the computation or get more information which cannot be achieved by the conventional methods. For example, the recursive projection method can be used for both the equilibrium point calculation and the decoupled time-domain simulation. The eigenvalues information of the stiff part achieved from RPM can also provide us the system stability change information for bifurcation analysis. Reference [73] applies RPM to extract the system steady state and small-signal stability information. The CIS method has been used in [38] to trace the trajectory of the critical eigenvalues as system parameter varies. It can also be used to identify various interacting dynamic phenomena related to eigenvalues. The successive sensitivities extracted from ICIS are proposed to identify the oscillatory stability

margin and the damping margin.

1.4 Organization

The thesis is divided into eight chapters and two appendices. The organization is as follows: Chapter 2 gives the mathematical model for power system stability analysis. Chapter 3 summaries the basic theorem and existing methods for eigenvalue and eigenvalue sensitivity calculation. Chapter 4 describes the improved continuation of invariant subspaces algorithm which is the basis of the thesis. Chapter 5 applies the ICIS method for critical eigenvalue tracing, oscillatory stability margin boundary estimation, and identification of various interacting power system dynamic phenomena, such as low-frequency oscillation, subsynchronous resonance, etc. Chapter 6 proposes an efficient identification of oscillatory stability margin and damping margin based on the successive eigenvalue sensitivity extracted during ICIS. Chapter 7 proposes a modified invariant subspace algorithm that can trace the equilibrium point and critical eigenvalues simultaneously. Chapter 8 gives the contributions of the research and discusses the future work.

CHAPTER 2. POWER SYSTEM DAE MODEL

2.1 Introduction

This chapter gives an overview of the mathematical models for a variety of power system components. The representation consists of both static and dynamic models. Based on detailed representation for each element, a generic mathematical formulation is presented for power system dynamic analysis.

2.2 Synchronous Generator Model

The studied power system is assumed to have n buses and m generators. Without loss of generality, the mth generator's rotor angle is chosen as the system angle reference. The two-axis generator model describing the synchronous machine dynamics is given as [64, 75]:

$$\dot{\delta}_i = (\omega_i - \omega_m)\omega_0 \qquad i = 1, 2, \ldots, m-1 \tag{2.1}$$

$$\dot{\omega}_i = [P_{mi} - D_i(\omega_i - \omega_m) - (E'_{qi} - X'_{di}I_{di})I_{qi} - (E'_{di} + X'_{qi}I_{qi})I_{di}]/M_i \qquad i = 1, 2, \ldots, m \tag{2.2}$$

$$\dot{E}'_{qi} = [E_{fdi} - E'_{qi} - (X_{di} - X'_{di})I_{di}]/T'_{d0i} \qquad i = 1, 2, \ldots, m \tag{2.3}$$

$$\dot{E}'_{di} = [-E'_{di} + (X_{qi} - X'_{qi})I_{qi}]/T'_{q0i} \qquad i = 1, 2, \ldots, m \tag{2.4}$$

where δ_i is the ith generator angle, ω_m is the system speed, ω_i is the machine speed, namely, generator angular speed, ω_0 is the system rated speed (377.0 rad/s for 60 Hz rated frequency); I_{di} and I_{qi} are direct axis (d-axis) and quadrature axis (q-axis) currents, respectively; E'_{di} and E'_{qi} are transient d-axis and q-axis EMFs (Electric and Magnetic Fields), respectively; X_{di} and X_{qi} represent d-axis and q-axis synchronous reactances; X'_{di} and X'_{qi} represent d-axis and q-axis transient reactances; T'_{d0i} and T'_{q0i} are d-axis and q-axis open circuit transient time constants;

M_i is the machine inertia constant and D_i is the machine damping constant. Note that all the other quantities are in per unit except ω_0.

The ith machine currents I_{di} and I_{qi} can be eliminated by solving the generator interface equations to the network. Therefore, we have

$$\begin{aligned} I_{di} &= [R_{si}[E'_{di} - V_i\sin(\delta_i - \theta_i)] + X'_{qi}[E'_{qi} - V_i\cos(\delta_i - \theta_i)]]/A_i \\ I_{qi} &= [R_{si}[E'_{qi} - V_i\cos(\delta_i - \theta_i)] - X'_{di}[E'_{di} + V_i\sin(\delta_i - \theta_i)]]/A_i \\ A_i &= R_{si}^2 + X'_{di}X'_{qi}. \end{aligned} \tag{2.5}$$

2.3 Excitation System Model

The simplified IEEE type DC-1 excitation system as shown in Fig. 2.1 is used to represent the excitation system. The corresponding mathematical model is as follows:

$$\dot{E}_{fdi} = [V_{ri} - [K_{ei} + S_{ei}(E_{fdi})]E_{fdi}]/T_{ei} \qquad i = 1, 2, \ldots, m \tag{2.6}$$

$$\dot{V}_{ri} = [-V_{ri} + K_{ai}(V_{refi} - V_i - R_{fi})]/T_{ai} \qquad i = 1, 2, \ldots, m \tag{2.7}$$

$$\text{if } V_{ri,\min} \le V_{ri} \le V_{ri,\max}, V_{pssi} = 0 \text{ (at steady state)}$$

$$\dot{R}_{fi} = [-R_{fi} - [K_{ei} + S_{ei}(E_{fdi})]K_{fi}E_{fdi}/T_{ei} + K_{fi}V_{ri}/T_{ei}]/T_{fi} \qquad i = 1, 2, \ldots, m \tag{2.8}$$

where V_{refi} is the reference voltage of AVR; V_{ri} and R_{fi} are the outputs of the AVR and exciter soft feedback; E_{fdi} is the voltage applied to generator field winding; T_{ai}, T_{ei}, and T_{fi} are AVR, exciter, and feedback time constants; K_{ai}, K_{ei}, and K_{fi} are the gains of AVR, exciter, and feedback, respectively; $V_{ri,\min}$ and $V_{ri,\max}$ are the lower and upper limits of V_{ri}.

2.4 Prime Mover and Speed Governor Model

Fig. 2.2 shows the block diagram of a simplified prime mover and speed governor. Two differential equations are used to describe the dynamics when no μ_i limit is hit.

$$\dot{P}_{mi} = (\mu_i - P_{mi})/T_{chi} \qquad i = 1, 2, \ldots, m \tag{2.9}$$

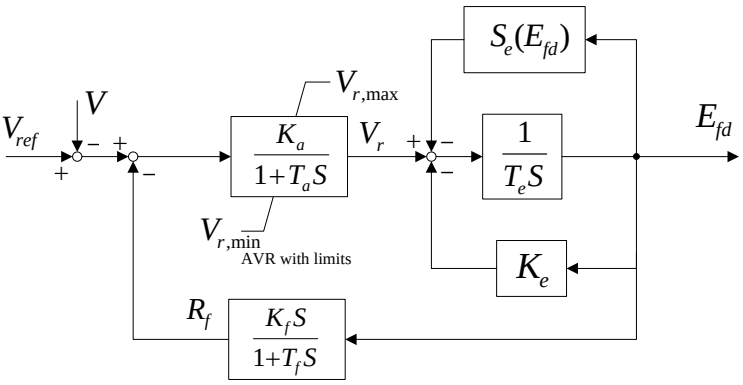

Figure 2.1 The IEEE Type DC-1 Excitation System.

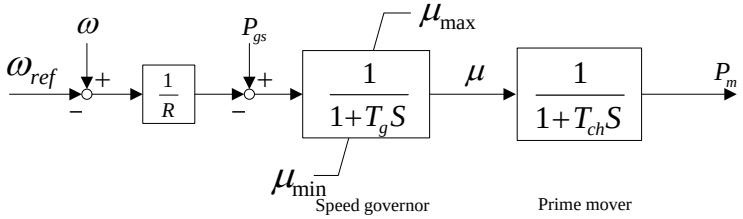

Figure 2.2 The Simplified Speed Governor and Prime Mover.

$$\dot{\mu}_i = [P_{gsi} - (\omega_i - \omega_{ref})/R_i - \mu_i]/T_{gi} \qquad i = 1, 2, \ldots, m \tag{2.10}$$

$$\text{if } \mu_{i,\min} \le \mu_i \le \mu_{i,\max}$$

where $P_{gsi} = P^0_{gsi}(1+K_{gi}p)$ is the designated real power generation, P^0_{gsi} is its setting at the base case; K_{gi} is the generator load pickup factor that can be determined by *automatic generation control* (AGC), *economic dispatch control* (EDC) or other system operating practices; P_{mi} is the mechanical power of prime mover and μ_i is the steam valve or water gate opening; $\mu_{i,\min}$ and $\mu_{i,\max}$ are the lower and upper limits of μ_i; R_i is the governor regulation constant representing its inherent speed-droop characteristic; ω_{ref} $(= 1.0)$ is the governor reference speed; T_{chi} and T_{gi} are the time constants related to the prime mover and speed governor, respectively. Parameter p is introduced to designate the system operating condition. At the base case, p is equal to zero.

2.5 Nonlinear Load Model

Load model may be voltage and frequency dependent. In power system analysis, common load models can be constant power model, constant current model, and constant impedance model. The representation for these static load models is shown as follows.

- Constant power load:

$$P_{li} = P_{li0} \qquad Q_{li} = Q_{li0}. \tag{2.11}$$

- Constant current load:

$$P_{li} = P_{li0}(V_i/V_{i0}) \qquad Q_{li} = Q_{li0}(V_i/V_{i0}). \tag{2.12}$$

- Constant impedance load:

$$P_{li} = P_{li0}(V_i/V_{i0})^2 \qquad Q_{li} = Q_{li0}(V_i/V_{i0})^2. \tag{2.13}$$

The generic load model which has been widely used to represent the voltage dependency of loads is the polynomial model:

$$\begin{cases} P_{li} = P_{li0}[K_{p1} + K_{p2}(V_i/V_{i0}) + K_{p3}(V_i/V_{i0})^2] \\ Q_{li} = Q_{li0}[K_{q1} + K_{q2}(V_i/V_{i0}) + K_{q3}(V_i/V_{i0})^2]. \end{cases} \tag{2.14}$$

This model is called the ZIP model, as it is composed of constant impedance (Z), constant current (I), and constant power (P) components. The parameters K_{p1}, K_{p2}, K_{p3} define the proportion of constant power, constant current, and constant impedance load for real power; the parameters K_{q1}, K_{q2}, K_{q3} define the proportion of constant power, constant current, and constant impedance load for reactive power.

The generic load model may also have frequency dependent component. The frequency dependency of load characteristics is usually represented by multiplying the exponential model of the polynomial model by a factor as follows:

$$\begin{cases} P_{li} = P_{li0}[K_{p1} + K_{p2}(V_i/V_{i0}) + K_{p3}(V_i/V_{i0})^2][1 + K_{pf}(\omega_m - 1)] \\ Q_{li} = Q_{li0}[K_{q1} + K_{q2}(V_i/V_{i0}) + K_{q3}(V_i/V_{i0})^2][1 + K_{qf}(\omega_m - 1)] \end{cases} \quad i = 1, 2, \ldots, n \tag{2.15}$$

where P_{li} and Q_{li} are the real and reactive power of the load at bus i; P_{li0} and Q_{li0} are the real and reactive power consumed by the load at the nominal voltage V_{i0}; parameters K_{pf} and K_{qf} are the load changing factors with respect to system frequency.

2.6 Network Power Equations

Network power equations represent the power flow model for power system network. The simplified form of the power flow equations is as follows.

$$g(x, y) = 0 \tag{2.16}$$

where algebraic variables y represent the solution of power flow; the algebraic equations g represent network equations. At each bus of the power system, power injection is balanced. The process of solving the algebraic equations (2.16) for given loads and generator power outputs is referred to as the *load flow* or *power flow calculation*. It requires an iterative procedure. There are several alternative iteration methods, all of which produce a solution in the form of a stated magnitude and phase angle of the power frequency voltage phasor for each bus.

The network equations g can be divided into the nonlinear forms consisting of real and reactive power balance.

$$\begin{cases} 0 = P_{gi} - (1 + K_{lpi}p)P_{li} - P_{ti} \\ 0 = Q_{gi} - (1 + K_{lqi}p)Q_{li} - Q_{ti} \end{cases} \qquad i = 1, 2, \ldots, n \tag{2.17}$$

where P_{gi} and Q_{gi} are the real and reactive power generation of the generator at bus i; P_{ti} and Q_{ti} are the net real and reactive power injection at bus i; K_{lpi} and K_{lqi} are the load changing factors specified for bus i.

The real and reactive power generations are primarily determined by the inherent characteristics of the speed governor and AVR regulations. They will change if real power generation rescheduling and secondary voltage control are activated. They are described as follows.

$$\begin{cases} P_{gi} = I_{di}V_i\sin(\delta_i - \theta_i) + I_{qi}V_i\cos(\delta_i - \theta_i) \\ Q_{gi} = I_{di}V_i\cos(\delta_i - \theta_i) - I_{qi}V_i\sin(\delta_i - \theta_i) \end{cases} \qquad i = 1, 2, \ldots, n \tag{2.18}$$

The real and reactive loads are determined by the load characteristics. The net real and reactive power injection are constrained by the physical characteristics, which are represented by the following equations.

$$\begin{cases} P_{ti} = \sum_{k=1}^{n} V_i V_k Y_{ik} \cos(\theta_i - \theta_k - \varphi_{ik}) \\ Q_{ti} = \sum_{k=1}^{n} V_i V_k Y_{ik} \sin(\theta_i - \theta_k - \varphi_{ik}) \end{cases} \qquad i = 1, 2, \ldots, n. \tag{2.19}$$

The variables V_i and θ_i in (2.18) and (2.19) are bus voltage magnitude and angle respectively. These variables belong to the unknown variables y in (2.16) in power flow calculation. The variables Y_{ik} and φ_{ik} are given parameters from power system model representing bus connections.

2.7 Power System DAE Model

Corresponding to the above models, there are both differential equations and algebraic equations in power systems. As a result, power systems can be represented generally by a DAE model. The mathematical formulation is as follows.

$$\begin{cases} \dot{x} = f(x, y, p) \\ 0 = g(x, y, p) \end{cases} \tag{2.20}$$

where $x \in \mathbb{R}^n$ and $y \in \mathbb{R}^m$ are state and algebraic variable vectors of dimensions n and m, respectively. The dynamics of the generators, motors, control devices, and generally the load dynamics together define the dynamic equations $f : \mathbb{R}^n \times \mathbb{R}^m \times \mathbb{R} \longrightarrow \mathbb{R}^n$, while the algebraic equations $g : \mathbb{R}^n \times \mathbb{R}^m \times \mathbb{R} \longrightarrow \mathbb{R}^m$ typically consist of the power flow equations of the network. $p \in \mathbb{R}$ is the parameter to represent the load level of the entire or part of the system. It should be pointed out that the system parameter is very flexible to be chosen. Any arbitrary system operating parameter (e.g., nodal injection, controller gain) or power network parameter (line impedance, transformer tap, etc) can also be chosen as the system parameter. When applying the continuation method, this parameter p is the continuation parameter to be used during the tracing process through the thesis.

CHAPTER 3. POWER SYSTEM SMALL-SIGNAL STABILITY ANALYSIS

3.1 Introduction

This chapter introduces the basic theorem and existing conventional methods for eigenvalue and eigenvalue sensitivity calculations in power systems. It also describes some eigenvalue-related concepts together with their applications in power system analysis.

3.2 Eigenvalue and Eigenvalue Sensitivity

For a fixed value of system parameter p, the equilibrium points (x^*, y^*) of the DAE model of power system (2.20) are solutions of the system:

$$\begin{cases} f(x, y, p) = 0 \\ g(x, y, p) = 0. \end{cases} \tag{3.1}$$

To a large extent, the current research and industry tools for stability analysis and design of power system controllers consist of applying the technique of *linearization*. Assume that matrices f and g are both continuous and differentiable, the stability of equilibrium points can be determined by linearizing (2.20) around the equilibrium (x^*, y^*).

$$\begin{bmatrix} \Delta\dot{x} \\ 0 \end{bmatrix} = A(p) \begin{bmatrix} \Delta x \\ \Delta y \end{bmatrix} \tag{3.2}$$

where $A(p) \in \mathbb{R}^{(m+n)\times(m+n)}$ is called the Jacobian matrix of the power system DAE model:

$$A(p) = \begin{bmatrix} f_x(p) & f_y(p) \\ g_x(p) & g_y(p) \end{bmatrix}. \tag{3.3}$$

In power system small-signal stability analysis, there are generally two techniques to calculate the Jacobian matrix once the steady state solutions are obtained at a certain system operating point: state perturbation and symbolic computation. In the state perturbation method, each state is perturbed in turn by a very small value (e.g., 10^{-4}). When the ith state is perturbed, the ith column of the Jacobian will be calculated. The Jacobian can be formulated once all the state and algebraic variables have been perturbed. The advantage of this method is that it is easy to implement. The disadvantage is that sometimes the results might not be accurate since it is only an approximation method. The symbolic computation derives the derivatives of each DAE with respect to x and y in order to calculate f_x, f_y, g_x, and g_y, respectively. We need to have explicit knowledge of system equations to perform the symbolic derivative calculation. In the thesis, the Jacobian is calculated using the symbolic computation with the help of MATLAB symbolic computing functions.

The Jacobian matrix $A(p)$ is a sparse matrix. For the New England 39-bus system at a certain steady state condition, Fig. 3.1 shows the sparsity pattern of the Jacobian. The non-zero elements are shown in black. Assume g_y is nonsingular, we can eliminate the vector of algebraic variables Δy in (3.2):

$$\Delta \dot{x} = [f_x - f_y g_y^{-1} g_x]\Delta x = A_s \Delta x. \tag{3.4}$$

The equivalent system state matrix is

$$A_s(p) = f_x(p) - f_y(p) g_y^{-1}(p) g_x(p) \tag{3.5}$$

whose eigenvalues determine the small-signal stability of the system. It is the Schur complement of the algebraic equation Jacobian g_y in the unreduced Jacobian $A(p)$. For this reason, $A_s(p)$ is often called the reduced Jacobian. Fig. 3.2 shows the sparsity pattern of the reduced Jacobian $A_s(p)$ in the New England system. Since the state matrix A_s is not sparse anymore, it is now generally accepted that it is better to work directly with (3.3) instead of (3.5) in computing eigenvalues and eigenvectors, especially for large power systems [53, 76]. In addition to this, the advantages of using structure-preserving form (3.3) in power system analysis include [77]: numerical efficient eigenvalue computation methods; it facilitates analytical study of how

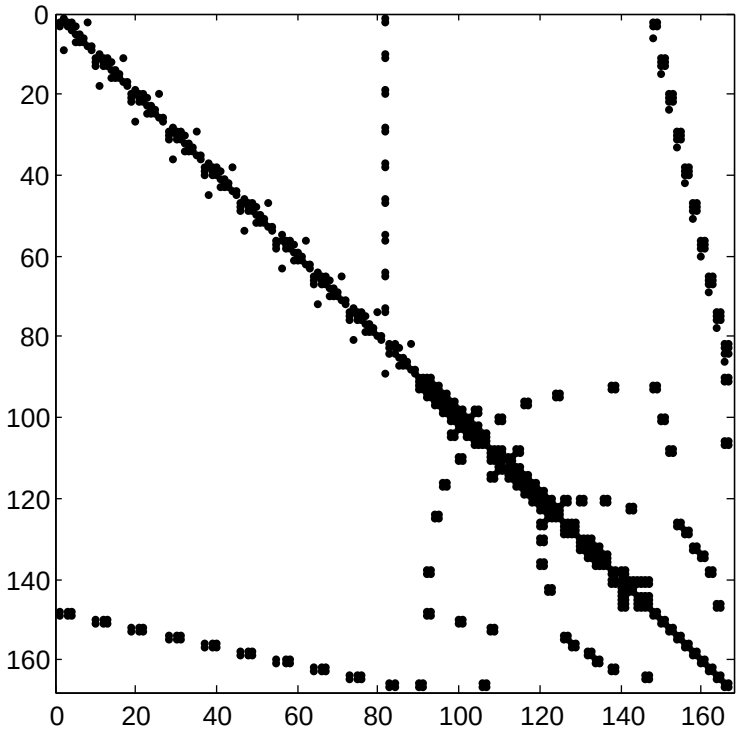

Figure 3.1 The Jacobian Matrix.

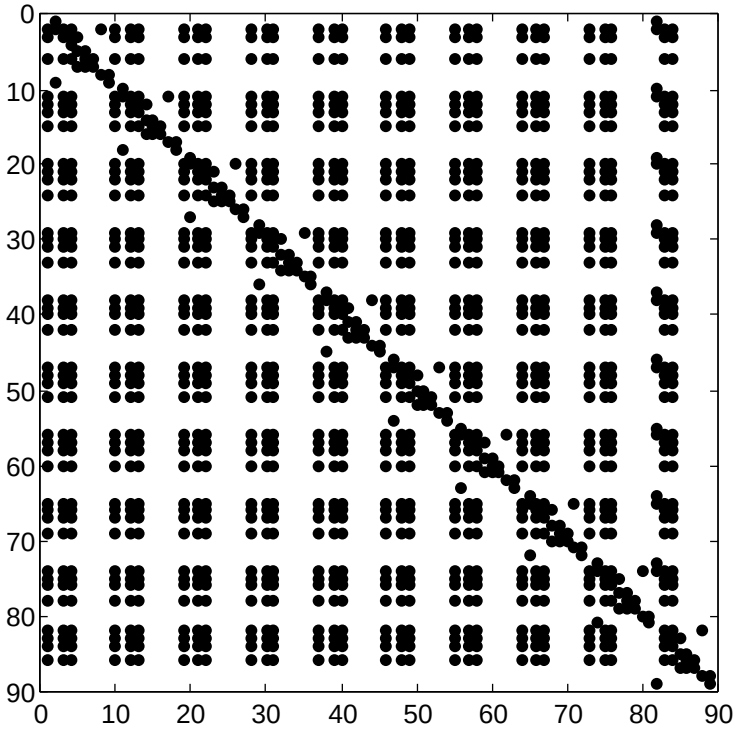

Figure 3.2 The Reduced Jacobian Matrix.

parameters in the algebraic equations affect the system eigenvalues; the eigenvalue sensitivity problem can be decomposed into network-dependent and device-dependent parts which provide more physical insight.

It should also be mentioned that the system sparsity pattern changes as system size varies. Table 3.1 shows the sparsity of Jacobian for different power system DAE models. One can see that with the increase in system size and order of the Jacobian, the ratio between the number of non-zero elements and the total number of elements in the Jacobian decreases, which reflects that the system model becomes more sparse.

Table 3.1 Sparsity of Jacobian for Different System Models

No.	Order	Total Number of Elements (TN)	Non-Zero Elements (NZ)	NZ/TN
1	167	27,889	1,298	4.65E-2
2	653	426,409	5,150	1.21E-2
3	1,138	1,295,044	4,054	3.13E-3
4	7,135	50,908,225	34,738	6.82E-4
5	13,251	175,589,001	48,737	2.78E-4
6	21,476	461,218,576	76,512	1.66E-4

Assume g_y is nonsingular, for each eigenvalue λ_i and the corresponding n-element right eigenvector ϕ_i of A_s, define $\varphi_i = -g_y^{-1} g_x \phi_i$, then we can work directly on (3.6) to calculate λ_i and ϕ_i instead of solving (3.7) [76]:

$$\begin{bmatrix} f_x & f_y \\ g_x & g_y \end{bmatrix} \begin{bmatrix} \phi_i \\ \varphi_i \end{bmatrix} = \begin{bmatrix} \lambda_i \phi_i \\ 0 \end{bmatrix} \tag{3.6}$$

$$A_s \phi_i = \lambda_i \phi_i. \tag{3.7}$$

Similarly, for each eigenvalue λ_i and the corresponding n-element left eigenvector ψ_i of A_s, define $\chi_i^T = -\psi_i^T f_y g_y^{-1}$, we can work directly on (3.8) instead of (3.9) to calculate λ_i and ψ_i:

$$\begin{bmatrix} \psi_i^T & \chi_i^T \end{bmatrix} \begin{bmatrix} f_x & f_y \\ g_x & g_y \end{bmatrix} = \begin{bmatrix} \lambda_i \psi_i^T & 0 \end{bmatrix} \tag{3.8}$$

$$\psi_i^T A_s = \psi_i^T \lambda_i. \tag{3.9}$$

Eigenvalue sensitivity analysis involves the study of changes in the dynamic characteristic of a system with respect to parameter variations. The conventional way to calculate eigenvalue

sensitivity uses the reduced Jacobian A_s. The eigenvalues depend continuously on parameter p. If the ith eigenvalue λ_i is distinct, then it is even differentiable and we also have $\psi_i^T \phi_i \neq 0$. In this case, one can carry through a first-order perturbation analysis. Take the partial derivative of both sides of (3.7) with respect to p:

$$\frac{\partial A_s}{\partial p}\phi_i + A_s \frac{\partial \phi_i}{\partial p} = \frac{\partial \lambda_i}{\partial p}\phi_i + \lambda_i \frac{\partial \phi_i}{\partial p}. \tag{3.10}$$

Left multiplying both sides of (3.10) by ψ_i^T, and considering (3.9), the first-order sensitivity of eigenvalue λ_i with respect to parameter p can be written as [50, 52]

$$\frac{\partial \lambda_i}{\partial p} = \frac{\psi_i^T \frac{\partial A_s}{\partial p}\phi_i}{\psi_i^T \phi_i}. \tag{3.11}$$

Meanwhile, differentiate (3.5) with respect to p, we can get

$$\frac{\partial A_s}{\partial p} = \frac{\partial f_x}{\partial p} - \frac{\partial f_y}{\partial p} g_y^{-1} g_x - f_y \frac{\partial g_y^{-1}}{\partial p} g_x - f_y g_y^{-1} \frac{\partial g_x}{\partial p}. \tag{3.12}$$

Proposition 1. $\frac{\partial g_y^{-1}}{\partial p} = -g_y^{-1} \frac{\partial g_y}{\partial p} g_y^{-1}$.

Proof. From $I = g_y g_y^{-1}$, differentiate both sides with respect to p and use the product rule:

$$0 = \frac{\partial (g_y g_y^{-1})}{\partial p} = \frac{\partial g_y}{\partial p} g_y^{-1} + g_y \frac{\partial g_y^{-1}}{\partial p}. \tag{3.13}$$

Then we will have

$$\frac{\partial g_y^{-1}}{\partial p} = -g_y^{-1} \frac{\partial g_y}{\partial p} g_y^{-1}. \tag{3.14}$$

□

Finally we can get

$$\dot{A}_s = \frac{\partial A_s}{\partial p} = \dot{f}_x - \dot{f}_y g_y^{-1} g_x + f_y g_y^{-1} \dot{g}_y g_y^{-1} g_x - f_y g_y^{-1} \dot{g}_x. \tag{3.15}$$

Similar to the calculation of the Jacobian matrix, the derivative of the Jacobian can also be derived by the symbolic computing to simplify the calculation.

Since the left and right eigenvectors corresponding to different eigenvalues are orthogonal, assume all eigenvalues are distinct, consider two eigenvalues λ_i and λ_j, if we normalize the eigenvectors so that

$$\psi_i^T \phi_j = \begin{cases} 1, & i = j \\ 0, & i \neq j. \end{cases} \tag{3.16}$$

Then the eigenvalue sensitivity in (3.11) can further be simplified as

$$\dot{\lambda}_i = \frac{\partial \lambda_i}{\partial p} = \psi_i^T \dot{A}_s \phi_i. \tag{3.17}$$

Reference [53] proposed an eigenvalue sensitivity formula which works directly with A instead of A_s. First, a generalized eigenvalue problem is presented:

$$A\hat{\phi}_i = \lambda_i E \hat{\phi}_i \tag{3.18}$$

where,

$$E = \begin{bmatrix} I_n & 0 \\ 0 & 0 \end{bmatrix} \tag{3.19}$$

$$\hat{\phi}_i = \begin{bmatrix} \phi_i \\ \varphi_i \end{bmatrix}. \tag{3.20}$$

It is equivalent to (3.6) and (3.7) to calculate the eigenvalue λ_i and its right eigenvector ϕ_i.

Similarly, for the calculation of eigenvalue λ_i and the corresponding left eigenvector, we have the following formulation

$$\hat{\psi}_i^T A = \lambda_i \hat{\psi}_i^T E \tag{3.21}$$

where,

$$\hat{\psi}_i = \begin{bmatrix} \psi_i \\ \chi_i \end{bmatrix}. \tag{3.22}$$

It is equivalent to (3.8) and (3.9) to calculate the eigenvalue and left eigenvector.

From (3.18), the eigenvalue sensitivity can be derived as follows [53]:

$$\frac{\partial \lambda_i}{\partial p} = \frac{\hat{\psi}_i^T \frac{\partial A}{\partial p} \hat{\phi}_i - \lambda_i \hat{\psi}_i^T \frac{\partial E}{\partial p} \hat{\phi}_i}{\hat{\psi}_i^T E \hat{\phi}_i}. \tag{3.23}$$

Matrix E is a constant matrix as shown in (3.19), so $\partial E/\partial p = 0$, if E has no relationship with p. Furthermore, if the eigenvectors ψ_i and ϕ_i are normalized and satisfy (3.16), we will have the following standard normalization of finite eigenvectors

$$\hat{\psi}_i^T E \hat{\phi}_i = 1. \tag{3.24}$$

Finally, the structure-preserving formulation of eigenvalue sensitivity in (3.23) has the form

$$\dot{\lambda}_i = \hat{\psi}_i^T \dot{A} \hat{\phi}_i. \tag{3.25}$$

Eqs. (3.17) and (3.25) give the conventional ways to calculate the eigenvalue sensitivity at any given steady state operating condition for differential (standard) and differential-algebraic (generalized) models, respectively. For eigenvalue computation using QR method, it takes $\mathcal{O}(m(m^2+mn+n^2))$ to formulate the state matrix A_s and $25\mathcal{O}(n^3)$ to calculate the eigenvalues, where "$\mathcal{O}$" means *floating-point operations per second* (FLOPS). For solving the generalized eigenvalue problem (3.18) with QZ algorithm [40], it takes $30\mathcal{O}((m+n)^3)$ to calculate the eigenvalues, $16\mathcal{O}((m+n)^3)$ and $20\mathcal{O}((m+n)^3)$ to calculate Q and Z, respectively. For eigenvalue sensitivity calculation, it needs both the left and the right eigenvectors and costs more time to compute. It can be seen that the computation of eigenvalue and eigenvalue sensitivity using the conventional methods is not efficient. For large power system, with the increase in system size, it will result in excessive computation cost. The improved continuation of invariant subspaces provides us an effective, efficient, and robust way not only for eigenvalue computation but also for the calculation of eigenvalue sensitivity as shown in the next chapter.

3.3 Eigenvalue and Damping Ratio

A real eigenvalue corresponds to a non-oscillatory mode. A positive real eigenvalue represents an aperiodic growing mode, and a negative real eigenvalue represents a decaying mode. On the other hand, complex eigenvalues occur in conjugate pairs and each pair corresponds to an oscillatory mode. A pair of complex eigenvalues $\lambda_i = \sigma_i \pm j\omega_i$ include a real part σ_i and an imaginary part ω_i. The imaginary part $\omega_i = 2\pi f_i$ gives the frequency f_i of the corresponding oscillatory mode. The real part σ_i reveals the damping of the associated oscillatory mode: a positive value means a negative damping with a growing oscillatory response, while a negative value represents a positive damping with a decreasing oscillatory response. A real part with zero value implies there is no damping with the mode. If all the eigenvalues of the system state Jacobian A_s have negative real parts, the equilibrium (x^*, y^*) is asymptotically stable for

"sufficiently small" initial perturbations from the equilibrium point. If at least one eigenvalue of the linearized system state matrix has a positive real part, the equilibrium is unstable.

Damping plays an important role in power system oscillations. In the oscillatory stability assessment, an important criterion is to keep the system far away from a certain minimum damping ratio limit for each scenario or contingency. Usually, the small-signal stability problem is one of ensuring sufficient damping of system oscillations. The damping ratio corresponding to a complex pair of eigenvalues $\lambda_i = \sigma_i \pm j\omega_i$ is given by

$$\zeta_i = \zeta(\lambda_i) = -\frac{\sigma_i}{\sqrt{\sigma_i^2 + \omega_i^2}}. \tag{3.26}$$

The damping ratio ζ_i determines the rate of decay of the amplitude of oscillation. The time constant of amplitude decay is $1/|\sigma_i|$. In other words, the amplitude decays to $1/e$ or 36.8% of the initial amplitude in $1/|\sigma_i|$ seconds or in $1/(2\pi\zeta_i)$ cycles of oscillation. For example, a damping ratio of 5% means that in three cycles of oscillation periods, the amplitude is damped to about 34.7% of its initial value.

3.4 Participation Factor and Modal Analysis

The right eigenvector associated with an eigenvalue may not always give a reliable measure of the activity of a variable in a mode as it depends on the physical units of the corresponding variable. In other words, the right eigenvectors account for mode shape, but they are unit dependent. Their scaling depends on the dimensions of the state variables and also the case for the left eigenvectors. This makes it difficult to compare the relative importance of different types of states. Consequently, the concept of participation factor was introduced successfully in [21] to overcome these difficulties as a means of expressing the coupling between modes and state variables.

Given that the eigenvectors product $\psi_i^T \phi_i$ is normalized to unity as in (3.16), *participation factor* is the product of the jth components of the left and right eigenvectors corresponding to the ith mode

$$p_{ij} = \psi_{ij}^* \phi_{ij} \tag{3.27}$$

where ϕ_{ij} is the ith element of the jth right eigenvector, ψ_{ij}^* is the complex conjugate of the ith element of the jth left eigenvector. ϕ_{ij} measures the activity of the ith state variable x_i in the jth mode, and ψ_{ij} weighs the contribution of this activity to the jth mode. Thus the factor p_{ij} gives a measure of the relative participation of the ith state variable in the jth mode, and vice versa. It should be mentioned that as pointed out in [78], this factor is also the partial derivative of the jth eigenvalue with respect to the ith diagonal element of the state matrix.

Originally proposed in [21], a matrix called the *participation matrix* denoted by P, provides a measure of association between the state variables and the oscillatory modes. It is defined as

$$P = \begin{bmatrix} P_1 & P_2 & \cdots & P_n \end{bmatrix} \tag{3.28}$$

with the participation vector P_i determined by

$$P_i = \begin{bmatrix} p_{1i} \\ p_{2i} \\ \vdots \\ p_{ni} \end{bmatrix} = \begin{bmatrix} \psi_{1i}^* \phi_{1i} \\ \psi_{2i}^* \phi_{2i} \\ \vdots \\ \psi_{ni}^* \phi_{ni} \end{bmatrix} \qquad i = 1, 2, \ldots, n. \tag{3.29}$$

It should be mentioned that in power system controller design, the right eigenvector gives information about the observability of oscillation mode, the left eigenvector gives information about the controllability. Hence, the combination of the right and left eigenvectors (residues) indicates the location of the controllers to be installed.

CHAPTER 4. AN IMPROVED CONTINUATION OF INVARIANT SUBSPACES WITH SENSITIVITY

4.1 Introduction

This chapter describes the improved continuation of invariant subspaces algorithm in detail. With proper initialization, the successive eigenvalue sensitivity extracted during ICIS is proposed and proved mathematically. The initialization and update of invariant subspaces are also described.

4.2 Improved Continuation of Invariant Subspaces With Sensitivity

4.2.1 Improved Continuation of Invariant Subspaces

Low-dimensional invariant subspaces of parameterized large matrix $A(p)$ (or $A_s(p)$) play an important role in the numerical analysis of dynamical systems. Invariants subspaces that belong to part of the spectrum which is close to the imaginary axis provide the information about stability, bifurcation, and more generally, about locally invariant manifolds [36]. However, for traditional eigenvalue computation methods, these eigenvalues are usually obtained from a full resolution of the spectrum. For big and sparse power system state matrix, it will be important to apply the continuation of invariant subspaces to this problem for saving computation time as well as improving efficiency.

We consider a family of matrices $A_s(p)$ depending smoothly on parameter p. Our aim is to compute smooth matrices $\Phi(p) \in \mathbb{R}^{n\times r}$, the columns of which form a basis of an r-dimensional subspace $S(\Phi(p))$ invariant under $A_s(p)$ [36], i.e.

$$A_s(p)\Phi(p) = \Phi(p)\Lambda(p) \tag{4.1}$$

for some $\Lambda(p) \in \mathbb{R}^{r\times r}$ which has exactly the eigenvalues of $A_s(p)$ that correspond to the eigenvectors spanning $\Phi(p)$. If the eigenvalues of A_s are distinct, then A_s can be diagonalized. Specially, when $\Lambda(p)$ is a diagonal matrix with the r eigenvalues on its diagonals, there is

$$\Lambda(p) = \mathrm{diag}(\lambda_1, \lambda_2, \ldots, \lambda_r) = \begin{bmatrix} \lambda_1 & 0 & \cdots & 0 \\ 0 & \lambda_2 & \cdots & 0 \\ \vdots & \vdots & \ddots & \vdots \\ 0 & 0 & \cdots & \lambda_r \end{bmatrix} \tag{4.2}$$

and

$$\Phi_0 = \begin{bmatrix} \phi_1 & \phi_2 & \cdots & \phi_r \end{bmatrix}. \tag{4.3}$$

It is easily seen that (4.1) represents nr equations for $(nr + r^2)$ unknowns. Therefore, r^2 extra conditions have to be added. A natural choice would be to require $\Phi(p)^T\Phi(p) = I_r$, where I_r denotes the $r \times r$ identity matrix. In other words, $\Phi(p)$ would span an orthonormal basis. However, the usual normalization condition $n(\Phi) = \Phi(p)^T\Phi(p) - I_r$ is not differentiable, except at $\Phi = 0$. Hence, it is generally preferred to consider a "linearized" constraint [36]:

$$\widehat{\Phi}^T\Phi(p) = I_r \tag{4.4}$$

with a fixed $\widehat{\Phi} \in \mathbb{R}^{n\times r}$.

Note for power systems with DAE models, the system state matrix A as defined in (3.3) will be used directly to maintain the system sparsity. Then the extended eigenvector matrix can be defined as $\Omega = -g_y^{-1}g_x\Phi$, and the equation set for the invariant subspace becomes [38]

$$T(\Phi, \Omega, \Lambda, p) = \begin{bmatrix} f_x(p)\Phi(p) + f_y(p)\Omega(p) - \Phi(p)\Lambda(p) \\ g_x(p)\Phi(p) + g_y(p)\Omega(p) \\ \widehat{\Phi}^T\Phi(p) - I_r \end{bmatrix} = 0. \tag{4.5}$$

In (4.5), there are totally $(m + n + r)r$ equations and the same number of unknowns for (Φ, Ω, Λ). The equation set can be solved by the continuation method along the parameter path. The predictor-corrector techniques are applied to (4.5).

Assume that $\Phi_0 = \Phi(p_0)$, $\Omega_0 = \Omega(p_0)$, and $\Lambda_0 = \Lambda(p_0)$ are the solutions of (4.5) at $p = p_0$, and the tangent to $(\Phi(p), \Omega(p), \Lambda(p))$ at p_0 is $(H_0, L_0, \Delta_0) = (\dot{\Phi}(p_0), \dot{\Omega}(p_0), \dot{\Lambda}(p_0))$. By

differentiating (4.5), the following linear system of dimension $(m+n+r)r$ can be obtained for the predictor:

$$\begin{bmatrix} f_x(p_0)H_0 - H_0\Lambda_0 + f_y(p_0)L_0 - \Phi_0\Delta_0 \\ g_x(p_0)H_0 + g_y(p_0)L_0 \\ \widehat{\Phi}^T H_0 \end{bmatrix} = \begin{bmatrix} -\dot{f}_x(p_0)\Phi_0 - \dot{f}_y(p_0)\Omega_0 \\ -\dot{g}_x(p_0)\Phi_0 - \dot{g}_y(p_0)\Omega_0 \\ 0 \end{bmatrix}. \tag{4.6}$$

Equation (4.6) is called the bordered matrix equation of Sylvester type (or Riccati equation) [36]. An effective method called the *bordered Bartels-Stewart algorithm* [40] is available for solving this matrix equation. The algorithm computes Schur decomposition of matrix Λ and reduces the linear algebra to solve a sequence of r bordered linear systems. The computation cost of using the algorithm to calculate the bordered matrix equation (4.6) is $\mathcal{O}(r(m+n)(m+n+r))$. The detailed implementation of the algorithm is described in the next section.

Once the tangent (H_0, L_0, Δ_0) has been found by solving (4.6), the prediction can be made as

$$\begin{bmatrix} \Phi_1 \\ \Omega_1 \\ \Lambda_1 \\ p_1 \end{bmatrix} = \begin{bmatrix} \Phi_0 \\ \Omega_0 \\ \Lambda_0 \\ p_0 \end{bmatrix} + s \begin{bmatrix} H_0 \\ L_0 \\ \Delta_0 \\ 1 \end{bmatrix} \tag{4.7}$$

where s is an appropriate step size.

For $\Lambda(p)$ as shown in (4.2), Λ_0 in (4.6) is a diagonal matrix. But since the derivative Δ_0 is not a diagonal matrix after solving the predictor (4.6), Λ_1 in (4.7) is also not diagonal.

Suppose Δ_0 is given as

$$\Delta_0 = \dot{\Lambda}(p) = \begin{bmatrix} \delta_{11} & \delta_{12} & \cdots & \delta_{1r} \\ \delta_{21} & \delta_{22} & \cdots & \delta_{2r} \\ \vdots & \vdots & \ddots & \vdots \\ \delta_{r1} & \delta_{r2} & \cdots & \delta_{rr} \end{bmatrix}. \tag{4.8}$$

Proposition 2. *When $\Lambda(p)$ is a diagonal matrix as defined in (4.2), the diagonal elements of its derivative Δ_0 in (4.8) $(\delta_{11}, \delta_{22}, \ldots, \delta_{rr})$ give the eigenvalue sensitivities of the traced*

eigenvalues $(\lambda_1, \lambda_2, \ldots, \lambda_r)$ *with respect to parameter* p. *In other words,* $\forall\, i \in [1, r]$, *we have*

$$\delta_{ii} = \frac{\partial \lambda_i}{\partial p} = \psi_i^T \dot{A}_s \phi_i. \tag{4.9}$$

Proof. For $\Omega_0 = -g_y^{-1} g_x \Phi_0$, differentiate both sides with respect to p, then

$$L_0 = \dot{\Omega}_0 = g_y^{-1} \dot{g}_y g_y^{-1} g_x \Phi_0 - g_y^{-1} \dot{g}_x \Phi_0 - g_y^{-1} g_x H_0. \tag{4.10}$$

Left multiply the first equation in (4.6) by ψ_i^T, we get

$$\psi_i^T f_x H_0 - \psi_i^T H_0 \Lambda_0 + \psi_i^T f_y L_0 - \psi_i^T \Phi_0 \Delta_0 = -\psi_i^T \dot{f}_x \Phi_0 + \psi_i^T \dot{f}_y g_y^{-1} g_x \Phi_0. \tag{4.11}$$

Substitute (4.10) into (4.11),

$$\psi_i^T (f_x - f_y g_y^{-1} g_x) H_0 - \psi_i^T H_0 \Lambda_0 - \psi_i^T \Phi_0 \Delta_0 = -\psi_i^T (\dot{f}_x - \dot{f}_y g_y^{-1} g_x + f_y g_y^{-1} \dot{g}_y g_y^{-1} g_x - f_y g_y^{-1} \dot{g}_x) \Phi_0. \tag{4.12}$$

Consider (3.5) and (3.15), then

$$\psi_i^T A_s H_0 - \psi_i^T H_0 \Lambda_0 - \psi_i^T \Phi_0 \Delta_0 = -\psi_i^T \dot{A}_s \Phi_0. \tag{4.13}$$

Suppose $H_0 = [\ h_1 \quad h_2 \quad \cdots \quad h_r\ ]$, introduce (4.2) and (4.8) into (4.13), then

$$\lambda_i \psi_i^T \begin{bmatrix} h_1 & h_2 & \cdots & h_r \end{bmatrix} - \psi_i^T \begin{bmatrix} h_1 & h_2 & \cdots & h_r \end{bmatrix} \begin{bmatrix} \lambda_1 & 0 & \cdots & 0 \\ 0 & \lambda_2 & \cdots & 0 \\ \vdots & \vdots & \ddots & \vdots \\ 0 & 0 & \cdots & \lambda_r \end{bmatrix}$$

$$-\psi_i^T \begin{bmatrix} \phi_1 & \phi_2 & \cdots & \phi_r \end{bmatrix} \begin{bmatrix} \delta_{11} & \delta_{12} & \cdots & \delta_{1r} \\ \delta_{21} & \delta_{22} & \cdots & \delta_{2r} \\ \vdots & \vdots & \ddots & \vdots \\ \delta_{r1} & \delta_{r2} & \cdots & \delta_{rr} \end{bmatrix} = -\psi_i^T \dot{A}_s \begin{bmatrix} \phi_1 & \phi_2 & \cdots & \phi_r \end{bmatrix}. \tag{4.14}$$

For the ith equation in (4.14), consider (3.16), there is

$$\lambda_i \psi_i^T h_i - \psi_i^T \begin{bmatrix} h_1 & h_2 & \cdots & h_r \end{bmatrix} \begin{bmatrix} 0 & \cdots & 0 & \lambda_i & 0 & \cdots & 0 \end{bmatrix}^T$$

$$-\psi_i^T \begin{bmatrix} \phi_1 & \phi_2 & \cdots & \phi_r \end{bmatrix} \begin{bmatrix} \delta_{1i} & \delta_{2i} & \cdots & \delta_{ri} \end{bmatrix}^T = -\psi_i^T \dot{A}_s \phi_i \tag{4.15}$$

$$\lambda_i \psi_i^T h_i - \psi_i^T h_i \lambda_i - \delta_{ii} = -\psi_i^T \dot{A}_s \phi_i. \tag{4.16}$$

Finally

$$\delta_{ii} = \psi_i^T \dot{A}_s \phi_i. \tag{4.17}$$

□

The real part of δ_{ii} is the sensitivity of the real part of λ_i with respect to p, and the imaginary part of δ_{ii} gives the sensitivity of the imaginary part of λ_i. These eigenvalue sensitivities are very useful for the selection of critical eigenvalue and step size control in the predictor iteration. They indicate the direction for driving the critical eigenvalue to the imaginary axis. Eigenvalue sensitivity information is also very useful in power system control, parameter estimation, and model reduction, etc. The efficient identification of oscillatory stability margin and damping margin can be achieved using the eigenvalue sensitivities during ICIS and will be described later.

Proposition 3. *Although $H_0 = \dot{\Phi}_0$, the columns of H_0 in (4.7) do not provide the eigenvector sensitivities information. In other words, assume $H_0 = [\ h_1 \quad h_2 \quad \cdots \quad h_r\ ]$, $\forall\ i \in [1, r]$, there is*

$$h_i \neq \frac{\partial \phi_i}{\partial p}. \tag{4.18}$$

Proof. Similarly, for the jth equation in (4.14), we have

$$\lambda_i \psi_i^T h_j - \psi_i^T h_j \lambda_j - \psi_i^T \phi_i \delta_{ij} = -\psi_i^T \dot{A}_s \phi_j \tag{4.19}$$

$$\delta_{ij} = \frac{(\lambda_i - \lambda_j)\psi_i^T h_j + \psi_i^T \dot{A}_s \phi_j}{\psi_i^T \phi_i}. \tag{4.20}$$

It can be seen that although Λ_0 is a diagonal matrix, its derivative Δ_0 is not diagonal anymore. Thus,

$$\delta_{1i}\phi_1 + \delta_{2i}\phi_2 + \cdots + \delta_{ri}\phi_r \neq \delta_{ii}\phi_i = \frac{\partial \lambda_i}{\partial p}\phi_i. \tag{4.21}$$

Since $\Omega_0 = -g_y^{-1} g_x \Phi_0$, then

$$\begin{aligned} L_0 &= \dot{\Omega}_0 \\ &= -\dot{g}_y^{-1} g_x \Phi_0 - g_y^{-1} \dot{g}_x \Phi_0 - g_y^{-1} g_x \dot{\Phi}_0 \\ &= g_y^{-1} \dot{g}_y g_y^{-1} g_x \Phi_0 - g_y^{-1} \dot{g}_x \Phi_0 - g_y^{-1} g_x H_0. \end{aligned} \tag{4.22}$$

Substitute (4.22) into the first equation in (4.6), at the same time consider (3.5) and (3.15), we can get

$$A_s H_0 - H_0 \Lambda_0 - \Phi_0 \Delta_0 = -\dot{A}_s \Phi_0 \tag{4.23}$$

Applying (4.21) to the ith equation in (4.23), we get

$$A_s h_i - \lambda_i h_i - \frac{\partial \lambda_i}{\partial p} \phi_i \neq -\dot{A}_s \phi_i \tag{4.24}$$

$$(A_s - \lambda_i I) h_i \neq -(\frac{\partial A_s}{\partial p} - \frac{\partial \lambda_i}{\partial p}) \phi_i. \tag{4.25}$$

This shows that $h_i \neq \partial \phi_i / \partial p$. Otherwise, they are supposed to equal to each other by eigenvector sensitivity definition when we take the derivative with respect to p on both sides of (3.7) [49, 79]. It means although $H_0 = \dot{\Phi}_0$, the columns of H_0 do not give the eigenvector sensitivities information because of non-diagonal form of matrix Δ_0. □

It should be mentioned that even when matrix Λ_0 is a diagonal matrix, its derivative matrix Δ_0 is not diagonal anymore. However, even if Δ_0 is not diagonal, its diagonal elements still provide the corresponding eigenvalue sensitivity information as long as Λ_0 is a diagonal matrix. The reason that matrix Δ_0 is not diagonal is because matrix H_0 which is the derivative of right eigenvector matrix Φ_0 does not provide the eigenvector sensitivity information as proved above. Hence, to make the linear matrix equation in (4.6) hold true, Δ_0 needs to be a non-diagonal matrix. Further analysis shows that Δ_0 will be a diagonal matrix if and only if H_0 is an eigenvector sensitivity matrix. The proof can be given similar to the above description considering the eigenvector sensitivity definition and is omitted.

Corrector steps are based on the standard Newton's method applied to (4.5) with $(\widehat{\Phi}, \Phi, \Omega, p)$ replaced by $(\Phi_0, \Phi_1, \Omega_1, p_1)$, i.e., the normalization condition is adapted. Starting at $(\Phi_1, \Omega_1, \Lambda_1)$, Newton's method generates a sequence of corrector iterations $(\Phi_k, \Omega_k, \Lambda_k), k \geq 1$, defined by

$$\begin{bmatrix} f_x(p_1)\Phi_{k+1} - \Phi_{k+1}\Lambda_k + f_y(p_1)\Omega_{k+1} - \Phi_k \Lambda_{k+1} \\ g_x(p_1)\Phi_{k+1} + g_y(p_1)\Omega_{k+1} \\ \Phi_0^T \Phi_{k+1} \end{bmatrix} = \begin{bmatrix} -\Phi_k \Lambda_k \\ 0 \\ I_r \end{bmatrix}. \tag{4.26}$$

The system is of the same type as (4.6) and again we use the same algorithm to solve it.

Assume the corrector iterations (4.26) converge to solution $(\Phi_{\nu+1}, \Omega_{\nu+1}, \Lambda_{\nu+1})$ after ν Newton's iterations (generally $\nu \leq 5$), the corrected eigenvalues can be obtained easily from the eigenvalue decomposition on matrix $\Lambda_{\nu+1}$ in the corrector solution. We can use the conventional methods, such as QR method, to compute the whole spectrum of $\Lambda_{\nu+1}$. Notice $\Lambda_{\nu+1}$ is not diagonal, the eigenvalue decomposition yields $\Lambda_{\nu+1}P = P\Lambda'$, where Λ' is a diagonal matrix whose diagonal elements are the tracing eigenvalues after one continuation step. Since r is very small compared with n, the decomposition cost is very cheap. At the next continuation step, $(\Phi_0, \Omega_0, \Lambda_0) = (\Phi_{\nu+1}P, \Omega_{\nu+1}P, \Lambda')$. This re-initialization guarantees the initial matrix Λ_0 at any continuation iteration is always a diagonal matrix in the predictor if necessary. Thus, Δ_0 always provides us eigenvalue sensitivity information. It should be mentioned that the re-initialization is not always needed during the ICIS process. In any case, the eigenvalues of Λ_0 contain eigenvalues of A_s which correspond to the invariant subspaces spanning $\Phi(p)$.

For each iteration, the computational cost to calculate r eigenvalues of an $(m+n)\times(m+n)$ matrix $A(p)$ is $\mathcal{O}(r(m+n)(m+n+r))$ [40]. It can be seen that the ICIS method has the computational advantage in eigenvalue calculation over the conventional methods, especially for large-scale power systems. Furthermore, as a by-product of the ICIS method, eigenvalue sensitivity is a very useful tool for step size control to further decrease the number of iterations to reach the stability margin boundary which will be described later.

4.2.2 The Bordered Bartels-Stewart Algorithm

The linear systems (4.6) and (4.26) are of the same form

$$\begin{bmatrix} AH - H\Lambda - \Psi\Delta \\ \hat{\Psi}^T H \end{bmatrix} = \begin{bmatrix} B \\ C \end{bmatrix} \tag{4.27}$$

where $H, B, \hat{\Psi} \in \mathbb{R}^{n\times r}$, $C, \Lambda, \Delta \in \mathbb{R}^{r\times r}$, and $\rho(\Lambda) \subset \rho(A)$. It is called the bordered matrix equation of Sylvester type for the unknowns (H, Δ). The bordered Bartels-Stewart algorithm [36, 37, 38] is very effective for solving this matrix equation and is described as follows. The algorithm reduces the linear algebra to solve a sequence of bordered linear systems. First

compute the complex Schur decomposition of the matrix Λ

$$Q^H \Lambda Q = \tilde{\Lambda}, Q^H Q = I_r, \tilde{\Lambda} \text{ upper triangular.} \tag{4.28}$$

Note that this only involves solving an eigenvalue problem of very small dimension for $r \ll n$, it can be done very cheaply. Also even Λ in the predictor (4.6) is diagonal, it is not diagonal in the corrector (4.26). By right-multiplying Q to both sides of (4.27), we transform it into

$$\begin{bmatrix} A\tilde{H} - \tilde{H}\tilde{\Lambda} - \Psi\tilde{\Delta} \\ \hat{\Psi}^T \tilde{H} \end{bmatrix} = \begin{bmatrix} \tilde{B} \\ \tilde{C} \end{bmatrix} \tag{4.29}$$

where

$$\tilde{H} = HQ, \tilde{\Delta} = \Delta Q, \tilde{B} = BQ, \tilde{C} = CQ. \tag{4.30}$$

Since $\tilde{\Lambda}$ is upper triangular, we can compute the columns $\tilde{H}_j, \tilde{\Delta}_j$ of $\tilde{H}, \tilde{\Delta}$ similar to the Bartels-Stewart algorithm from a sequence of bordered linear systems [40]

$$\begin{bmatrix} A - \tilde{\Lambda}_{jj} I_n & -\Psi \\ \hat{\Psi}^T & 0 \end{bmatrix} \begin{bmatrix} \tilde{H}_j \\ \tilde{\Delta}_j \end{bmatrix} = \begin{bmatrix} \tilde{B}_j + \sum_{k=1}^{j-1} \tilde{\Lambda}_{kj} \tilde{H}_k \\ \tilde{C}_j \end{bmatrix} \qquad j = 1, 2, \ldots, r. \tag{4.31}$$

After solving the linear systems in (4.31) sequentially for $j = 1, 2, \ldots, r$, we can get $\tilde{H}_j$ and $\tilde{\Delta}_j$. Finally the solution (H, Δ) can be obtained from $(\tilde{H}, \tilde{\Delta})$ in (4.30).

4.3 Initialization and Update of Invariant Subspaces

To have the ICIS method started, we need to calculate a defined subset of eigenvalues and their invariant subspace for a given initial parameter value. The main interest is the subspaces that belong to spectral sets close to zero or to the imaginary axis, since the invariant subspace corresponding to a few eigenvalues near the imaginary axis provides information about stability and bifurcations. For the oscillatory stability, we are interested in the rightmost eigenvalues which satisfy a certain real part criterion, since these eigenvalues are most likely to cross the imaginary axis when the parameter changes.

If we want to trace the rightmost eigenvalues, we need to guarantee that the invariant subspace span contains all eigenvalues satisfying

$$\mathrm{Re}(\lambda_i) > -\gamma \tag{4.32}$$

for a given $\gamma > 0$. The idea is to detect the eigenvalues passing the imaginary axis in advance for the purpose of stability analysis. This is because these eigenvalues are the candidates for transition through the imaginary axis. More generally, we would like to choose $\Lambda(p)$ in (4.2) so that the gap between the real parts of the leftmost eigenvalue in $\Lambda(p)$ and the rightmost eigenvalue in the rest of the eigenvalue spectrum is greater than a certain threshold.

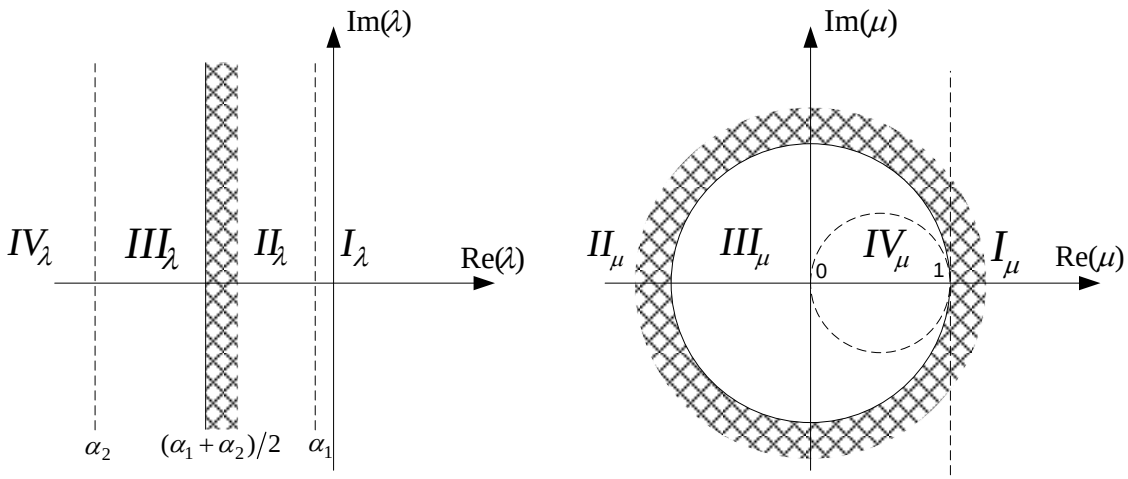

Figure 4.1 Generalized Cayley Transform for Calculation of Rightmost Eigenvalues.

To find the eigenspace corresponding to the rightmost eigenvalues, we need to find a transformation of A_s which maps eigenvalues with largest moduli to the rightmost eigenvalues. This is because the conventional dominant eigenvalue computation methods can only converge to the eigenvalues with largest moduli. The so-called *generalized Cayley transform* possesses such a property [80, 81], as shown in Fig. 4.1. Let $\alpha_1 > \alpha_2$ be chosen so that $(A_s - \alpha_1 I)$ is regular. In other words, α_1 is not an eigenvalue of matrix A_s. The generalized Cayley transform $C(A_s)$

is defined as

$$C(A_s) = (A_s - \alpha_1 I)^{-1}(A_s - \alpha_2 I) = I + (\alpha_1 - \alpha_2)(A_s - \alpha_1 I)^{-1}. \tag{4.33}$$

The following propositions are derived from [80] and have been reformulated here for better illustration.

Proposition 4. *This rational transform maps eigenvalues $\lambda \in \rho(A_s)$ to $\theta \in \rho(C(A_s))$ as follows:*

$$\mu = C(\lambda) = \frac{\lambda - \alpha_2}{\lambda - \alpha_1}. \tag{4.34}$$

Proof. For any $\lambda \in \rho(A_s)$ with eigenvector ϕ, we have $A_s\phi = \lambda\phi$. So

$$(A_s - \alpha_1 I)\phi = (\lambda - \alpha_1)\phi \tag{4.35}$$

$$(A_s - \alpha_2 I)\phi = (\lambda - \alpha_2)\phi. \tag{4.36}$$

Multiply both sides of (4.35) and (4.36) by $(\lambda - \alpha_2)$ and $(\lambda - \alpha_1)$ respectively, then we can get

$$(\lambda - \alpha_2)(A_s - \alpha_1 I)\phi = (\lambda - \alpha_1)(\lambda - \alpha_2)\phi \tag{4.37}$$

$$(\lambda - \alpha_1)(A_s - \alpha_2 I)\phi = (\lambda - \alpha_1)(\lambda - \alpha_2)\phi. \tag{4.38}$$

Therefore, there is

$$(\lambda - \alpha_2)(A_s - \alpha_1 I)\phi = (\lambda - \alpha_1)(A_s - \alpha_2 I)\phi. \tag{4.39}$$

From (4.39), consider $(A_s - \alpha_1 I)$ is regular, we have

$$(A_s - \alpha_1 I)^{-1}(A_s - \alpha_2 I)\phi = \frac{\lambda - \alpha_2}{\lambda - \alpha_1}\phi. \tag{4.40}$$

This means $\mu = (\lambda - \alpha_2)/(\lambda - \alpha_1)$ is the mapping eigenvalue of $C(A_s)$ with eigenvector ϕ. □

Proposition 5. *Let $\theta = c(\mu)$ where $\mu \in \mathbb{C}$. Then*

$$\begin{aligned}
Re(\mu) \in [\alpha_1, \infty) &\iff \theta \in \{z \in \mathbb{C} : Re(z) > 1\} \\
Re(\mu) \in \left[\frac{\alpha_1 + \alpha 2}{2}, \alpha_1\right) &\iff \theta \in \{\{z \in \mathbb{C} : Re(z) \le 1\} - B(0,1)\} \\
Re(\mu) \in \left[\alpha_2, \frac{\alpha_1 + \alpha 2}{2}\right) &\iff \theta \in \left\{B(0,1) - B(\frac{1}{2}, \frac{1}{2})\right\} \\
Re(\mu) \in (-\infty, \alpha_2) &\iff \theta \in B(\frac{1}{2}, \frac{1}{2})
\end{aligned} \tag{4.41}$$

Proof. The results follow after straightforward calculation as illustrated in Fig. 4.1. □

It can be seen that the half plane $\mathrm{Re}(\lambda) > (\alpha_1 + \alpha_2)/2$ in the original spectral domain is mapped outside the unit circle in the transformed spectral domain, and the farthest eigenvalue of the matrix $C(A_s)$ corresponds to the rightmost eigenvalue of A_s. It follows that well-chosen parameters α_1 and α_2 enable us to detect the presence of eigenvalues satisfying the condition (4.32). The advantages and shortcomings of the generalized Cayley transform have been discussed in detail in [14]. The main advantage of the Cayley transform is that it only needs to be applied one time to calculate all of the critical eigenvalues. The calculation is performed in real arithmetic for real shift points α_1 and α_2 when A_s is real matrix. In addition, for the initialization of rightmost eigenvalues using the Cayley transform, a suitable choice of α_1 and α_2 should help in two ways. First, it should be able to help separate close rightmost eigenvalues in the new spectral domain after the Cayley transform. Second, an appropriate choice can maximize the convergence rate of the dominant eigenvalue computation. Reference [80] explores more details on how to properly choose these parameters.

To trace the eigenvalues with the least damping ratio, we need to find the invariant subspace contains the eigenvalues satisfying

$$\zeta(\lambda_i) > \zeta_c \tag{4.42}$$

where ζ_c is a certain damping ratio threshold.

Reference [38] proposes a method which includes coordinate transform by rotating the axes and the Cayley transform. The disadvantages of this method have two aspects. First, the calculation needs to be performed in complex arithmetic for the Cayley transform after rotating the real and imaginary axes, which increases the complexity of calculation. Second, we cannot guarantee that all the eigenvalues satisfying the damping ratio requirement will be included. The parameters α_1 and α_2 need to be carefully chosen so that the eigenvalues close to the imaginary axis will not be neglected.

To overcome these shortcomings, the so-called *"semi-complex" Cayley transform* is proposed to calculate those eigenvalues, as shown in Fig. 4.2. The advantage of this transforma-

tion is that it can easily discriminate between complex conjugate pairs. Moreover, since α_1 remains real, the matrix transformation (4.33) is still performed in real arithmetic.

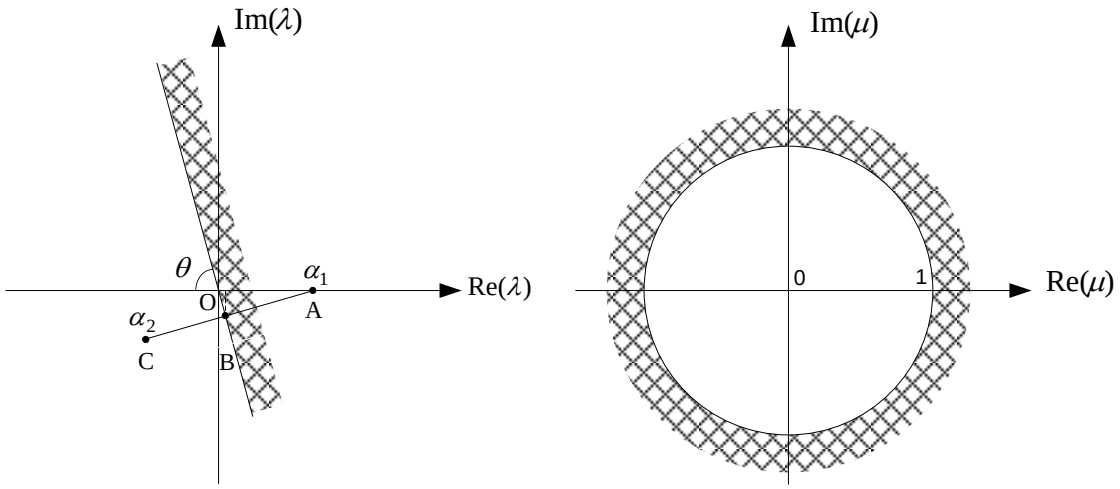

Figure 4.2 "Semi-complex" Cayley Transform for Calculation of Least Damping Ratio Eigenvalues.

For certain damping ratio requirement, the damping angle is $\theta = \cos^{-1}\zeta = \tan^{-1}(\frac{\sqrt{1-\zeta^2}}{\zeta})$. The parameters α_1 and α_2 can be chosen as follows.

Proposition 6. *For a proper chosen parameter $\alpha_1 > 0$, parameter α_2 can be determined by the following formula:*

$$\alpha_2 = \alpha_1(cos2\theta - jsin2\theta). \tag{4.43}$$

Proof. The coordination of point A is $A = \alpha_1$, since the line OB is perpendicular to the line AB, the coordination of point B is

$$B = \alpha_1 \cos^2\theta - j\alpha_1 \sin\theta\cos\theta. \tag{4.44}$$

Since point B is the midpoint of line segment AC in Fig. 4.2. According to the midpoint formula, there is

$$\begin{aligned} C &= 2B - A \\ &= 2\alpha_1\cos^2\theta - j2\alpha_1\sin\theta\cos\theta - \alpha_1 \\ &= \alpha_1(\cos2\theta - j\sin2\theta). \end{aligned} \tag{4.45}$$

So we can get

$$\alpha_2 = \alpha_1(\cos 2\theta - j\sin 2\theta). \tag{4.46}$$

□

Once the transformation is performed, the dominant eigenvalue computation methods can be used to calculate the largest moduli eigenvalues and the corresponding eigenvectors, such as the Arnoldi method [38], power method, subspace iteration, etc. Subspace iteration (sometimes called simultaneous iteration or orthogonal iteration) is a well-known algorithm that computes eigenspace corresponding to eigenvalues with the largest moduli [36], which is a generalization of the power method for finding the dominant eigenspace of a matrix. It is especially suitable for solving eigenvalue problem involving large, sparse nonsymmetric matrices [82], such as power system eigenvalue computation. Reference [82] provides a Fortran program to calculate the dominant invariant subspace to the eigenvalues of the largest moduli for a nonsymmetric matrix by the method of subspace iteration. Let r be the number of eigenvalues we want to calculate ($r \ll n$). Assume $S = C(A_s)$ is a matrix of order n with eigenvalues $(\mu_1, \mu_2, \ldots, \mu_n)$ ordered so that

$$|\mu_1| \geq \cdots \geq |\mu_r| > |\mu_{r+1}| \geq \cdots \geq |\mu_n|$$

i.e., there is a spectral gap between the two clusters. Consider the following subspace iterative process:

do $V^{(k+1)} = C(A_s)V^{(k)}$;

orthonormalize $V^{(k+1)}$;

$k = k + 1$;

until *convergence.*

The iterative process produces a sequence of matrices $V^{(k)} \in \mathbb{R}^{n\times r}$ which converge to the eigenspace corresponding to $(\mu_1, \mu_2, \ldots, \mu_r)$ provided that the initial matrix $V^{(0)}$ contains components in this eigenspace. It is automatically satisfied in computer arithmetic due to round-off errors. Therefore, we can initialize $V^{(0)}$ randomly. The orthonormalization is implemented via the *modified Gram-Schmidt* process [40]. In addition, the method can be accelerated by the application of acceleration techniques. For example, the Fortran program SRRIT [82] makes

use of a "Schur-Rayleigh-Ritz step" to accelerate the iteration process. Some other subspace iteration methods, such as the Jacobi-Davidson method [31], is applied to compute the rightmost eigenvalues without the need of Cayley transform.

To trace the movement of a number of specified oscillatory modes with parameter change, the initialization is different since these eigenvalues are only associated with certain modes of the system that we are interested in. In this case, first the conventional eigenvalue computation methods (such as the QR method) will be used to calculate the eigenvalues at a starting point. Then modal analysis will be performed to associate the eigenvalues with different modes (elements of the system). The eigenvalues and eigenvector space corresponding to the specified modes will then be extracted. Once the invariant subspace is obtained at the starting point, the interaction between these oscillatory modes can be identified subsequently when the ICIS method is used to trace them.

Since we cannot guarantee that all the eigenvalues satisfying the criterion will be captured during the tracing process, the update of invariant subspace is needed when a new single eigenvalue or a complex conjugate pair satisfying (4.32) or (4.42) occurs. Therefore, at regular intervals of change in parameter value, a routine check will be performed to compute all eigenvalues satisfying the criterion. Since some of them have been included in the invariant subspace spanned by $\Phi(p)$ obtained from ICIS, reference [37] proposes to perform a projection in each step of subspace iterations to compute only those eigenvalues satisfying (4.32) or (4.42) which are not included in the tracing set. Similarly, reference [38] proposes the projected Arnoldi method to avoid the recalculation of these eigenvalues.

4.4 Computational Cost Comparison

About the computational cost, the ICIS method has the advantage over the traditional eigenvalue calculation methods since it only calculates a set of critical eigenvalues instead of the whole eigenvalue spectrum. For the Sylvester equation $AX + XB = C$, where A, B, and C are real matrices of dimensions $m \times m, n \times n$, and $m \times n$, respectively, to solve it by the Bartels-Stewart algorithm, the number of multiplications required for the solution is estimated

by [83]

$$(2+4\xi)(m^3+n^3)+5(mn^2+m^2n)/2$$

where ξ is the average number of QR steps required to make a subdiagonal element negligible. The first term is due to the reduction of A and B to real Schur form.

In general, the computational cost to calculate r eigenvalues of an $n \times n$ matrix A is $\mathcal{O}(nr(n+r))$ [40]. As a comparison, it costs $\mathcal{O}(25n^3)$ to calculate r eigenvalues using the QR method. So it can be seen that the ICIS method has big computational advantage over the traditional methods, especially for large-scale eigenvalue computation problem.

The detailed performance comparison between the ICIS method and the conventional methods will be described later in Chapter 6.

4.5 Conclusion

It is of great value to efficiently compute not only the mode related to the least damping eigenvalue, but also the mode related to the eigenvalue that moves the fastest or most likely to cross the imaginary axis. The ICIS method can provide us an efficient way to implement it. The ICIS algorithm consists of a predictor based on the first derivative information, and a corrector based on an iterative refinement technique for improving the accuracy of a computed invariant subspace. The bordered Bartels-Stewart algorithm is applied to solve the matrix equations in the predictor and the corrector. Generalized Cayley transform and subspace iteration are employed to update the invariant subspace and guarantee that it contains all the critical modes for rightmost eigenvalues trace. The "semi-complex" Cayley transform is proposed to calculate the least damping ratio eigenvalues.

The ICIS method can trace the movement of a number of particular critical eigenvalues with parameter change. On the other hand, the QR method can only calculate a bunch of discrete eigenvalues for each parameter value. The eigenvalue sequences are not ordered in the same way for different parameter values. Hence, it is difficult to link them together as parameter varies. The QR method frequently changes the positions of eigenvalues, causing

difficulties in tracing the *same* eigenvalue. The ICIS method does not have the difficulty to trace any set of critical eigenvalues of interest.

The eigenvalue sensitivities can also be extracted during the ICIS process [67, 71, 72]. At each iteration, we not only know the location of each traced eigenvalue, but also the direction and speed of the eigenvalue movement. This information is very useful in ranking eigenvalues, controller design, and many other purposes.

CHAPTER 5. SYSTEMATIC IDENTIFICATION OF INTERACTING POWER SYSTEM DYNAMIC PHENOMENA WITH THE PROPOSED METHOD

5.1 Introduction

This chapter applies the improved continuation of invariant subspaces to trace the critical eigenvalues of power system and extract the eigenvalue sensitivity information. Furthermore, the stability margin boundary is predicted at each iteration by Newton's method, it gives us an index to measure the distance of the current operating point to the stability boundary. As a result, only the critical eigenvalues that might affect the system stability change will be traced. We can get the movement of those critical eigenvalues together with the eigenvalue sensitivities effectively and accurately. The ICIS method will be used to deal with close eigenvalues and eigenvalue collision. It will also be applied to identify various interacting dynamic phenomena, such as low-frequency oscillation, subsynchronous resonance, etc. A heuristic procedure based on the ICIS method is proposed to identify the potential modal resonance phenomenon. The detailed simulation results based on the proposed ICIS algorithm in Chapter 4 are given as follows.

5.2 Numerical Examples

5.2.1 New England System Description

The improved continuation of invariant subspaces is tested on the New England 39-bus system. The schematic diagram of the system is shown in Appendix A. The system has 10 generators, 19 loads, and 46 transmission lines. Each generator consists of a two-axis generator

model, an IEEE DC-1 excitation system, and a governor model. There are nine state variables for each generator and two algebraic variables for each bus. With system angle reference excluded, the total state and algebraic variables are 89 and 78, respectively. The total number of eigenvalues at any given equilibrium operating point is 89. Load consists of 50% constant power, 30% constant current, and 20% constant impedance. Load on all buses will increase with the same percentage unless specified. The system load is chosen at the control parameter p. All of the numerical results are performed in MATLAB environment.

Fig. 5.1 shows the distribution of eigenvalues of the New England system at 4300 MW load level by MATLAB eigenvalue computation function "eig". It can be seen that the system is very stiff because it has both small eigenvalues (e.g., -100) and large eigenvalues (e.g., -0.02). The system stiffness ratio is $S = \max|\mathrm{Re}(\lambda_i)|/\min|\mathrm{Re}(\lambda_i)| \approx 5000$ which is very large. For power system eigenvalues computation, the rightmost eigenvalues and eigenvalues with the least damping ratio are most of interest, which are only a small part of the whole eigenvalue spectrum.

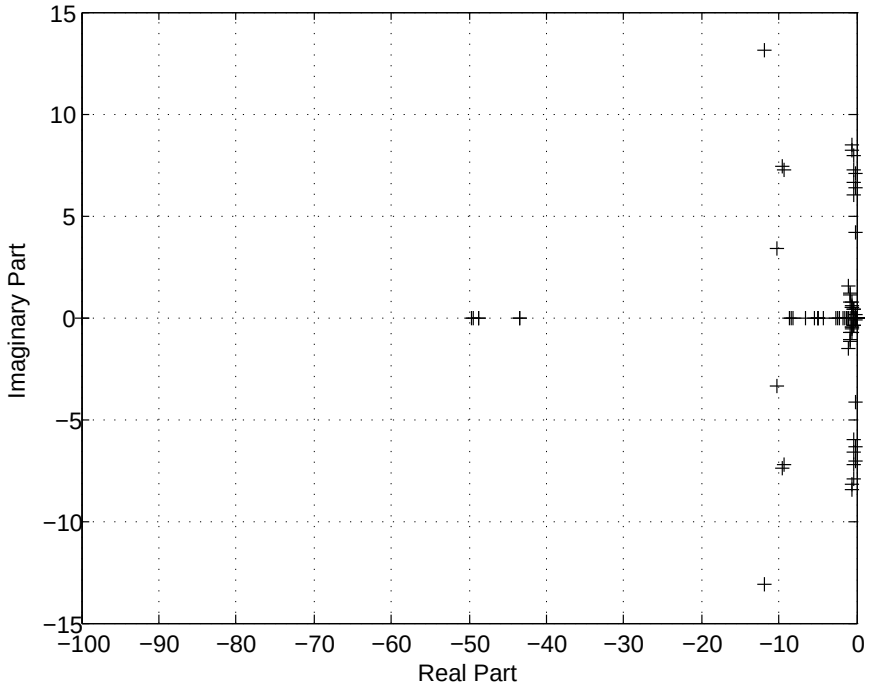

Figure 5.1 Distribution of Eigenvalues at 4300 MW Load.

5.2.2 Rightmost Eigenvalues Trace

For the rightmost eigenvalues trace, getting the subspace continuation started is a crucial problem. If no complete spectrum is available, we use a combination of the generalized Cayley transform and orthogonal subspace iteration, as introduced in Section 4.3. In this way, we can obtain an invariant subspace of the eigenvalues satisfying a certain real part criterion. During the continuation process, we keep the dimension of the invariant subspace minimal but above some critical number. However, as pointed in [36], no device is currently implemented to guarantee that the continued spectral set contains the rightmost eigenvalues. For this reason, at regular intervals of 500 MW incremental changes in system load, a routine check will be performed to ensure that all of the rightmost eigenvalues in the critical margin are included in the invariant subspaces.

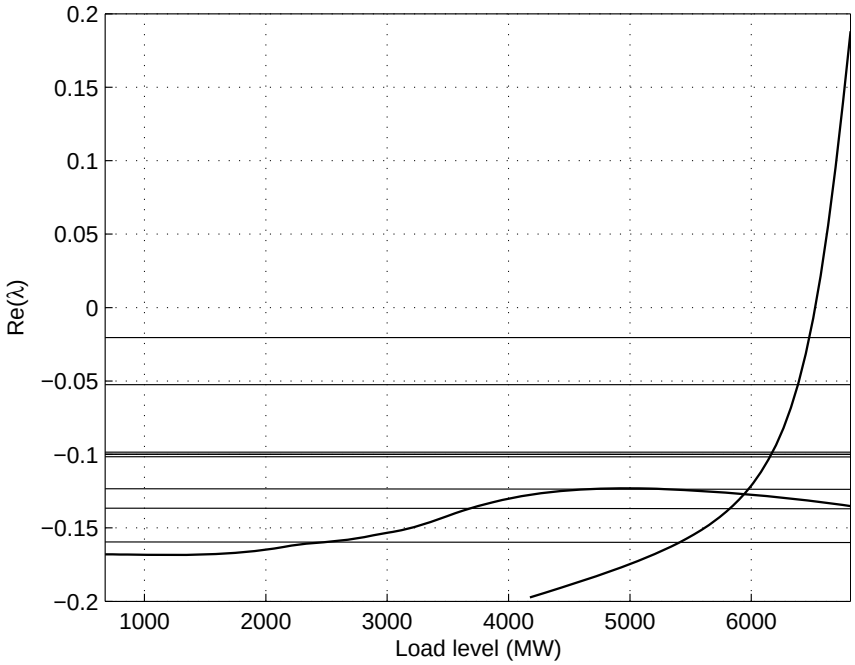

Figure 5.2 Rightmost Eigenvalues Movement.

Fig. 5.2 shows the results by ICIS for all of the eigenvalues satisfying real part criterion ($\mathrm{Re}(\lambda) > -0.2$) when load changes from 614 MW to 6817 MW. Although such an initial load is unrealistic for the New England system, it is a good practice to test the algorithm robustness

for study purpose. Thick lines correspond to the complex conjugate pairs of eigenvalues, regular lines represent real eigenvalues. Since eigenvalues are symmetrical to the real axis, only the eigenvalues with positive imaginary parts are considered to save the computation time. The constant step size s used in the continuation method is 61.4 MW, which equals to 10% of the initial load. Initially, nine eigenvalues are located in the critical region. One more complex eigenvalue enters into the critical region as load increases to 4176 MW. The tracing process will end when one of the eigenvalues crosses the imaginary axis. One can see that among the rightmost eigenvalues, only complex eigenvalues move dramatically as system load changes. The movement of real eigenvalues is not obvious compared with complex eigenvalues. In other words, complex eigenvalues have much bigger eigenvalue sensitivities than real eigenvalues in this case. If these real eigenvalues (or any other complex eigenvalue) insensitive to load change are filtered out during the tracing process based on their sensitivity information, the process can be further speeded up. In the next chapter, an eigenvalue sensitivity-based method will be proposed to reduce the number of traced eigenvalues in order to efficiently identify stability margin boundary.

5.2.3 Least Damping Ratio Eigenvalues Trace

The eigenvalues with least damping ratios less than 10% are traced by ICIS in this case. For the damping threshold $\zeta_c = 0.1$ in (4.42), damping angle is $\theta = \cos^{-1}0.1 = 84.26^{\circ}$. For parameter $\alpha_1 = 1$, it can be calculated from (4.43) that parameter $\alpha_2 = -0.98 - j0.199$. Using the "semi-complex" Cayley transform with the above parameters, the eigenvalues with the least damping ratio will become the eigenvalues with largest moduli. In addition, only the eigenvalues with positive imaginary parts are considered since complex eigenvalues are symmetric with respect to the real axis. Then the subspace iteration method is used to calculate the dominant eigenvalues that correspond to the largest moduli eigenvalues and the corresponding eigenvectors. It is used for the initialization and update of the invariant subspaces.

Table 5.1 gives the traced eigenvalues with the least damping ratio and the load condition

Table 5.1 Traced Eigenvalues with Least Damping Ratio

No.	Load (MW)	λ_i	f_i (Hz)	$\zeta_i(\%)$
1	614	$-0.1679 + j7.1878$	1.1440	2.34
2	614	$-0.2342 + j5.7371$	0.9131	4.08
3	614	$-0.2547 + j6.1023$	0.9712	4.17
4	614	$-0.2726 + j6.2658$	0.9972	4.35
5	614	$-0.3609 + j6.6533$	1.0589	5.42
6	614	$-0.2744 + j4.0656$	0.6471	6.73
7	2640	$-0.6702 + j7.5370$	1.1996	8.86
8	2640	$-0.5620 + j5.9359$	0.9447	9.43
9	3070	$-0.7734 + j8.1405$	1.2956	9.46

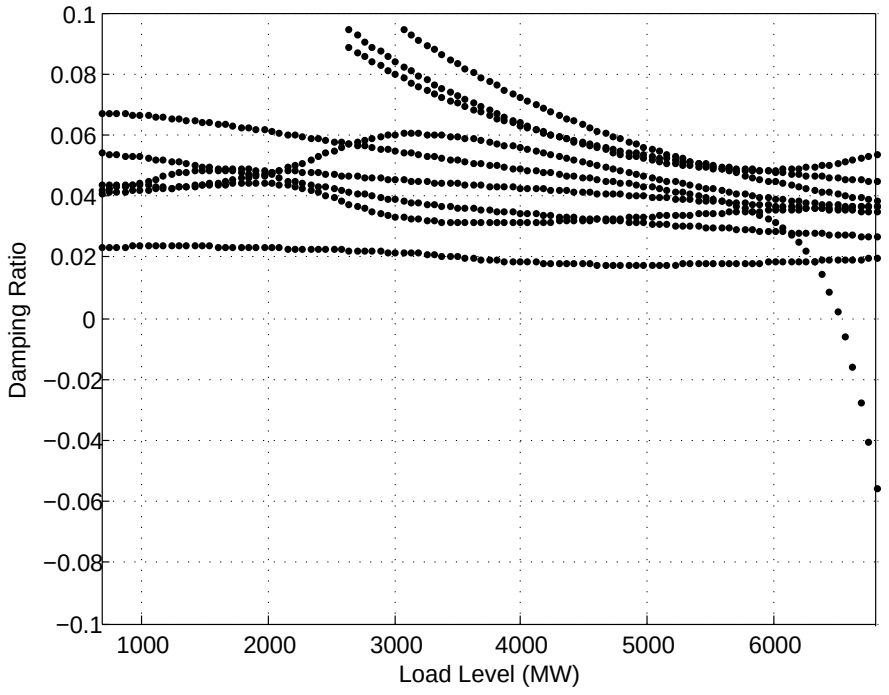

Figure 5.3 Least Damping Ratio Eigenvalues Movement.

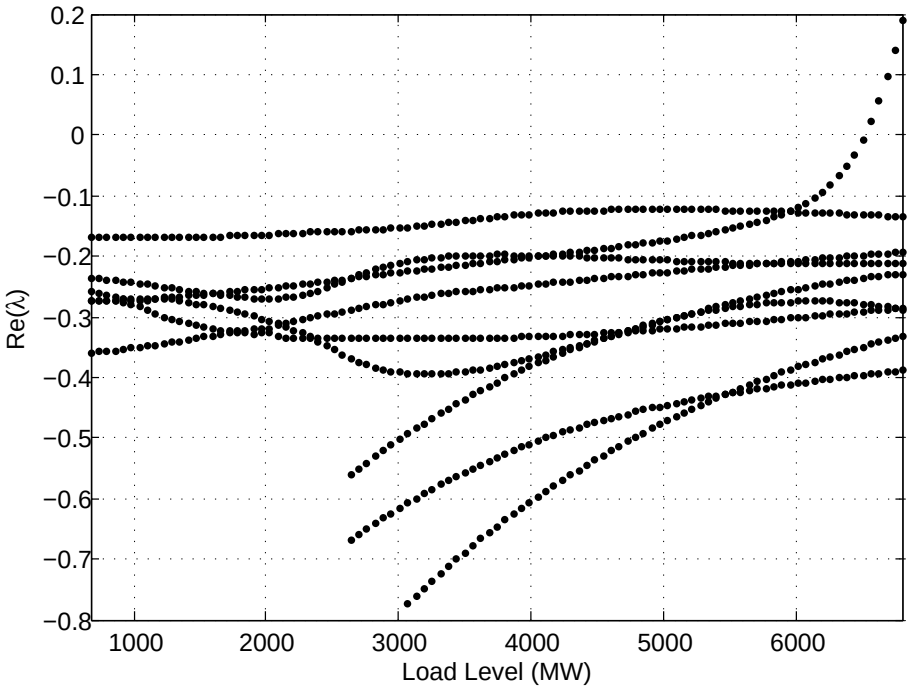

Figure 5.4 Real Parts of Least Damping Ratio Eigenvalues.

at which those eigenvalues are captured during the iterative procedure. Damping ratios of all of the critical eigenvalues with respect to load variation are plotted in Fig. 5.3. Initially, six eigenvalues are located in the critical region when the load level is 614 MW. The number of critical eigenvalues increases to eight and nine during the tracing process when load increases to 2640 MW and 3070 MW, respectively. The real parts of these least damping ratio eigenvalues are plotted in Fig. 5.4.

5.2.4 Eigenvalue Sensitivity

To verify the accuracy of the proposed method, the eigenvalue sensitivities extracted during the ICIS process have been compared with the eigenvalue sensitivities calculated by the conventional methods. Table 5.2 gives the rightmost eigenvalues ($\sigma > -0.5$) and their sensitivities information when the system load is 4300 MW. The detailed comparison results confirm that the eigenvalue sensitivities calculated from ICIS are the same as that by the conventional method. The schematic figure of the complex eigenvalue locations and their sensitivities are

Table 5.2 Rightmost Eigenvalues and Their Sensitivities at 4300 MW Load

No.	λ_i	ICIS		Conventional Method	
		$\partial\sigma_i/\partial p$	$\partial\omega_i/\partial p$	$\partial\sigma_i/\partial p$	$\partial\omega_i/\partial p$
1	$-0.0525 + j0.0982$	−5.9377E-6	−3.1926E-4	−5.9377E-6	−3.1926E-4
2	$-0.1261 + j7.0702$	9.4457E-4	−3.0119E-3	9.4457E-4	−3.0119E-3
3	$-0.1942 + j4.1239$	2.5508E-3	2.8751E-3	2.5508E-3	2.8751E-3
4	$-0.2007 + j6.3352$	−8.4974E-4	−8.9467E-3	−8.4974E-4	−8.9467E-3
5	$-0.2415 + j7.2522$	2.1491E-3	1.0440E-2	2.1491E-3	1.0440E-2
6	$-0.3305 + j7.9058$	9.4690E-4	2.8318E-2	9.4690E-4	2.8318E-2
7	$-0.3508 + j6.6306$	5.6534E-3	6.5148E-3	5.6534E-3	6.5148E-3
8	$-0.3551 + j5.9727$	8.3411E-3	−6.2773E-3	8.3411E-3	−6.2773E-3
9	$-0.3696 + j0.4187$	1.2604E-3	1.0462E-3	1.2604E-3	1.0462E-3
10	$-0.4469 + j0.4249$	1.7653E-3	1.0829E-3	1.7653E-3	1.0829E-3
11	$-0.4735 + j0.4400$	1.9227E-3	1.3988E-3	1.9227E-3	1.3988E-3
12	$-0.4759 + j0.5232$	1.8981E-3	1.8885E-3	1.8981E-3	1.8885E-3
13	$-0.4870 + j8.1914$	7.4598E-3	3.2961E-2	7.4598E-3	3.2961E-2
14	$-0.4935 + j0.7235$	−2.1590E-5	4.1323E-3	−2.1590E-5	4.1323E-3
15	−0.0205	−2.7233E-6		−2.7233E-6	
16	−0.0985	−4.4064E-7		−4.4064E-7	
17	−0.09989	−1.5724E-6		−1.5724E-6	
18	−0.09994	−3.8624E-7		−3.8624E-7	
19	−0.1016	−2.7436E-6		−2.7436E-6	
20	−0.1236	−3.1409E-6		−3.1409E-6	
21	−0.1368	−2.9819E-7		−2.9819E-7	
22	−0.1598	−7.1009E-6		−7.1009E-6	
23	−0.3337	6.4056E-6		6.4056E-6	
24	−0.3338	1.1082E-5		1.1082E-5	
25	−0.3508	8.4736E-5		8.4736E-5	

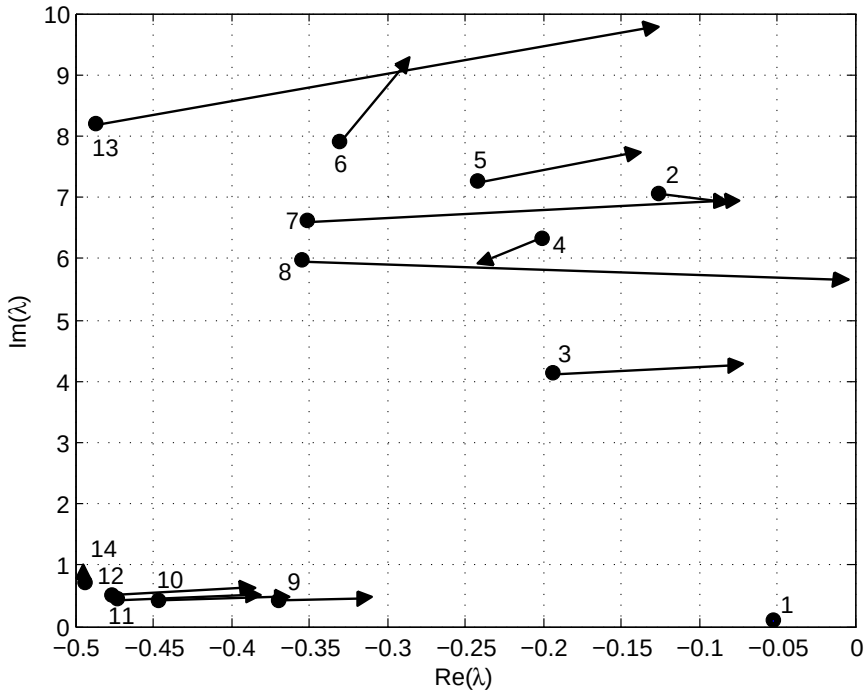

Figure 5.5 Rightmost Eigenvalues and Eigenvalue Sensitivities.

plotted in Fig. 5.5. The arrow shows the moving direction of each eigenvalue when the system load level increases. The length of the arrow shows the relative speed of eigenvalue movement with respect to the change in load.

During the continuation process, at each predictor step, after solving the matrix equation set in the predictor, the eigenvalue sensitivities can be obtained as a by-product. As long as proper re-initialization is performed after the convergence of corrector iterations, matrix Λ_0 in (4.6) is always diagonal in the next continuation iteration, the eigenvalue sensitivities will be extracted successively during the ICIS process.

Eigenvalue derivatives are extremely useful for determining the sensitivity of dynamic responses to system parameter variations as well as power system controller design. The eigenvalue sensitivities can be used as an indicator in eigenvalue ranking and selection for small-signal stability analysis. Since eigenvalue sensitivity quantifies the expected change in the eigenvalue in response to a change in the parameter. A positive sensitivity indicates that an

increase in the parameter value will increase the eigenvalue. An eigenvalue sensitivity-based method will be proposed in the next chapter to efficiently identify the oscillatory stability margin and damping margin boundaries.

Furthermore, the eigenvalue sensitivity provides useful information for power system planning and control. By examining the sensitivity of critical eigenvalues with respect to the specific control or operating parameters when the parameters experience changes, one can determine possible measures to improve the small-signal stability of the system.

Compared with the conventional methods, the advantages of eigenvalue sensitivity calculation using ICIS are as follows.

- The computations of the inverse of G_y and the reduced Jacobian matrix A_s are avoided since the calculation is in a structure-preserving formulation;

- Left eigenvector calculation is avoided. The conventional method differentiates (3.7) at first, then to solve the new equation set (3.10), introduces the left eigenvector ψ_i to calculate the eigenvalue sensitivity $\dot{\lambda}_i$. If there is a way to solve the equation set (3.10) directly, there is no need to use the left eigenvector in calculating eigenvalue sensitivity. In the proposed ICIS algorithm, instead of using the left eigenvector information, a normalization condition for the invariant subspace is introduced. We then get a bordered equation set of Sylvester type, and the bordered Bartels-Stewart algorithm is used to solve it efficiently. With proper initialization in the predictor step, the eigenvalue sensitivities can be achieved as a by-product during the process without the need of left eigenvector.

5.2.5 Oscillatory Stability Margin Boundary Estimation

To identify the oscillatory stability margin, reference [39] proposes an eigenvalue index to identify the critical eigenvalue to be traced by an integration-based method. In [62], a voltage stability index using tangent vector is developed to identify "weak" buses in power system that are most prone to voltage collapse. In [26], various indices based on eigenvalue and singular values are proposed to detect and predict oscillatory instabilities associated with Hopf bifurcations in power systems for online applications. For the ICIS method, the eigenvalue

sensitivities are by-products. At each iteration, we not only know the location of each traced eigenvalue, but also the direction and speed of the eigenvalue movement. Therefore, we can make use of this information to identify critical eigenvalues and estimate the stability margin.

For the ith eigenvalue λ_i ($\lambda_i = \sigma_i + j\omega_i$) traced by ICIS, the following eigenvalue index (EI) is defined as in [39]:

$$EI_i = -\frac{\sigma_i}{\dot{\sigma}_i} \tag{5.1}$$

where $\dot{\sigma}_i = \partial\sigma_i/\partial p = \delta_{ii}$, which is the ith row, ith column element of the matrix Δ_0 in (4.8). Δ_0 provides the traced eigenvalues sensitivity information when the parameter (such as the load level) changes. So the eigenvalue index is very easy to calculate.

Once we know the eigenvalues and their derivatives at a certain load level p_k, based on Newton's method, the margin boundary with respect to λ_i is

$$MB_k^i = p_k - \frac{\sigma_i}{\dot{\sigma}_i} = p_k + EI_i \tag{5.2}$$

where MB_k^i is the estimated margin boundary based on the ith eigenvalue at the kth iteration.

So the stability margin boundary at the kth iteration can be predicted as

$$MB_k = \min\{MB_k^1, MB_k^2, \ldots, MB_k^r\}. \tag{5.3}$$

After each iteration, the corresponding margin boundary can be obtained easily. It can tell us approximately how far the system's operating point is away from the instability boundary. Moreover, the step size s can be adjusted automatically from the margin boundary information.

In this example, the rightmost eigenvalues together with their sensitivities information are used to define the critical eigenvalue set. The critical eigenvalues mean the eigenvalues that are most likely to cross the imaginary axis and affect the stability of the system. To define the critical eigenvalues, first the eigenvalues satisfying a certain real part criterion are calculated by the Cayley transform, then ICIS is used to trace these eigenvalues. The sensitivities information and the estimated stability margin boundary for each eigenvalue can be obtained, too. During the continuation process, the eigenvalues that are moving away from the imaginary axis or have smaller sensitivities corresponding to bigger estimation margins will be filtered out to save computational cost. As a result, only a small number of the dominant eigenvalues need to

be traced to estimate the stability margin boundary. This is useful because these eigenvalues are most critical to the system stability change even though they may not necessarily be the least stable modes for a particular operating condition.

5.2.6 Close Eigenvalues Trace

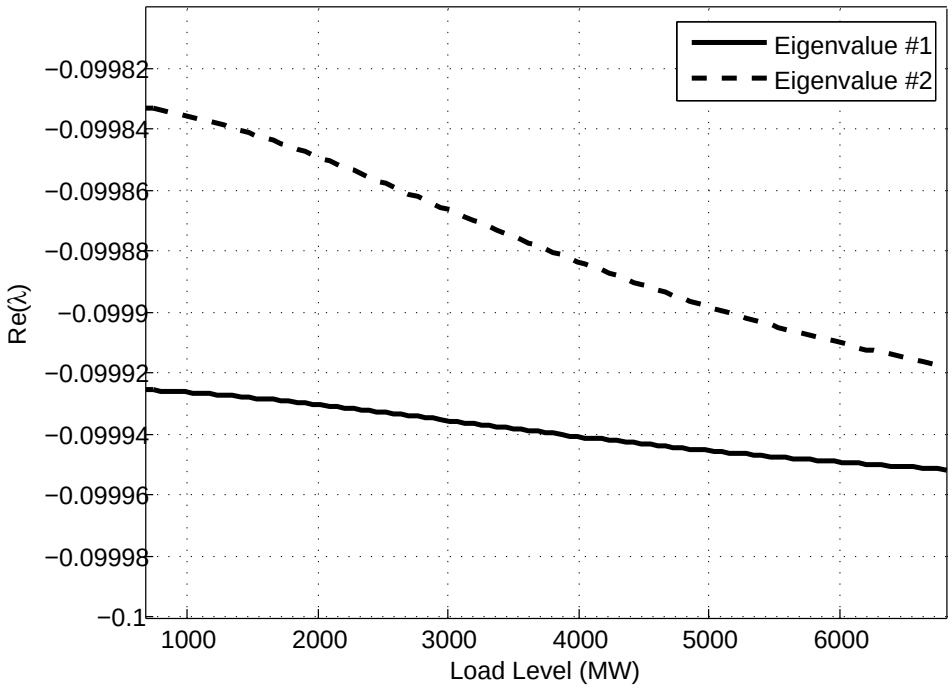

Figure 5.6 Close Eigenvalues Movement with Load Increase.

One advantage of the invariant subspace-based method over the derivative-based method is the treatment of eigenvalues with multiplicity and very close eigenvalues.

For the New England system, Fig. 5.6 gives the movement of the two close real eigenvalues with load variation obtained by the ICIS method. These two eigenvalues #1 and #2 correspond to λ_{17} and λ_{18} in Table 5.2, respectively. It shows that the ICIS method can be used to trace and differentiate very close eigenvalues too.

For example, assume that there are a cluster of eigenvalues which are very close to one another in a power system. Suppose we are interested in one or more specified eigenvalue trajectories. For the traditional methods (such as the Arnoldi method), we can only get a

bunch of discrete eigenvalues in the complex plane. It is difficult to associate these close eigenvalues for different parameter values. If the ICIS method is used to trace the movement of these eigenvalues, we can easily get the accurate trajectories of the close eigenvalues, as shown in Fig. 5.6.

Further advantages of ICIS over the conventional methods in treating close eigenvalues will be given in the next subsection.

5.2.7 Eigenvalues Collision Identification

Fig. 5.7 shows the eigenvalues collision in the New England system captured by ICIS without re-initialization when load increases from 4975 MW to 5902 MW. Fig. 5.8 shows a three-dimensional figure of eigenvalues collision for better illustration. In the beginning, when the load condition is 4975 MW, there are two real eigenvalues in the system, -1.4532 and -1.3751. With the increase in load, the two real eigenvalues (denoted by "o" and "+" in Fig. 5.7) are moving closer and finally collide at 5835.2 MW load level. As the load continues to increase, they will form a pair of complex conjugate eigenvalues and move apart, as shown in Fig. 5.8. Similar phenomenon has also been observed in [1]. It is indicated as a *node-focus* (NF) point.

The mathematical description of the advantages of ICIS in treating close or multiple eigenvalues is described as follows. In linear algebra, a *defective matrix* is a square matrix that does not have a complete basis of eigenvectors, and therefore is not diagonalizable. In particular, for an $n \times n$ matrix A_s, the matrix is defective if and only if it does not have n linearly independent eigenvectors. In the case of close or multiple eigenvalues, A_s is defective (or almost defective), and the computed eigenvectors corresponding to the relevant eigenvalues will be almost linear dependent. In addition, a small perturbation in matrix A_s may yield the change of A_s from a defective matrix to a non-defective matrix. This leads to a challenging numerical question for this scenario [12]: How can we compute the eigenvalues and eigenvectors in an efficient and accurate manner?

The convergence of the ICIS method for close eigenvalues and eigenvalues collision can

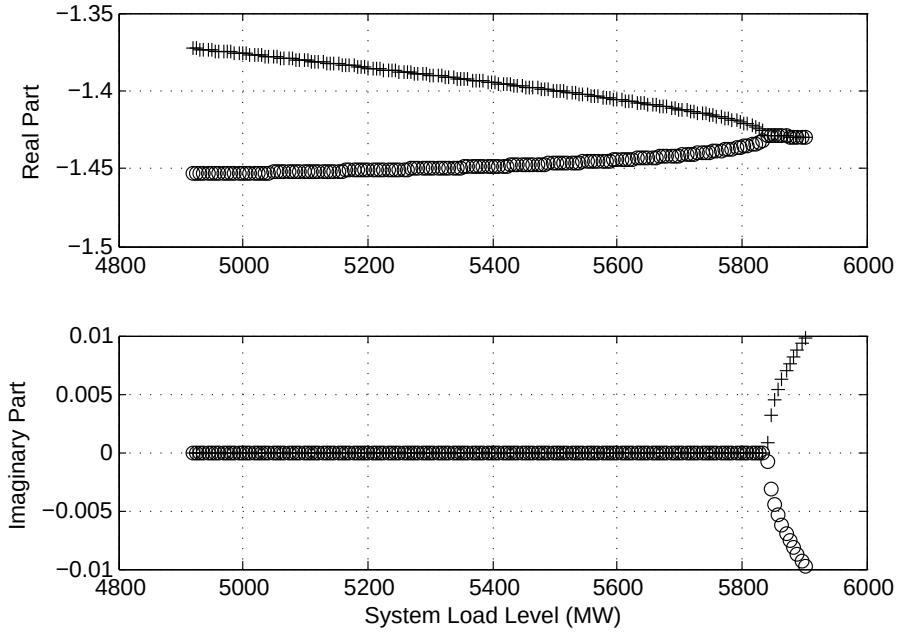

Figure 5.7 Eigenvalues Collision Captured by the ICIS Method.

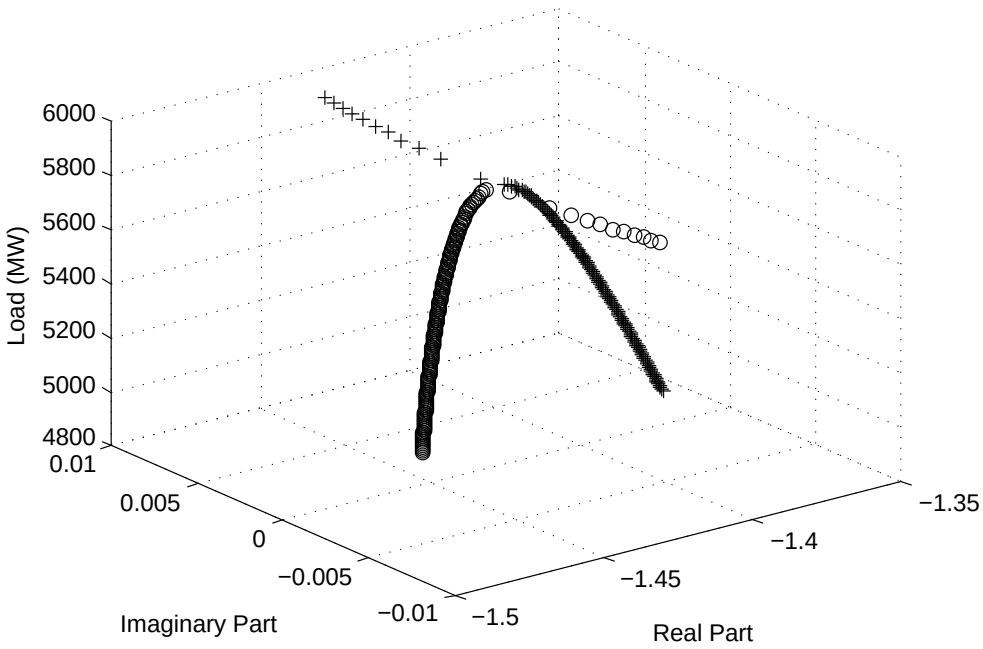

Figure 5.8 Three-Dimensional Graph of Eigenvalues Collision.

be explained mathematically as follows. In the case of close or multiple eigenvalues, the corresponding eigenvectors are not unique. This has the consequence that the eigenvectors corresponding to a tight cluster of eigenvalues will be ill-conditioned. In addition, a small perturbation of a matrix may result in a large change in its eigenvalues. This affects both the performance and the error bounds of the conventional eigenvalue computation methods such as Newton's method [24]. It also makes the computation of derivatives numerically ill-conditioned [41], since the Jacobian becomes ill-conditioned in case of nearby eigenvalues and singular for defective eigenvalues using Newton's method.

It is well known that invariant subspaces of a matrix tend to be more stable than eigenvectors. For interacting eigenvalues (such as eigenvalue collision, strong resonance, etc.), the eigenvectors associated with the interacting eigenvalues are highly unstable. Hence, the eigenvalue and eigenvector derivatives-based tracing method in [39] will fail in this case. However, the invariant subspace that represents the span of these interacting eigenvalues is much better conditioned, as pointed out in [30]. Therefore, it is of great importance to develop algorithms to identify and trace the stable invariant subspaces.

In order to circumvent the difficulties associated with multiple eigenvalues, an invariant subspace is used to follow these eigenvalues simultaneously. Although in this case, the individual eigenvectors are ill conditioned, the space spanned by these eigenvectors is an invariant subspace, which does not need to be sensitive to perturbations in the matrix. The invariant subspace associated with a cluster containing those two eigenvalues can be well determined, if the cluster is well separated from the remaining eigenvalues [84]. As a result, the invariant subspace-based method will work much better in such cases. When applying the ICIS method, the matrices of the equation set for the invariant subspace (4.1) are not ill-conditioned even though square matrix A_s has close or multiple eigenvalues. The continuation procedure provides bases of the invariant subspaces that depend smoothly on the parameter as long as the continued spectral subset does not collide with another eigenvalue.

The invariant subspace-based method provides us an efficient and robust way to deal with these issues. When λ is one of a set of r ill conditioned eigenvalues (close or multiple), one

should still be able to determine accurately an $n \times r$ matrix X and an $r \times r$ matrix M such that $A_s X = XM$, where the columns of X accurately define the relevant invariant subspace. Consequently, we can use ICIS to trace those eigenvalues without having any convergence problem. Similarly, the ICIS method can be used to investigate the interaction of different oscillatory modes (such as subsynchronous resonance) and model resonance [27] in power systems.

5.3 Low-Frequency Oscillation

5.3.1 Determination of Electromechanical Modes

For $\Delta\dot{x} = A_s \Delta x$, where A_s is an $n \times n$ matrix, there are n eigenvalues for any given equilibrium point. To choose the eigenvalues which are strongly related to part of the state variables (or a kind of state variables), the concept of *relative coefficient* will be introduced. For example, for the low-frequency oscillation problem, the eigenvalues which are strongly associated with $\Delta\omega$ and $\Delta\delta$ (electromechanical modes) should be selected. Those eigenvalues are the eigenvalues corresponding to the low-frequency oscillation. It is not reliable to make the judgment only based on the frequency information of the eigenvalues.

For the low-frequency oscillation, the electromechanical relative coefficient ρ_i of the complex eigenvalue λ_i (or participation ratio [85]) is defines as

$$\rho_i = \left| \frac{\sum_{x_j \in (\Delta\omega, \Delta\delta)} p_{ji}}{\sum_{x_j \notin (\Delta\omega, \Delta\delta)} p_{ji}} \right| \tag{5.4}$$

where p_{ji} is the participation factor similar to the definition in (3.27). It gives a measure of the relative participation of the jth state variable in the ith mode λ_i.

For a power system model, if any of its eigenvalues λ_i satisfies

$$\begin{cases} \rho_i > 1 \\ \lambda_i = \sigma_i \pm j\omega_i \quad f_i = \omega_i/(2\pi) \in 0.2 \sim 2.5\text{Hz} \end{cases} \tag{5.5}$$

then we can say that λ_i is a low-frequency oscillation mode (or electromechanical mode).

In the New England power system, we calculate all of the 89 eigenvalues when the load condition is 798 MW. There are totally 24 conjugate pairs of complex eigenvalues. If we only

Table 5.3 Relative Coefficients of the New England System

No.	λ_i	f_i (Hz)	ρ_i	States
1	$-0.1681 \pm j7.1869$	1.14	105.9256	δ_1, ω_1
2	$-0.2643 \pm j6.1664$	0.98	50.6123	δ_4, ω_4
3	$-0.2384 \pm j5.7765$	0.92	37.1478	δ_2, ω_2
4	$-0.2739 \pm j6.2882$	1.00	27.5098	δ_9, ω_9
5	$-0.3571 \pm j6.6677$	1.06	20.8464	δ_3, ω_3
6	$-0.2732 \pm j4.0720$	0.65	18.1027	ω_{10}, δ_5
7	$-0.9968 \pm j6.8994$	1.10	7.3933	ω_6, δ_6
8	$-0.9382 \pm j5.6801$	0.90	5.7617	ω_5, δ_5
9	$-1.3439 \pm j7.3976$	1.18	5.3627	δ_8, ω_8
10	$-1.3967 \pm j1.4172$	0.23	0.0067	E'_{q7}, R_{f7}, E_{fd7}
11	$-9.2942 \pm j7.1681$	1.14	7.6721E-4	R_{f4}, V_{r4}
12	$-0.7738 \pm j1.3083$	0.21	5.3390E-4	E'_{q10}, E_{fd10}
13	$-9.3956 \pm j7.3198$	1.17	3.0516E-4	V_{r3}, R_{f3}
14	$-10.3001 \pm j3.4377$	0.55	4.2978E-5	V_{r2}, R_{f2}
15	$-11.9004 \pm j13.0509$	2.08	3.4200E-5	V_{r1}, R_{f1}

Table 5.4 Participation Factor and State Information of Eigenvalue λ_6

Participation Factor	State
0.1755	ω_{10}
0.1154	δ_5
0.0879	ω_5
0.0856	δ_4
0.0855	δ_6
0.0734	δ_7
0.0613	ω_4
0.0588	ω_6
0.0519	ω_7
0.0469	δ_9

consider the eigenvalues whose imaginary parts are bigger than zero, there are 15 of the 48 complex eigenvalues whose frequencies are between 0.2 Hz and 2.5 Hz. Table 5.3 gives the 15 complex eigenvalues and their relative coefficients information. There are nine complex eigenvalues ($\lambda_1 \sim \lambda_9$) satisfying the criterion described in (5.5). So we can determine that the system has nine electromechanical modes. Since the electromechanical oscillation modes involve the generator swing equations, their number is one less than the number of generators in the system. For a power system with n generators, there are $(n-1)$ electromechanical modes in the system. The New England power system has ten generators, so it has nine electromechanical modes, which matches the results in Table 5.3.

To verify the results in Table 5.3, we can calculate the participation factor of each mode for modal analysis. Table 5.4 describes the participation factor and the corresponding state information for the eigenvalue $\lambda_6 = -0.2732 \pm j4.0720$. The participation factor information shows how strong each state will be related when the mode is excited. From the participation factors, we see that λ_6 is strongly related to states ω_{10} and δ_5. Similarly, we can calculate the relatedness of other eigenvalues with state variables. The detailed results are shown in Table 5.3. It can be seen that the first nine modes ($\lambda_1 \sim \lambda_9$) are strongly related to the angle or speed of the generators, which confirms that they are the electromechanical modes of the system.

To further investigate the relationship between each oscillation mode and the state variables, we can plot the mode shapes (normalized eigenvector components corresponding to rotor speed of the generators) to have a visual analysis of the rotor angle modes. Fig. 5.9 describes the participation factors associated with the mode λ_6. Since the participation factors are generally indicative of the relative participation of the respective states in the corresponding modes. Fig. 5.9 shows that among the 89 state variables ($x_1 \sim x_{89}$), the mode λ_6 is strongly related to state $x_{82}(\omega_{10})$, $x_{37}(\delta_5)$, $x_{38}(\omega_5)$, $x_{28}(\delta_4)$, $x_{46}(\delta_6)$, and $x_{55}(\delta_7)$, etc. Fig. 5.10 shows the mode shape of rotor angle modes corresponding to λ_6. The mode shape gives the relative activity of the state variables when a particular mode is excited. We can see that the big swing happens between generators G10 and G5, and the swings among other generators are much

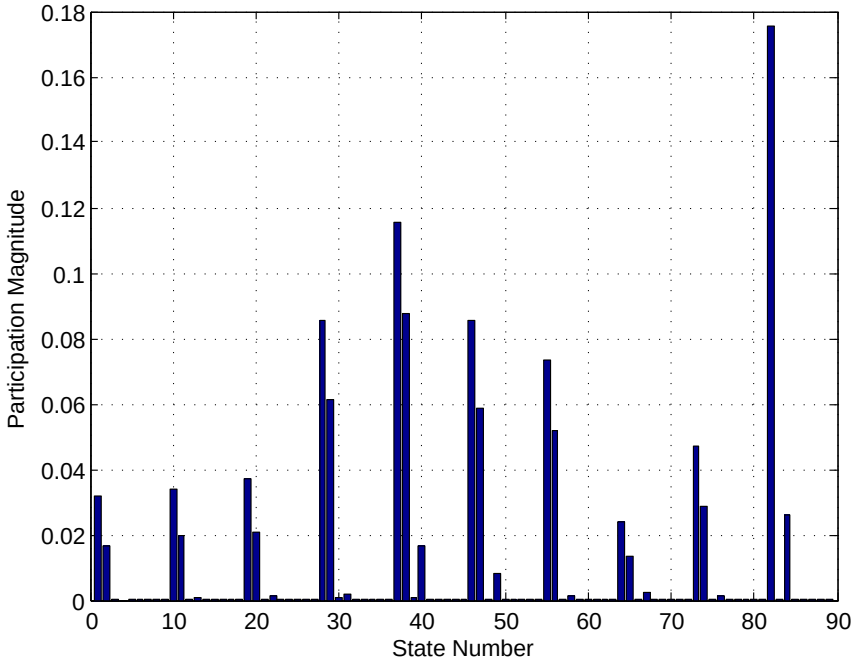

Figure 5.9 Participation Factors Associated with Eigenvalue λ_6.

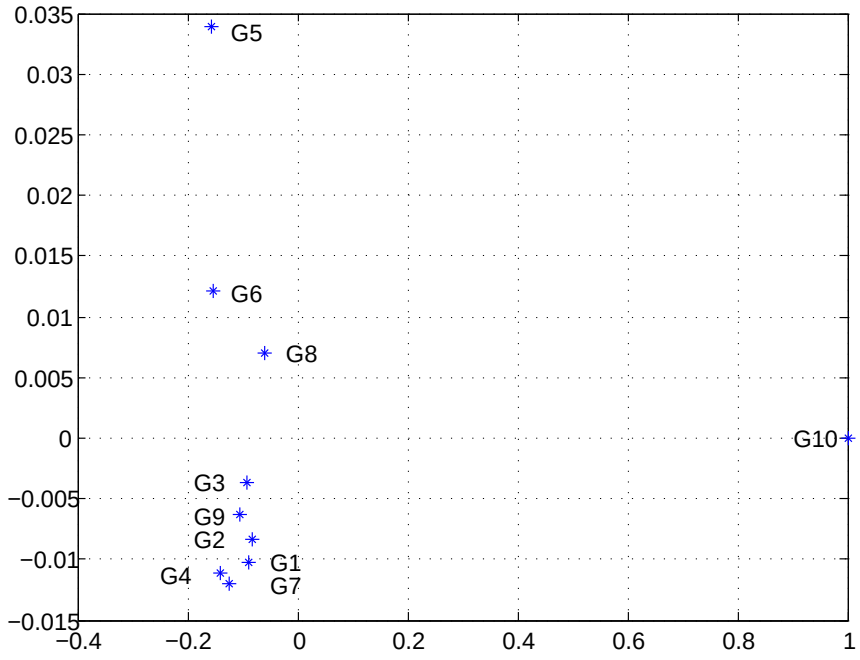

Figure 5.10 Mode Shape of Rotor Angle Modes corresponding to Eigenvalue λ_6.

smaller. It furthermore verifies the participation factor results.

5.3.2 Mode Tracing and Interaction

In order to apply the ICIS method to investigate the interaction of oscillatory modes, we first try to use ICIS to trace the movement of a set of complex eigenvalues with load variation. Fig. 5.11 shows the eigenvalues movement of the nine electromechanical modes. The load scenario is the same as shown in Fig. 5.2. The '+' represents the starting point (614 MW load), and 'o' represents the end point (6817 MW load). It can be seen that the eigenvalues movement is very nonlinear. With the increase in load, the direction and speed are changing too. The ICIS method provides us an efficient and accurate way to trace the trajectory of eigenvalues movement.

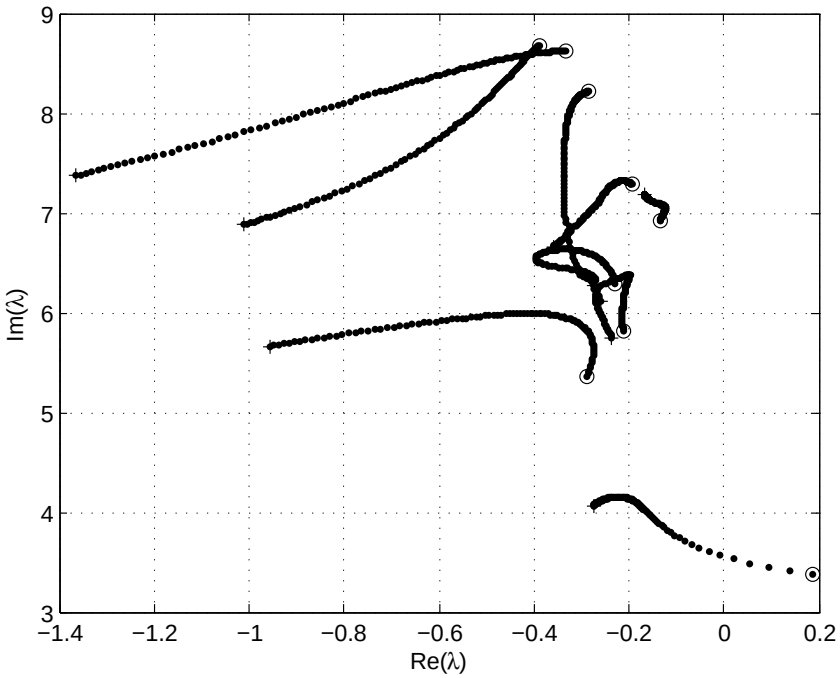

Figure 5.11 Electromechanical Modes Movement with Load Change.

Fig. 5.12 shows the eigenvalues movement with intersection which is part of the magnification of Fig. 5.11. The load increases from 1670 MW at the starting point to 2200 MW at the end point. During the increase in load, the two complex eigenvalues will intersect each other.

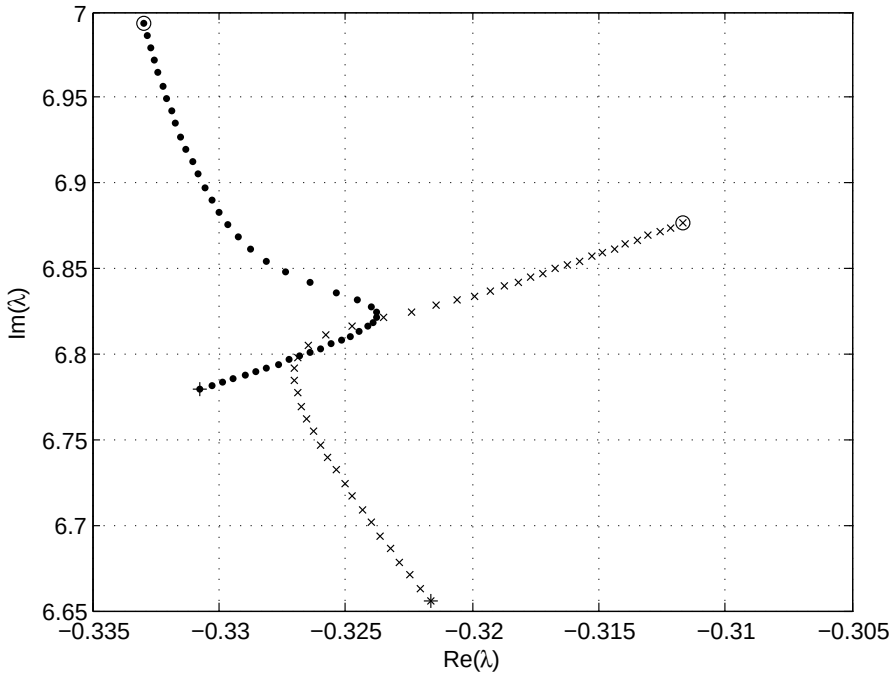

Figure 5.12 Magnification of Eigenvalues Movement with Intersection.

It can be observed that the intersection causes sharp turn in the eigenvalues movement.

The methodology of the ICIS method for low-frequency mode tracing can also be applied to investigate the interaction between difference electromechanical modes or inter-area oscillations in large-scale power systems. The application of ICIS to investigate a special eigenvalue interaction phenomenon in power systems is described in the next section.

5.3.3 Discussions

It is well-known that power system stabilizers are very efficient to damp the electromechanical oscillations in interconnected power systems. When the stabilizers are correctly tuned, the resulting damping control is robust. ICIS provides us a useful tool not only for power system operation but also for power system controller design. It utilizes the linearized system analysis to get a better understanding of power system oscillations and help ensure the system security. In addition, it can also be applied to the parameter setting of power system stability controller, such as power system stabilizers. Reference [44] describes the design, location and tuning of

PSS in detail.

ICIS can also be applied for the evaluation of power system stabilizer performance for changing system operating conditions. In the small-signal performance, the critical eigenvalues corresponding to the dominant modes need to be traced under a range of system conditions in order to verify the effectiveness of power system stabilizers.

5.4 Subsynchronous Resonance Analysis

5.4.1 Introduction

SSR is a power system dynamic oscillation phenomenon which is caused by the electrical resonance of the synchronous generator and the series capacitor compensated transmission lines. The formal definition of SSR is provided by the IEEE [45]:

Subsynchronous resonance is an electric power system condition where the electric network exchanges energy with a turbine generator at one or more of the natural frequencies of the combined system below the synchronous frequency of the system.

In power systems, series capacitors are being installed by many electric utilities to increase the power transfer capability of the transmission lines, as well as to improve the stability of the system. However, the occurrence of undesirable oscillations may lead to the destruction of the shaft of the turbine or the loss of synchronism of the generator. SSR is an interaction between the subelectrical mode and the torsional modes of the generator. There are several techniques proposed to study the phenomenon of SSR [42, 43]. The most common approaches are eigenvalue analysis, frequency scanning, and numerical time-domain simulation.

We are interested in the interaction between the subsynchronous electrical mode and the torsional modes when the capacitor compensation level changes. It has been known that the number of eigenvalues of a system matrix is equal to the number of state variables of the system, and each eigenvalue or eigenvalue pair can be associated with a system component. The conventional eigenvalue computation methods, such as the QR method, can only be used to calculate all eigenvalues of the state matrix at a given starting point. The identification of an eigenvalue or eigenvalue pair associated with the corresponding system component can be

implemented by modal analysis or some other techniques as described in [42, 43, 45]. For the conventional eigenvalue analysis methods, in order to investigate the SSR phenomenon, the eigenvalue computation needs to be repeated each time when the compensation level increases by a small amount, then the modal analysis will be applied to identify eigenvalues. The eigenvalue analysis method calculates all of the eigenvalues of the system. Among these eigenvalues, we are only interested in the eigenvalues associated with the torsional modes and subelectrical mode, which are a very small part of whole eigenvalues of the system. For example, for the IEEE SSR first benchmark model [86], the DAE model of the SMIB system has 27 differential equations and 11 algebraic equations. Among the 27 eigenvalues, there are five torsional modes and one subelectrical mode. As the system size increases, the repeated calculation of all the eigenvalues will cost a lot of extra computational cost.

The ICIS method is used to investigate the interaction between different oscillation modes that might cause SSR. For any given initial compensation level, the torsional modes and subelectrical mode are determined through modal analysis. Once those modes are extracted, the correlation between each torsional mode and the corresponding eigenvalue will not change as system compensation level increases. The ICIS method can then be used to efficiently trace the movement of those modes and identify the mode interaction among them. By using the ICIS method, the repeated calculation of whole eigenvalue spectrum and multiple modal analysis are avoided.

First, the eigenvalues corresponding to these oscillatory modes are associated with their invariant subspaces. By applying the continuation method, eigenvalue trajectory with parameter change can be obtained from the ICIS method. In this way, the interactions of oscillatory modes can be illustrated clearly. The relationship between the eigenvalues movement and the system mode change is explored.

The right eigenvector information obtained from the invariant subspace during the tracing process is also very useful in SSR analysis. It shows the distribution of modes of response (eigenvalues) through the state variables. Using this information, we can establish the relative magnitude of each mode's response due to each state variable. We can also determine the

state variables that have little or no effect on a given mode of response, and conversely those variables that play an important role in contributing to a given response. This often tells the engineers exactly those variables that need to be controlled in order to mitigate SSR in power systems.

5.4.2 IEEE SSR First Benchmark Model

We applied the ICIS method to the classic IEEE SSR first benchmark model [86]. The first benchmark model is recommended by an IEEE committee for SSR study shown in Fig. 5.13, which is a single machine infinite bus (SMIB) system. It includes the blocking filter, the line impedance, the series capacitor with dual gap protection for compensation, and the infinite bus. Also shown in the figure are two fault reactances X_F at two different locations. A fault may be assumed either at bus A or bus B, but not simultaneously. The system data is given in [86]. Fig. 5.14 gives the schematic diagram of the system with mass spring structure of the turbine generator. The six torsional masses include a high-pressure (HP) turbine section, an intermediate-pressure (IP) turbine section, two low-pressure (LPA and LPB) turbine sections, the rotor of the generator (GEN), and excitor (EX) rotor.

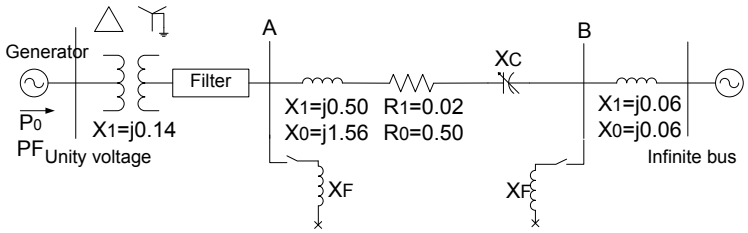

Figure 5.13 Network for SSR Studies [86].

Fig. 5.15 illustrates the mode shapes of the turbine generator. The relative rotational displacements of the individual mass for each mode of oscillation are given by the right eigenvector of the corresponding eigenvalue. The elements of the eigenvector associated with the angle deviations are used to draw the mode shape. In the plots shown in Fig. 5.15, each eigenvector has been normalized so that its largest element is equal to 1. The system has five torsional modes TM1 (15.7 Hz), TM2 (20.2 Hz), TM3 (25.6 Hz), TM4 (32.3 Hz), and TM5 (47.5 Hz).

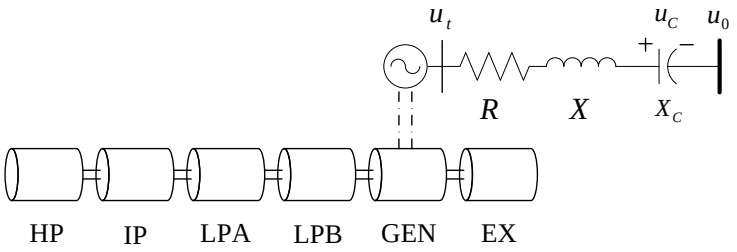

Figure 5.14 A Turbine Generator Power System with Series Capacitor Compensation.

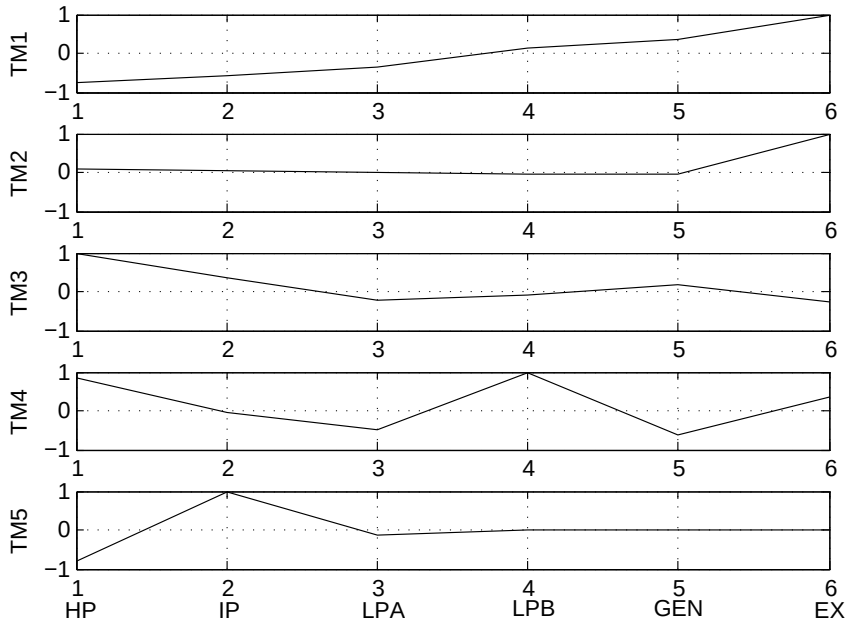

Figure 5.15 Mode Shapes of the Steam Turbine Generator.

The 15.7 Hz TM1 has one polarity reversal in the mode shape as shown in Fig. 5.15 (Similarly, TM2 has two polarity reversals, etc.). The polarities of eigenvector elements associated with the rotors of the HP, IP, and LPA sections are opposite to those associated with the rotors of the LPB, GEN, and EX sections. This indicates that the rotors of the HP, IP, and LPA sections oscillate against the other three rotors when TM1 is excited. Furthermore, the relative rotational displacement between LPA and GEN is the biggest, which suggests that the eigenvalue corresponding to TM1 is associated with the speed deviation or the angle deviation of the LPA or GEN rotors, when TM1 is excited. Similar analysis can be performed for the other four torsional modes. The detailed results are shown in Table 5.5. We will show later that the results of modal analysis are consistent with the mode shapes of the generator.

Table 5.5 Modal Analysis Results of Torsional Modes

Mode	Associated Rotors
TM1	GEN, LPA
TM2	EX, LPB or GEN
TM3	HP, LPA
TM4	LPB, GEN
TM5	HP, IP

5.4.3 Modal Analysis

We are interested in the interaction between the subsynchronous electrical mode and the torsional modes when the capacitor compensation level changes. At a given starting point, the modal analysis is performed to identify those eigenvalues.

Table 5.6 gives the eigenvalues, relative coefficients, and the related mode state information when the compensation level is $\mu = X_C/X_L = 0.5\%$. There are totally six complex pairs of eigenvalues whose relative coefficients are bigger than 1 (namely λ_{HP}, λ_{IP}, λ_{LPA}, λ_{LPB}, λ_{GEN}, and λ_{EX}), which are associated with the speed deviations ω_i or the angle deviations δ_i of the six turbine sections. These modes are associated with the five torsional modes and one system mode which represents the oscillation of the entire rotor against the power system. From the participation factor information corresponding to each pair of complex eigenvalues, each mode

Table 5.6 Eigenvalues of the 27th-Order System

	λ_i	f_i(Hz)	ρ_i
$\lambda_{E_{fd}}$	-499.9866		5.2718E-7
λ_{VR}	-101.9516		1.1216E-4
λ_S	-30.4085		1.6267E-2
λ_Q	-24.7465		3.2651E-4
λ_F	-8.7917		1.2667E-1
$\lambda_{d,q}$	$-6.8764 \pm j397.3176$	63.2351	4.4346E-4
λ_C	$-6.8103 \pm j356.6095$	56.7562	7.2520E-4
λ_{GOVR}	$-4.7377 \pm j0.8194$	0.1304	8.1021E-2
λ_{CO}	-4.6861		1.7277E-2
λ_{CH}	-2.7893		4.8463E-2
λ_D	-1.9514		4.0666E-2
λ_{EX}	$-0.6557 \pm j127.0134$	20.2148	1.5152E4
λ_{HP}	$-0.1818 \pm j298.1767$	47.4563	4.4290E6
λ_{LPA}	$-0.165 \pm j160.596$	25.5597	4.1971E3
λ_{LPB}	$-0.1507 \pm j99.0491$	15.7641	1.2977E3
λ_{RH}	-0.1416		8.9604E-3
λ_{IP}	$-0.0379 \pm j202.9609$	32.3022	2.4394E3
λ_{GEN}	$0.1952 \pm j7.6846$	1.2230	2.0639E1

Table 5.7 Participation Factor and State Information of Oscillation Modes

$\lambda_{HP} = -0.1818 \pm j298.1767$		$\lambda_{IP} = -0.0379 \pm j202.9609$		$\lambda_{LPA} = -0.165 \pm j160.596$	
Participation Factor	State	Participation Factor	State	Participation Factor	State
0.3463	ω_2	0.2923	ω_4	0.2434	ω_1
0.3463	δ_2	0.2923	δ_4	0.2434	δ_1
0.1282	ω_1	0.1122	ω_5	0.1196	ω_3
0.1282	δ_1	0.1119	δ_5	0.1196	δ_3
0.0245	ω_3	0.0714	ω_3	0.0634	ω_5
0.0245	δ_3	0.0714	δ_3	0.0634	δ_5
$\lambda_{LPB} = -0.1507 \pm j99.0491$		$\lambda_{EX} = -0.6557 \pm j127.0134$		$\lambda_C = -6.8103 \pm j356.6095$	
Participation Factor	State	Participation Factor	State	Participation Factor	State
0.1618	δ_5	0.4401	ω_6	0.8182	i_d
0.1615	ω_5	0.4401	δ_6	0.7284	i_q
0.1317	ω_3	0.0182	ω_4	0.4761	i_D
0.1317	δ_3	0.0182	δ_4	0.3160	i_Q
0.0745	δ_1	0.0160	δ_5	0.2639	E_{Cd}
0.0745	ω_1	0.0159	ω_5	0.2633	E_{Cq}

can be associated with a system component. For example, Table 5.7 shows the participation factors and the corresponding state variables information related to five torsional modes and one subelectrical mode. The participation factor p_{ij} is a measure of the relative participation of the state variables x_i and the oscillation mode λ_j. We know that the state variables i_d and i_q are connected to the subelectrical mode EM. Based on the participation factor information, it can be seen that eigenvalue λ_C corresponds to EM. From the eigenvalue frequency information shown in Table 5.6, λ_{LPB} is corresponding to TM1 since λ_{LPB} has the frequency of 15.76 Hz which is always the same as the natural frequency of TM1 (15.7 Hz). From Table 5.7, TM1 is associated with the state variables δ_5 and ω_5 which correspond to the generator rotor GEN. It matches with the modal analysis result of TM1 in Table 5.5. TM2 is related to the state variables δ_6 and ω_6 representing the excitor rotor EX. Similar analysis shows that TM3, TM4, and TM5 are associated with HP, LPB, and IP sections, respectively. The participation factor results are in accordance with the mode shapes of the generator shown in Fig. 5.15 and in Table 5.5.

5.4.4 Numerical Results

Table 5.8 shows the information of the six oscillatory modes (one subelectrical mode EM and five torsional modes TM1 $\sim$ TM5) obtained from the modal analysis results at the compensation level $\mu = 0.5\%$. From these eigenvalues, an orthonormal basis for the subspaces corresponding to these six eigenmodes can be calculated. Once the invariant subspace needed for the initialization is obtained at the starting point, then the ICIS method can be used to trace the eigenvalue trajectory of these oscillatory modes easily with the change in compensation level. The interactions between the EM and different TMs that will result in SSR can be identified subsequently.

The numerical results of the ICIS method are shown in Figs. 5.16–5.19. In order to better investigate the mode interactions, the step size s is chosen to be a constant value of 0.5%, which means the compensation level is increased by 0.005 at each iteration during the continuation process until it reaches 100%. It should be mentioned that this variation is for research purpose.

Table 5.8 Oscillatory Modes Traced by the ICIS Method

Mode	λ_i
EM	$-6.8103 + j356.6095$
TM1	$-0.1507 + j99.0491$
TM2	$-0.6557 + j127.0134$
TM3	$-0.165 + j160.596$
TM4	$-0.0379 + j202.9609$
TM5	$-0.1818 + j298.1767$

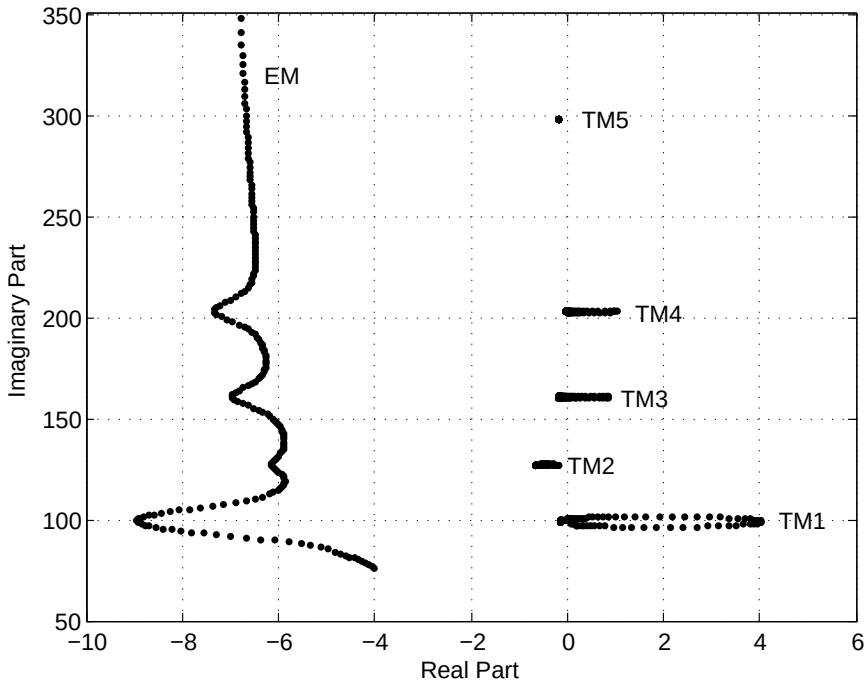

Figure 5.16 Eigenvalues Movement of Different Oscillatory Modes when the Compensation Level Changes from 0.5% to 100%.

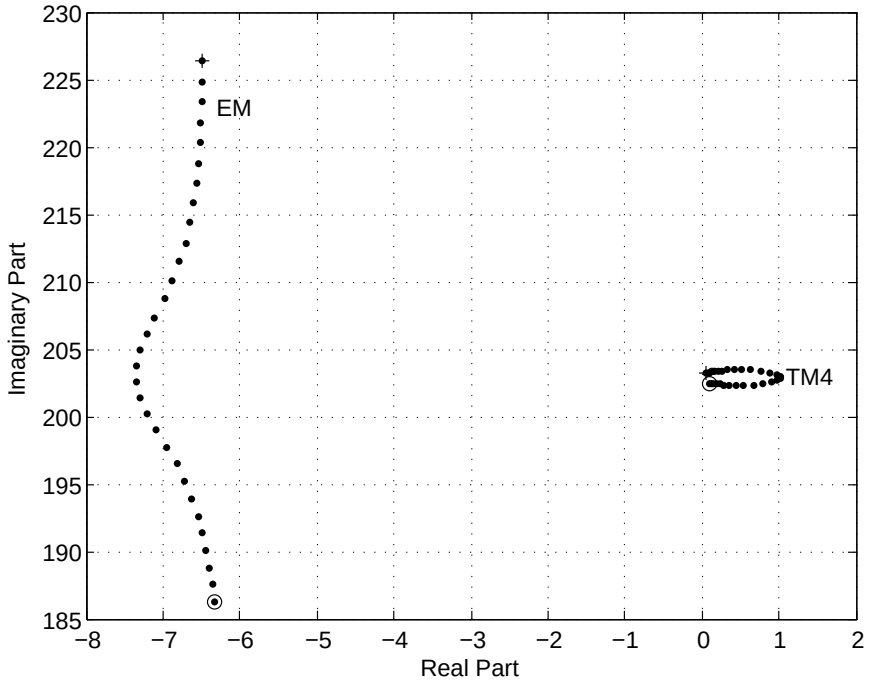

Figure 5.17 Mode Interaction between EM and TM4.

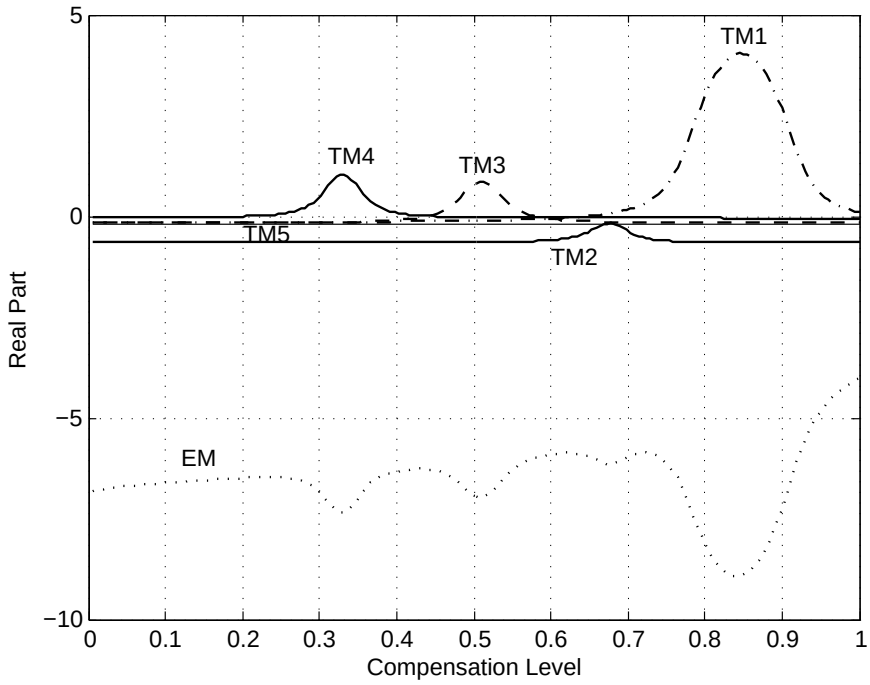

Figure 5.18 Real Parts of the Eigenvalues Movement with the Change in Compensation Level.

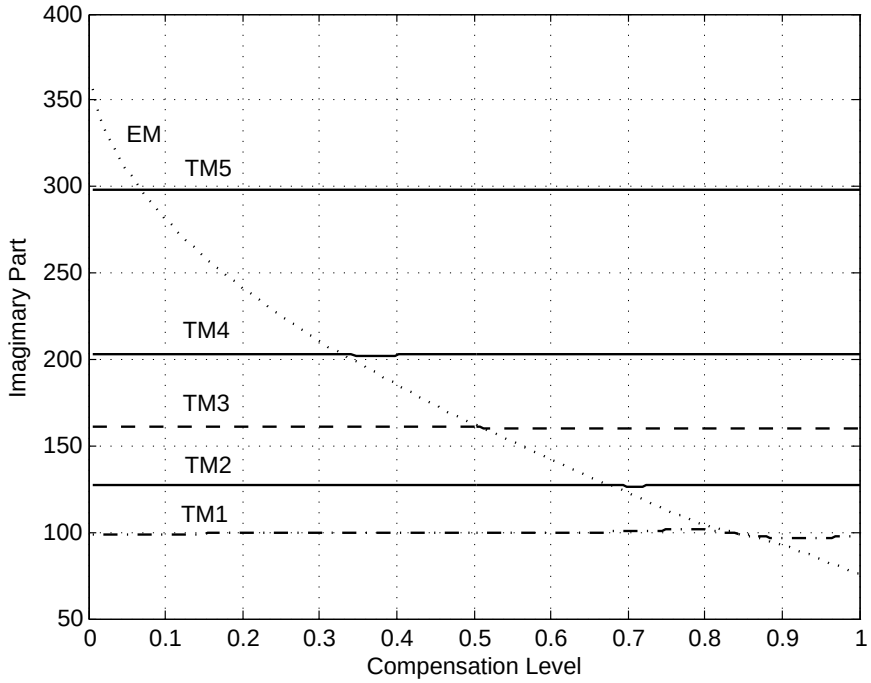

Figure 5.19 Imaginary Parts of the Eigenvalues Movement with the Change in Compensation Level.

Typically the inductive reactance of a transmission line is compensated to between 25% and 70% [87]. Fig. 5.16 describes the eigenvalues movement of different oscillatory modes with the change in compensation level. It gives a whole picture of the eigenvalues movement in the complex plane. Fig. 5.17 shows the mode interaction between subelectrical mode EM and the torsional mode TM4 , which is the magnification part of Fig. 5.16. The '+' and 'o' represent the starting and ending points of the eigenvalue trajectory, where the compensation levels are 14.6% and 44.7%, respectively. Figs. 5.18 and 5.19 show the real and imaginary parts of the oscillatory modes in terms of the compensation level. From Figs. 5.16 and 5.18, we can see that there are unstable eigenvalue modes of the mass-spring system when the capacitor compensation changes. For example, from Fig. 5.18, it can be seen that eigenvalue mode is unstable when compensation level $\mu \in (20.6\%, 45.1\%)$ for TM4, $(44\%, 57.9\%)$ for TM3, and $(64.6\%, 100\%)$ for TM1. There is also the coexistence of two unstable eigenvalue modes simultaneously. For example, both TM4 and TM3 are unstable when μ is between 44% and 45.1%. When the frequency of the subelectrical mode is equal to one of the torsional modes

(such as $\mu = 33\%$ for TM4, $\mu = 51\%$ for TM3, and $\mu = 84.4\%$ for TM1), the mode interaction happens. The mode interaction causes the sharp turns of eigenvalues movement and certain torsional modes to become unstable, as shown in Figs. 5.16 and 5.18. From Figs. 5.17 and 5.19, it can be seen that as μ increases from 14.6%, the impact of EM on torsional mode TM4 increases and causes TM4 to move from the left half plane closer to the right half plane. At the same time, the imaginary part of EM decreases and becomes closer to the imaginary part of TM4. The interaction between EM and TM4 near its natural frequency 32.3 Hz ($\omega = 203$ rad/sec) causes TM4 to cross the imaginary axis at $\mu = 20.6\%$ and become unstable. When μ increases to 45.1%, TM4 crosses the imaginary axis to come back into the left half complex plane and becomes stable again. For comparison purpose, we also tested the results using the conventional method using MATLAB routine to calculate the whole spectrum of eigenvalues. The results of the ICIS method match the results of the conventional method very well. So we can see that ICIS provides us an efficient and accurate way to identify the interacting dynamic phenomena. It is also a useful tool to investigate the interaction between different oscillation modes that could cause SSR.

An interesting phenomenon observed from Figs. 5.16 and 5.18 is that the movement of real part of EM is approximately symmetrical to the movements of real parts of TM1 $\sim$ TM5. In other words, a certain change in the real part of EM will cause roughly the same amount of change but in the reverse direction for the sum of the real parts in TM1 $\sim$ TM5. Further whole eigenvalue analysis results show that among the 15 eigenvalues other than the six oscillatory modes in Table 5.6, their movements are very minor. As a result, the sum of the whole 27 eigenvalues is always a constant value regardless of the change in the compensation level. Mathematically, we know that the sum of all the eigenvalues is equal to the negative of the coefficient of the degree $(n-1)$ term in the characteristic polynomial of a matrix. Also the trace of the matrix (defined as $\mathrm{tr}(A)$) is the sum of its eigenvalues as well. It means that the sum of the main diagonal of the state matrix in the IEEE SSR first benchmark system has no relationship with the compensation level. The examination of system state matrix verifies it.

5.5 Modal Resonance Analysis

Detection of modal resonance (strong or weak resonance, etc.) for a generic power system model can be a very long process, especially if the studied system is not well known. Based on the previous research results [27, 28, 29], it is summarized that the following two conditions need to be satisfied in order to increase the possibility of eigenvalues interaction:

1. Modes must be within a certain frequency range for them to interact;
2. The sensitivity of the eigenvalues with respect to the system parameter must be opposite to each other.

Since the ICIS method provides us a useful tool to trace any set of critical eigenvalues. The eigenvalue sensitivities can also be extracted during the process, which can be used to determine the direction and speed of the eigenvalues movement. Based on the ICIS method, a heuristic procedure to efficiently identify modal resonance is proposed. Fig. 5.20 shows the flowchart to identify modal resonance using the ICIS method.

The identification procedure can be described as follows: For a certain initial condition, the eigenvalues satisfying the above conditions are obtained at first. From the eigenvalue sensitivities using ICIS, a linear estimation of the eigenvalue movements is predicted to identify the resonance. Note that the nonlinear and rapid change in the eigenvalue movements yields poor estimation from $\partial\lambda_i/\partial p$ as pointed out in [27], we use transformed eigenvalues in the estimation similar to [27]. The step size will then be adjusted to reflect the estimation results and the system parameter will be modified accordingly. The iteration is repeated for ICIS until the model resonance has been identified.

5.6 Conclusion

This chapter applies the improved continuation of invariant subspaces to trace the critical eigenvalues and identify various interacting dynamic phenomena in power system. With this approach, one can trace the trajectory of different oscillatory modes with respect to system

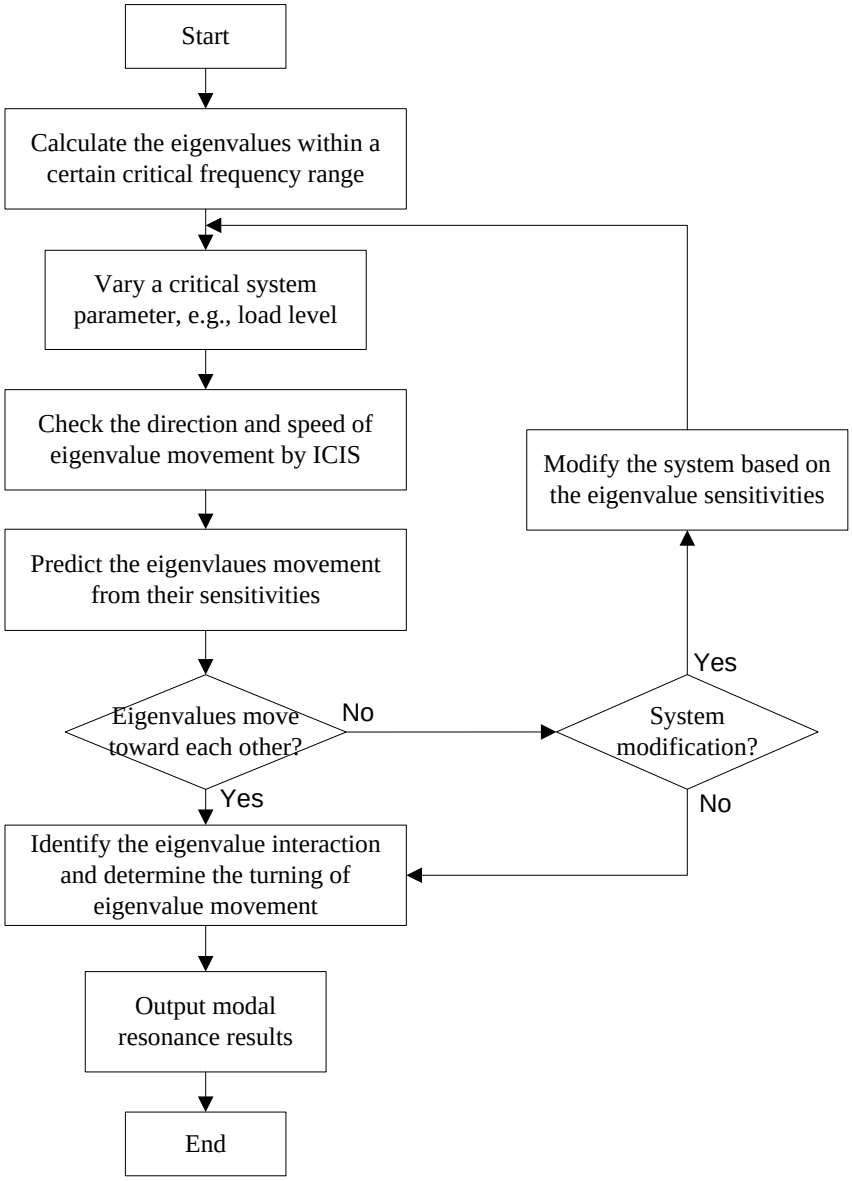

Figure 5.20 Heuristic Procedure to Identify Modal Resonance Using ICIS.

parameter variation. The ICIS algorithm can trace the nonlinear movement of eigenvalues efficiently and accurately.

An eigenvalue index is proposed to rank the critical eigenvalues that might cross the imaginary axis and estimate the oscillatory stability margin boundary. We can make use of this information to identify critical eigenvalues that might affect the oscillatory stability, and then use them to predict the behavior of the system as parameter changes. We can also use the information to design power system stabilizer or controller to mitigate the oscillations related to certain modes of interest.

The eigenvalue computation based on invariant subspace is practical and efficient for power system small-signal stability analysis. By using ICIS, we can trace any set of eigenvalues we are interested in (such as the rightmost eigenvalues or the eigenvalues with least damping ratio, etc.). The method is able to handle eigenvalues with any multiplicity and very close eigenvalues. Eigenvalue collision is also identified by ICIS. The method can be used to identify the interacting dynamic phenomena in power systems, such as low-frequency oscillation, SSR, etc. The ICIS method can be applied for the design of power system stabilizer and other control techniques. A heuristic procedure is proposed to identify modal resonance using the ICIS method.

CHAPTER 6. EFFICIENT IDENTIFICATION OF OSCILLATORY STABILITY MARGIN AND DAMPING MARGIN WITH THE PROPOSED METHOD

6.1 Introduction

In this chapter, the improved continuation of invariant subspaces together with the extracted eigenvalue sensitivity information is proposed to identify the oscillatory stability margin and damping margin. The ICIS method enables us to trace any set of critical eigenvalues of interest. The eigenvalue sensitivity, a by-product during the ICIS process, will be used to automatically adjust the step size at each iteration to improve the efficiency of calculation.

The oscillatory stability margin is defined as the amount of load increase for a specified load scenario which would lead to the onset of oscillations. Mathematically speaking, the system at the oscillatory stability margin boundary has a simple pair of purely imaginary eigenvalues, and there are no other eigenvalues on the imaginary axis and in the right half complex plane. Damping margin is defined as the amount of additional load on a certain pattern of incremental change in system load that would cause the damping ratio to reach its specified minimum limit.

With respect to the methods based on eigenvalue estimation, such as eigenvalue-based approaches to identify oscillatory stability margin or damping margin, reference [2] presented an algorithm to calculate the Hopf bifurcation-related oscillatory margin boundary. The method starts the iteration at a given initial operating point. After linearizing the DAE model at the operating point, the system Jacobian matrix is obtained. The eigenvalue with the maximum real part is chosen as the dominant eigenvalue and is updated by the power method or the modified Arnoldi method. The step size is selected by the secant method. To speed up the process, reference [13] discussed different techniques to calculate the critical eigenvalue clusters

in the small-signal stability analysis of large power systems. The method in [2] considers only one critical eigenvalue each time. Although the algorithm is fast, it might not work well to reach the Hopf bifurcation point since we cannot guarantee that the calculated eigenvalue is the critical eigenvalue that will cross the imaginary axis first as parameter varies. This is because in general the eigenvalues have a nonlinear behavior which means that determining which one is the dominant eigenvalue is very difficult. Reference [88] applied genetic algorithm and decision tree for eigenvalue region prediction in oscillatory stability assessment.

Another way to identify the Hopf bifurcation is through the direct method. Reference [89] and [90] applied the direct method in the identification of the oscillatory stability margin boundary. The bifurcation points are the solutions of a set of algebraic equations. In addition, a transfer function-based Hopf bifurcation algorithm was also proposed in [90] to determine the eigenvalue crossings of the stability or security boundaries. The direct method can identify the oscillatory stability margin directly without computing any intermediate operating point. But solving these nonlinear algebraic equations is also very complex and slow, and sometimes the traditional Newton-based techniques can lead to difficulties or even failure when the initial solution is far away from the Hopf bifurcation point.

Reference [38] firstly applied the CIS method for eigenvalue tracing in power systems. In [38], a bordered version of the Bartels-Stewart algorithm is used to trace the critical eigenvalues of power system. The Cayley transform is used to map the rightmost eigenvalues to the eigenvalues with largest moduli, the projected Arnoldi method is then applied to calculate these eigenvalues. Here we further reduce the computational time with step size control using the eigenvalue sensitivities from the proposed ICIS in Chapter 4. The eigenvalue sensitivities will not be prominent without proper re-initialization during ICIS. The sensitivities can be achieved without adding computation cost.

In [39], a derivative-based method is applied to power system oscillatory stability analysis. From the eigenvalue sensitivity information, an eigenvalue index is derived to identify the changing rates and the movement directions of the eigenvalues with respect to change in any parameter of interest. Compared with [39], the process can be further improved by using other

efficient dominant eigenvalue computation methods. The ICIS method can play a key role in it. Moreover, the integration-based method requires the computation of both eigenvalue sensitivities and eigenvector sensitivities, whereas only eigenvalue sensitivities are used in the identification process.

By combining the ideas of [38] and [39], an improved algorithm is proposed to trace the critical eigenvalues of power systems via ICIS by considering the eigenvalue sensitivity information. In this chapter, the successive eigenvalue sensitivities extracted from ICIS are proposed to identify the oscillatory stability margin as well as the damping margin. The ICIS method provides us an efficient tool to trace any set of critical eigenvalues of interest. The extracted eigenvalue sensitivities can be used to automatically adjust the step size in continuation iteration to improve the efficiency of calculation. The next sections provide the details about this approach.

6.2 Oscillatory Stability Margin and Damping Margin Identification Using Eigenvalue Sensitivity

For the oscillatory stability margin, the issue is to find the critical eigenvalue which will cross the imaginary axis first and the parameter value where the real part of the critical eigenvalue equals to zero. As we know, the eigenvalue movement is very nonlinear with the change in parameter. It is almost impossible to identify the critical eigenvalue before we actually reach the oscillatory stability margin boundary. This brings the difficulty for identification of the stability margin. In [38], constant parameter change is assumed until the system reaches the margin boundary. The eigenvalue sensitivities can provide an indicator to identify the margin boundaries and speed up the process. A good solution for this problem using eigenvalue sensitivities is proposed as follows: Given a real part criterion σ_c (e.g., $\sigma_c = -0.5$), we calculate the rightmost eigenvalues that satisfy the criterion for an initial parameter value (i.e., $\mathrm{Re}(\lambda_i) > \sigma_c$). The critical eigenvalue will be one of those rightmost eigenvalues with proper selection of σ_c. The ICIS method is used to trace these rightmost eigenvalues. At each iteration, the eigenvalue sensitivities will determine the optimal step size of the predictor by using Newton's

method. They can also help to eliminate some noncritical eigenvalues to save more computation cost. The algorithm uses the sensitivities for both determining the critical eigenvalue and driving it to the imaginary axis.

Suppose q rightmost eigenvalues are traced by ICIS ($\lambda_i = \sigma_i + j\omega_i, \sigma_i < 0, i = 1, 2, \ldots, q$). The real part of the eigenvalue sensitivity is $\dot{\sigma}_i = \partial\sigma_i/\partial p$. Among the q eigenvalues, there are r eigenvalues with $\dot{\sigma}_i > 0 (i = 1, 2, \ldots, r, r \leq q)$, which means those eigenvalues are moving closer to the imaginary axis and will determine the oscillatory stability margin. The step size is chosen as

$$s = \min\{-\frac{\sigma_1}{\dot{\sigma}_1}, -\frac{\sigma_2}{\dot{\sigma}_2}, \ldots, -\frac{\sigma_r}{\dot{\sigma}_r}, s_{\max}\} \tag{6.1}$$

where $s_{\max}$ is the step size upper limit to reduce the linear estimation error considering the nonlinear movements of eigenvalues. Another way is to introduce a scaling factor $\alpha < 1$ to balance the error when the point is far away from the solution.

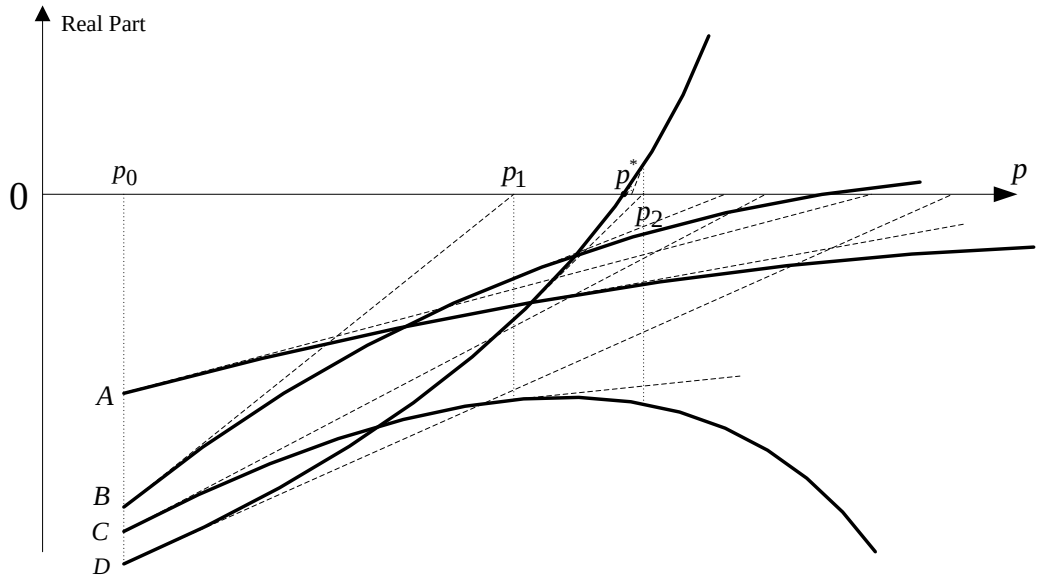

Figure 6.1 Step Size Control Using Eigenvalue Sensitivity.

Fig. 6.1 shows an illustration of how to use eigenvalue sensitivity for step size control. It describes the movements of real parts of four rightmost eigenvalues (A, B, C, and D) with respect to parameter p. The dashed lines indicate the slopes of the eigenvalues which are

the real parts of eigenvalue sensitivities. This information is used to define the optimal load change to reach the oscillatory stability margin boundary. At parameter value p_0, eigenvalue B gives the optimal step size since the intersection of eigenvalue slope and p-axis has the smallest load increase. Similarly, eigenvalue D decides the step size at p_1, etc. The critical eigenvalue shifts from eigenvalue B to eigenvalue D at p_1. At p_2, it can be seen that eigenvalue D is still the critical eigenvalue because only D has positive real part. Only critical eigenvalue D will be considered after p_2 to further reduce the computation cost, since D is the eigenvalue that crosses the imaginary axis first. The iteration will stop when it reaches the margin boundary point p^*. Like Newton's method, the convergence rate is quadratic once the critical eigenvalue is determined, which is faster than the secant method proposed in [2] since the latter is only superlinearly convergent. It should be pointed out that ICIS can capture the critical eigenvalue shift in tracing a subset of eigenvalues instead of one at a time such as in [39]. It also provides a structure-preserving technique to efficiently calculate critical eigenvalues as well as eigenvalue sensitivities. Furthermore, instead of repeated eigenvalue calculations by conventional methods, the ICIS method can trace the movements of eigenvalues as system parameter varies. Fig. 6.1 also shows that as parameter p moves closer to the boundary point p^*, Newton's method provides better linear estimation in the stability margin and step size adjustment error becomes smaller.

The damping ratio margin can be identified similar to the oscillatory stability margin. The only question is to calculate the derivative of damping ratio with respect to parameter p. For eigenvalue λ_i, the damping ratio is defined as

$$\zeta_i = -\frac{\sigma_i}{\sqrt{\sigma_i^2 + \omega_i^2}}. \tag{6.2}$$

Since both $\partial\sigma_i/\partial p$ and $\partial\omega_i/\partial p$ are available, then the derivative of damping ratio ζ_i to p can be derived as follows:

$$\frac{\partial\zeta_i}{\partial p} = \frac{\sqrt{1-\zeta_i^2}}{\sigma_i^2 + \omega_i^2}(\sigma_i\frac{\partial\omega_i}{\partial p} - \omega_i\frac{\partial\sigma_i}{\partial p}). \tag{6.3}$$

Fig. 6.2 describes the flowchart for oscillatory stability margin and damping margin identification using the ICIS method.

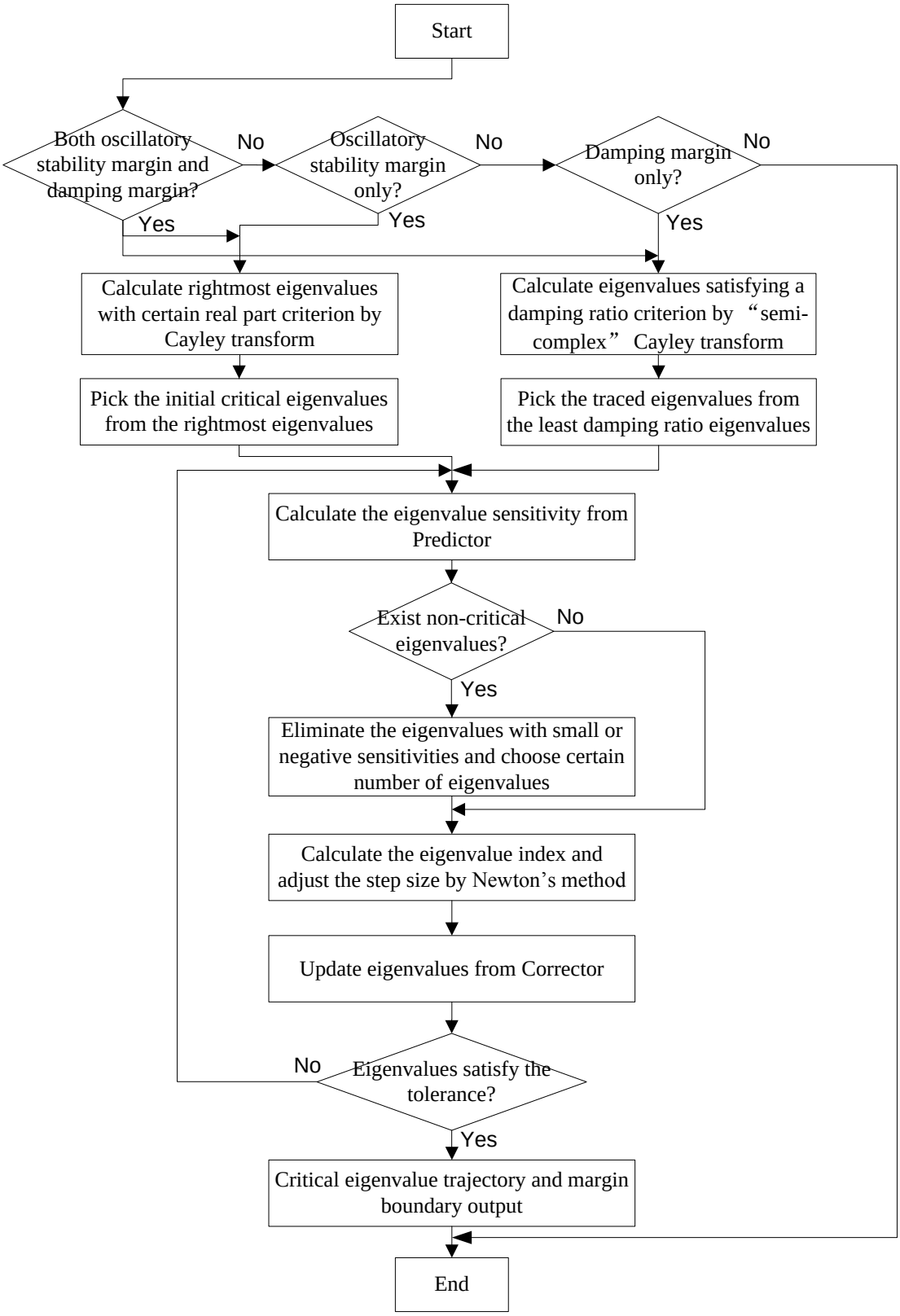

Figure 6.2 Flowchart for Oscillatory Stability Margin and Damping Margin Identification.

6.3 Simulation Results

The improved continuation of invariant subspaces with sensitivity for identification of oscillatory stability margin and damping margin is tested on the New England 39-bus system and IEEE 145-bus system, respectively. The detailed numerical results are described in the following.

6.3.1 New England 10-Generator, 39-Bus System

The New England 39-bus system has been described in Section 5.2.1. The schematic diagram of the system is shown in Appendix A. The system load level is chosen as the control parameter p.

Table 6.1 Rightmost Eigenvalues and Their Sensitivities at 4300 MW Load

No.	λ_i	$\partial\sigma_i/\partial p$	$-\sigma_i/\dot{\sigma}_i$
1	$-0.3551 \pm j5.9727$	8.3411E-3	42.57
2	$-0.3508 \pm j6.6306$	5.6534E-3	62.05
3	$-0.4870 \pm j8.1914$	7.4598E-3	65.28
4	$-0.1942 \pm j4.1239$	2.5508E-3	76.13
5	$-0.2415 \pm j7.2522$	2.1491E-3	112.4
6	$-0.1261 \pm j7.0702$	9.4457E-4	133.5
7	$-0.4735 \pm j0.4400$	1.9227E-3	246.3
8	$-0.4759 \pm j0.5232$	1.8981E-3	250.7
9	$-0.4469 \pm j0.4249$	1.7653E-3	253.2
10	$-0.3696 \pm j0.4187$	1.2604E-3	293.3
11	$-0.3305 \pm j7.9058$	9.4690E-4	349.1
12	$-0.2007 \pm j6.3352$	-8.4974E-4	-236.2
13	$-0.0525 \pm j0.0982$	-5.9377E-6	-8835
14	$-0.4935 \pm j0.7235$	-2.1590E-5	-2.286E4

6.3.1.1 Oscillatory Stability Margin Identification

By using the generalized Cayley transform with parameters $\alpha_1 = 0$ and $\alpha_2 = -1$, Table 6.1 gives the 14 complex conjugate pairs of eigenvalues whose real parts are greater than -0.5 at the base case. The total base case load is 4300 MW. These rightmost eigenvalues and their sensitivities are corresponding to the complex eigenvalues in Table 5.2 and also plotted in Fig. 5.5. For each eigenvalue λ_i, $\dot{\sigma}_i = \partial\sigma_i/\partial p$ shows the real part of its sensitivity calculated by ICIS, $s_i = -\sigma_i/\dot{\sigma}_i$ gives the corresponding step size. Positive $\dot{\sigma}_i$ means the corresponding eigenvalue moves toward the imaginary axis if load increases, negative value means that it moves away from the imaginary axis. For example, for eigenvalue $\lambda_1 = -0.3551 + j5.9727$, its real and imaginary parts of eigenvalue sensitivity are 8.3411E-3 and -6.2773E-3, respectively. If we use linear estimation to project eigenvalue movement, it means that λ_1 will change to $-0.3468 + j5.9664$ when the load increases to 4400 MW. In fact, the actual value of λ_1 at 4400 MW load is $-0.3469 + j5.9656$, which is only slightly different from the projected value using eigenvalue sensitivities. Since eigenvalue movement is very nonlinear, the linear approximation is accurate for small parameter change and less accurate for large parameter change. Note that for eigenvalue located in the left half plane, negative $\dot{\sigma}_i$ will result in negative step size, such as λ_{12}. Therefore, it will not be considered for step size control. Table 6.1 shows that at base case, λ_1 determines the optimal step size $s = 42.57$, which corresponds to 4257 MW load increase. We also compared the eigenvalue sensitivity results with the conventional methods using (3.11) or (3.23), both CIS and the conventional methods gave the same results.

From Table 6.1, it can also be seen that some eigenvalues, e.g., $\lambda_{13} = -0.0525 + j0.0982$, although very close to the imaginary axis, their sensitivities are very small. On the other hand, λ_1 has much bigger sensitivity though it is far away from the imaginary axis. Considering eigenvalue sensitivities, λ_1 is better than λ_{13} to be chosen as a critical eigenvalue, even λ_{13} is closer to the imaginary axis than λ_1. Therefore, it is not reliable to use only the eigenvalue locations to determine the critical eigenvalues. A natural and reasonable choice is to use eigenvalue sensitivities as guiding principle in the selection of critical eigenvalues. The selection criterion of critical eigenvalues should be based on the location, moving direction,

and movement speed of the eigenvalues of interest.

It should be pointed out that although eigenvalue λ_{13} is very small and appears to be zero eigenvalue of the system due to the redundant state variables (such as no angle reference, etc.). As we know, the zero eigenvalues may appear as very small eigenvalues since they might not be calculated exactly because of mismatches in the power flow solution and the limited accuracy of eigenvalue calculation algorithm [78]. In the eigenvalues result, since we have chosen one of the machines as angle reference and express the angle changes of all other machines with respect to this reference machine. The redundancy in rotor angle states as well as the zero eigenvalue is eliminated. Further modal analysis on λ_{13} shows that it is a mode corresponding to rotor speed and angle of all the ten generators as a whole part. In other words, it is a very low frequency mode involving all the generators in the system. The low frequency is caused by the big inertia constant related to the generator G1 at bus 39. It is an equivalent generator of the USA-Canada interconnected system. Its dynamic behavior approaches that of an infinite bus due to its own low impedance and high inertia characteristics which lead to low frequency mode.

After ranking the eigenvalues using $-\sigma/\dot{\sigma}$ as in (6.1), the next step is to determine the number of eigenvalues to be traced by ICIS. If we trace more eigenvalues, the effect of critical eigenvalue shift can be ignored. But at the same time, it will increase the computation cost, since it is proportional to the number of traced eigenvalues. There should be a trade-off in the number selection to balance between the speed and the efficiency. From Table 6.1, it can be seen that there is a relatively big difference in the step sizes between the first six eigenvalues $(\lambda_1, \lambda_2, \ldots, \lambda_6)$ and other rightmost eigenvalues $(\lambda_7, \lambda_8, \ldots, \lambda_{14})$. As a result, we trace the first six eigenvalues to identify the oscillatory stability margin.

Fig. 6.3 shows the real parts of all the six eigenvalues at each continuation iteration during the tracing process with step size control. Fig. 6.4 shows the eigenvalue movement in the complex plane during the iterative process. Fig. 6.5 shows the system load change during the iterative process. Each iteration number is highlighted by different symbol. The algorithm takes only four iterations to converge to the oscillatory stability boundary point, where the

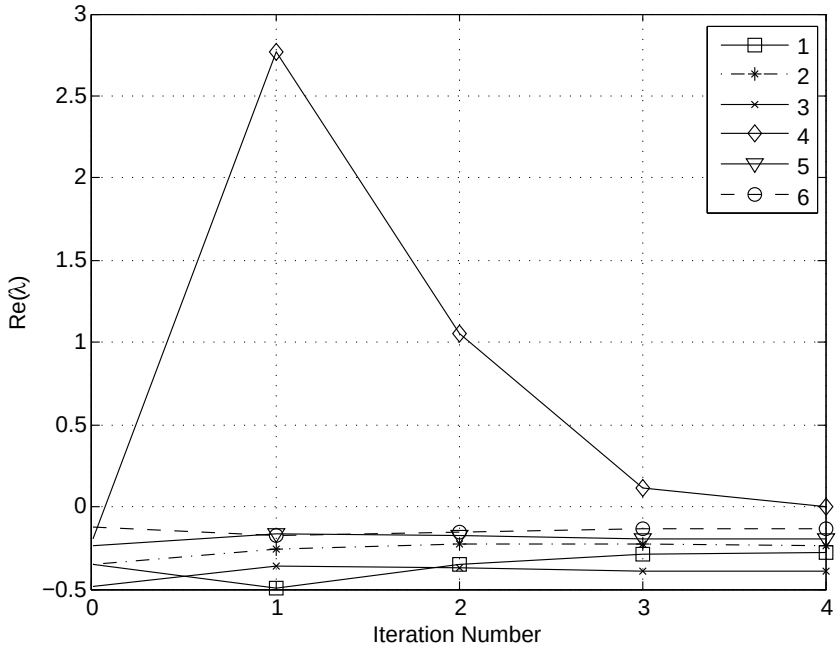

Figure 6.3 Eigenvalues Real Parts during the Iterative Process.

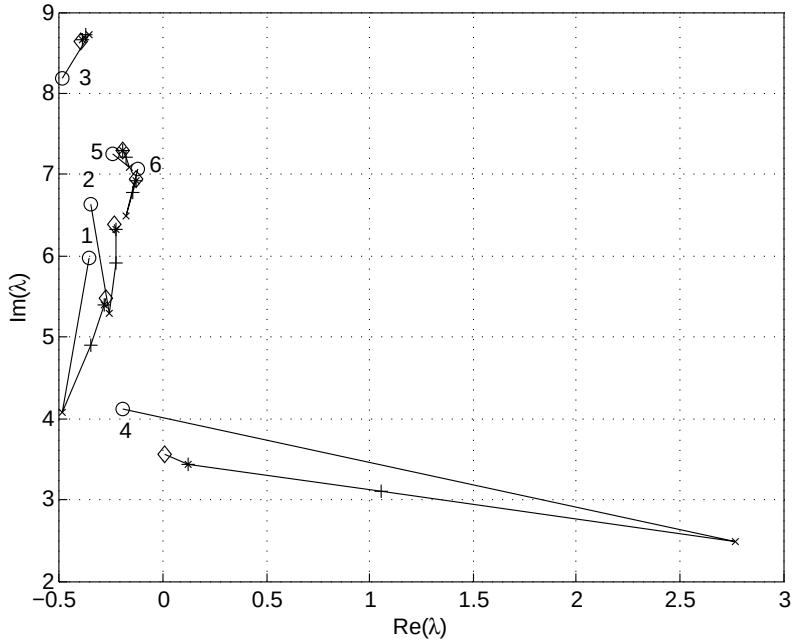

Figure 6.4 Eigenvalues Movement during the Iterative Process.

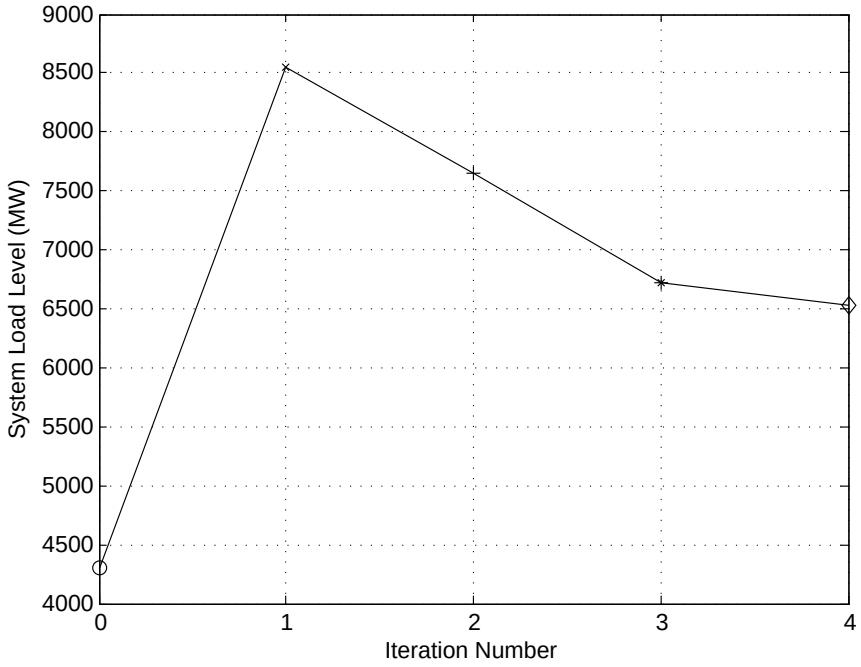

Figure 6.5 System Load Level Change during the Iterative Process.

critical eigenvalue is $\lambda_4 = 0.0004 + j3.5532$. Compared with Table 6.1, it can be observed that the critical eigenvalue changes from λ_1 at base case to λ_4 after the first iteration. The integration-based method will not be able to capture the critical eigenvalue change easily, since only the ranked number one eigenvalue is traced at a time [39]. The final load level is 6536 MW, which is 52% load increase compared with the base case. The exact oscillatory stability margin is 6526 MW. The difference is 10 MW, which is only 0.15% compared with the actual margin value. The ICIS method takes only four iterations to accurately identify the oscillatory stability margin.

To illustrate the effect of different initial points on the number of iterations, we choose another base case, where the total load is 614 MW. Although this load condition is impractical for the system, it is useful to test the convergence of the algorithm. Since the load level is very low at the base case, we select a bigger real part criterion for the rightmost eigenvalues calculation. Table 6.2 gives the sixteen complex eigenvalues with the real parts greater than -1. The eigenvalues sensitivities from the predictor and the corresponding step sizes are also

Table 6.2 Rightmost Eigenvalues and Their Sensitivities at 614 MW Load

No.	λ_i	$\partial\sigma_i/\partial p$	$-\sigma_i/\dot{\sigma}_i$
1	$-0.7242 \pm j1.1424$	1.1067E-2	65.44
2	$-0.5954 \pm j0.4021$	8.6522E-3	68.81
3	$-0.9656 \pm j5.6576$	1.3259E-2	72.83
4	$-0.2744 \pm j4.0656$	2.0289E-3	135.2
5	$-0.3609 \pm j6.6533$	2.1570E-3	167.3
6	$-0.1679 \pm j7.1878$	9.5579E-4	175.7
7	$-0.7555 \pm j0.3687$	4.2862E-3	176.3
8	$-0.6588 \pm j0.5223$	2.2707E-3	290.1
9	$-0.5683 \pm j0.7362$	1.8859E-3	301.3
10	$-0.6280 \pm j0.4088$	2.0163E-3	311.4
11	$-0.6859 \pm j0.5766$	1.7563E-3	390.5
12	$-0.2547 \pm j6.1023$	-4.9348E-3	-51.61
13	$-0.2342 \pm j5.7371$	-2.0870E-3	-112.2
14	$-0.2726 \pm j6.2658$	-2.8058E-4	-971.5
15	$-0.7725 \pm j1.3083$	-6.5960E-4	-1171
16	$-0.05245 \pm j0.09891$	-1.2141E-6	-4.320E4

shown in the table. The schematic figure of the eigenvalue locations and their sensitivities are plotted in Fig. 6.6. Similarly, after ranking these eigenvalues using $-\sigma/\dot{\sigma}$, we choose the first seven eigenvalues (λ_1, λ_2, ..., λ_7) as the critical eigenvalues based on their locations and sensitivities, and then use ICIS to trace them.

In order to reduce the linear estimation error, the maximum step size is restricted to 5000 MW for each iteration. Figs. 6.7 and 6.8 show the eigenvalues movement and the system load change during the iterative process, respectively. It takes only six iterations for the algorithm to converge to the boundary point, where the critical eigenvalue is $\lambda_4 = -0.0022 + j3.5627$. We can see that the critical eigenvalue shifts from λ_1 to λ_4 at the second iteration, since the critical eigenvalue is $\lambda_1 = -0.7242 + j1.1424$ at the base case. The final load level is 6522 MW. The error is 4 MW, which is only 0.06%. It can be seen that although the base load level is much far away from the oscillatory stability margin, it only takes two more iterations compared with

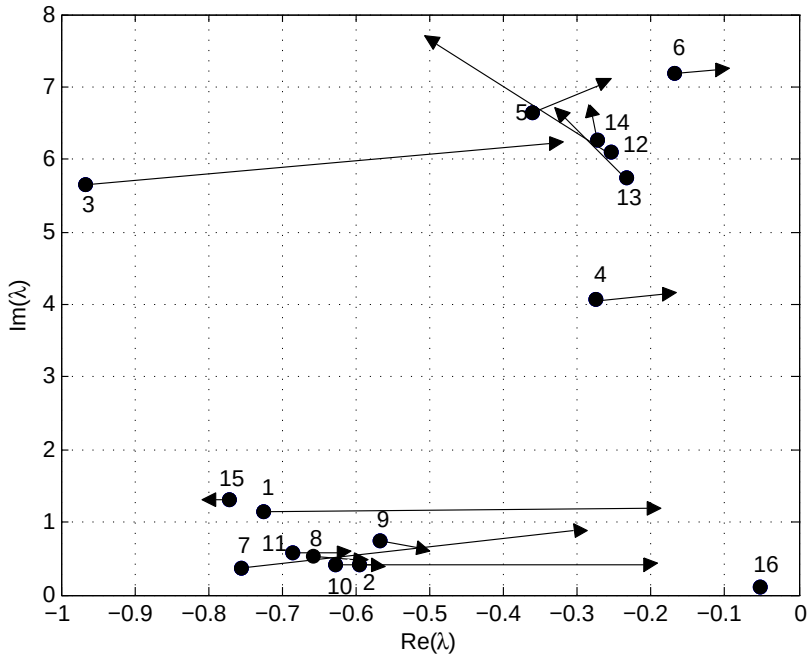

Figure 6.6 Rightmost Eigenvalues and Eigenvalue Sensitivities.

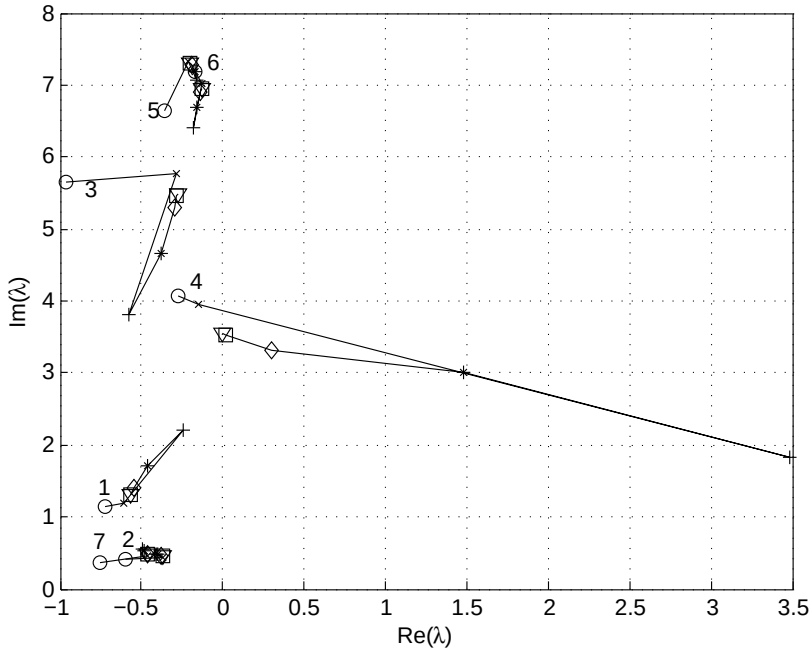

Figure 6.7 Eigenvalues Movement during the Iterative Process.

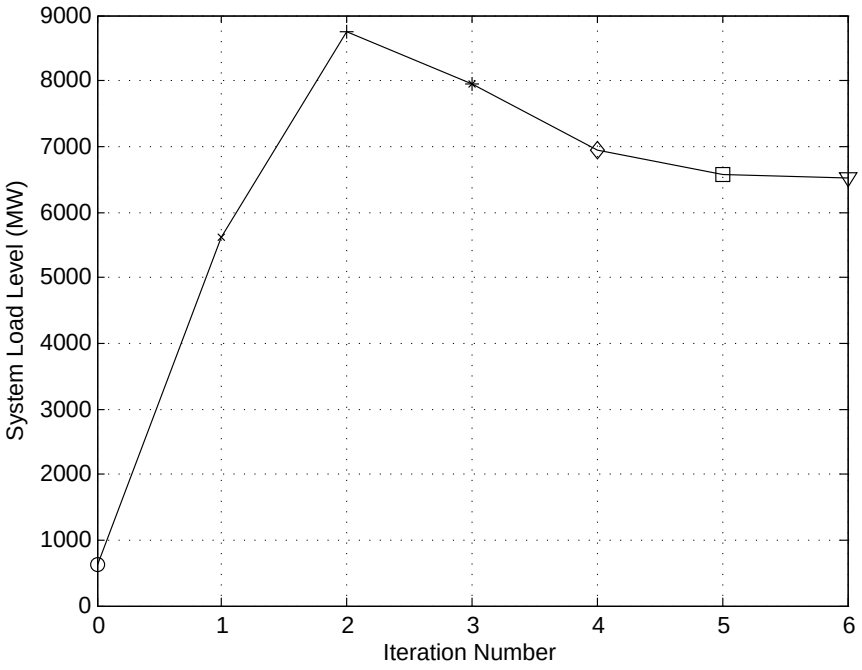

Figure 6.8 System Load Level Change during Oscillatory Stability Margin Identification.

the previous scenario. The proposed method is very efficient to identify the stability margin boundary. The efficiency of the algorithm comes from the quadratic convergence of step size control once the critical eigenvalue is determined.

6.3.1.2 Damping Margin Identification

Table 6.3 shows the results of nine least damping ratio eigenvalues with damping ratio less than 20% at the base case using the "semi-complex" Cayley transform, where the total load is 614 MW. The damping ratio of each eigenvalue and its sensitivity are also shown in Table 6.3.

Suppose we want to identify the damping margin with a damping ratio minimum limit $\zeta_c = 1\%$. We rank these nine least damping ratio eigenvalues by their corresponding step sizes. The first six eigenvalues are selected to identify the damping margin based on their initial damping ratios and the corresponding step sizes s_i. The maximum step size limit is chosen as 5000 MW. Fig. 6.9 shows the system load change during the tracing process. Fig. 6.10

Table 6.3 Least Damping Ratio Eigenvalues and Their Sensitivities at 614 MW Load

No.	λ_i	$\zeta_i(\%)$	$\partial\zeta_i/\partial p$	s_i
1	$-0.9656 + j5.6576$	16.82	−2.5674E-3	61.64
2	$-1.3762 + j7.3609$	18.38	−2.4194E-3	71.83
3	$-1.0154 + j6.8708$	14.62	−1.5179E-3	89.73
4	$-0.2744 + j4.0656$	6.73	−5.3398E-4	107.4
5	$-0.3609 + j6.6533$	5.42	−3.9015E-4	113.2
6	$-0.1679 + j7.1878$	2.34	−1.0765E-4	124.1
7	$-0.2726 + j6.2658$	4.35	−3.1536E-5	1061
8	$-0.2547 + j6.1023$	4.17	5.9545E-4	−53.24
9	$-0.2342 + j5.7371$	4.08	2.2530E-4	−1367

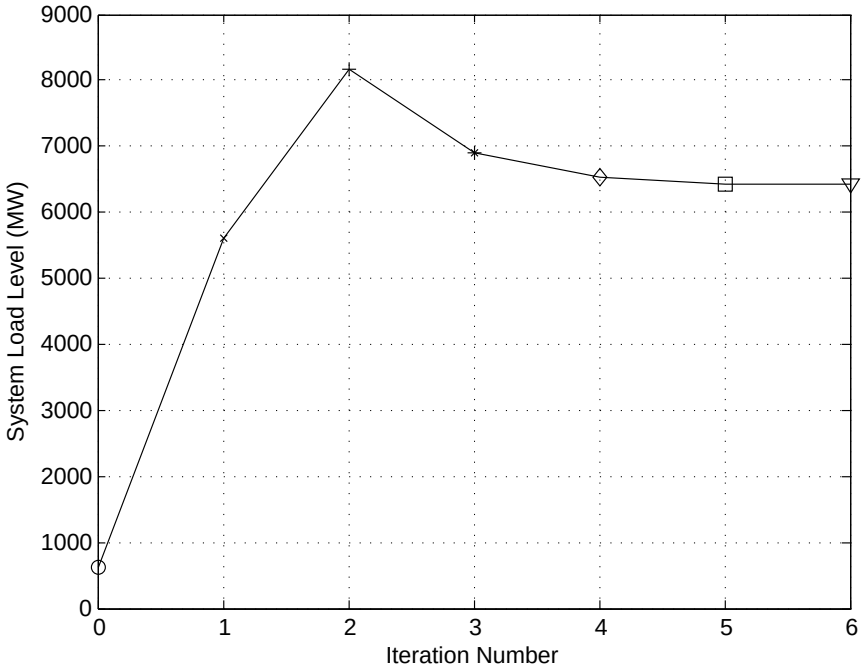

Figure 6.9 System Load Level Change during Damping Margin Identification.

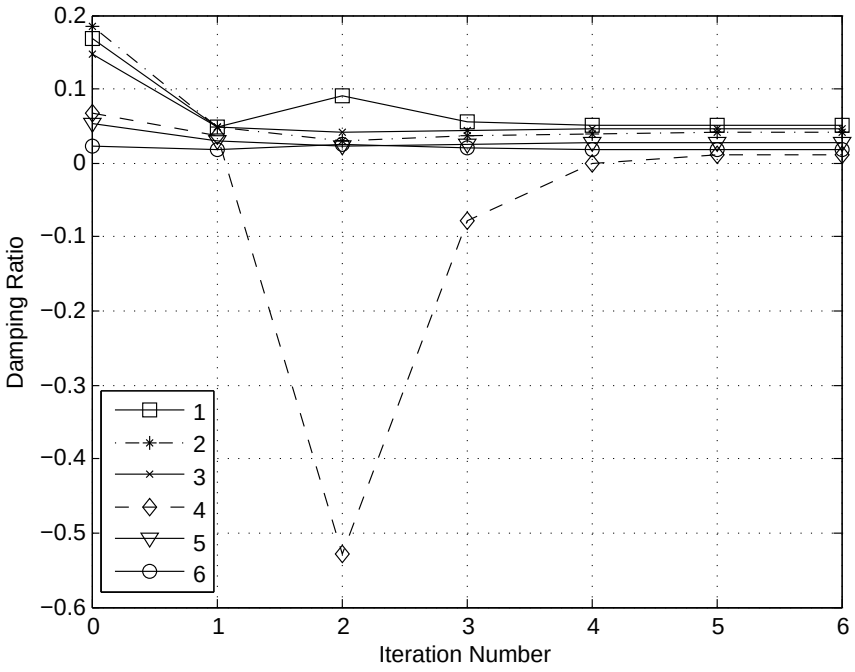

Figure 6.10 Damping Ratios of Tracing Eigenvalues during the Iterative Process.

gives the change in damping ratios of tracing eigenvalues in each iteration. The algorithm takes six iterations to converge to the damping margin. The critical eigenvalue at the damping margin boundary is $\lambda_4 = -0.0361 + j3.6167$ and its damping ratio is 0.997%. The system load level at damping margin boundary is 6436 MW. At the base case, the critical eigenvalue is $\lambda_6 = -0.1679 + j7.1878$ with damping ratio $\zeta = 2.34\%$. With the increase in load level, λ_4 has the smallest damping ratio and is successfully captured during the iterative process. The exact damping margin is 6435 MW. So the difference is only 1 MW.

In the computation cost comparison, we compared the performance of the proposed method with the integration-based method in [39], and repeated eigenvalue calculation. All the methods are implemented in MATLAB environment and tested for the same case. The simulations are performed on a computer with Intel Core 2 Duo 2.40 GHz processor and 3.00 GB of RAM. In the repeated eigenvalue calculation, first the eigenvalues are calculated by Arnoldi method at each step, then the eigenvalue sensitivities calculated from (3.11) provide the optimal load

change in (6.1) for the next calculation. The simulation performance is shown in Table 6.4. In the results, the average computational time to identify the oscillatory stability margin and damping margin is given for all of the three methods. From the computation cost perspective, the ICIS method is faster than both the integration-based method and repeated calculation by the conventional method in the margin identification.

Table 6.4 New England System Simulation Performance

	Oscillatory Stability Margin	Damping Margin
Average Time of ICIS with Sensitivity (s)	2.968	2.334
Average Time of Integration-Based Method (s)	6.145	5.046
Average Time of Repeated Eigenvalue Calculation (s)	3.794	2.606

6.3.2 IEEE 50-Generator, 145-Bus System

The system is a slightly modified version of the IEEE 50-generator system that was developed as a benchmark for stability studies [91]. Seven of the generators are represented by the two-axis model and IEEE AC-4 exciters, whereas the rest of the generators are modeled only with their swing equations. The total number of eigenvalues is 156, in which 112 are complex eigenvalues. The loads are modeled as constant power. The base load level is 16.33 GW. The system load level is chosen as parameter p. The schematic diagram of the system is shown in Appendix B. Two scenarios are studied in the simulation results. Both uniform and nonuniform changes in load at different buses are considered to show the generic formulation of the proposed method.

Scenario I: The load scenario is chosen such that the load at each load bus and generation at each generator bus uniformly increase with the same percentage from the base case loading.

We calculate the rightmost eigenvalues with real parts bigger than -0.25. Fig. 6.11 shows the locations of the five rightmost eigenvalues at base case which are denoted by the symbol "o". After each iteration step, the eigenvalue locations will change and are shown by different

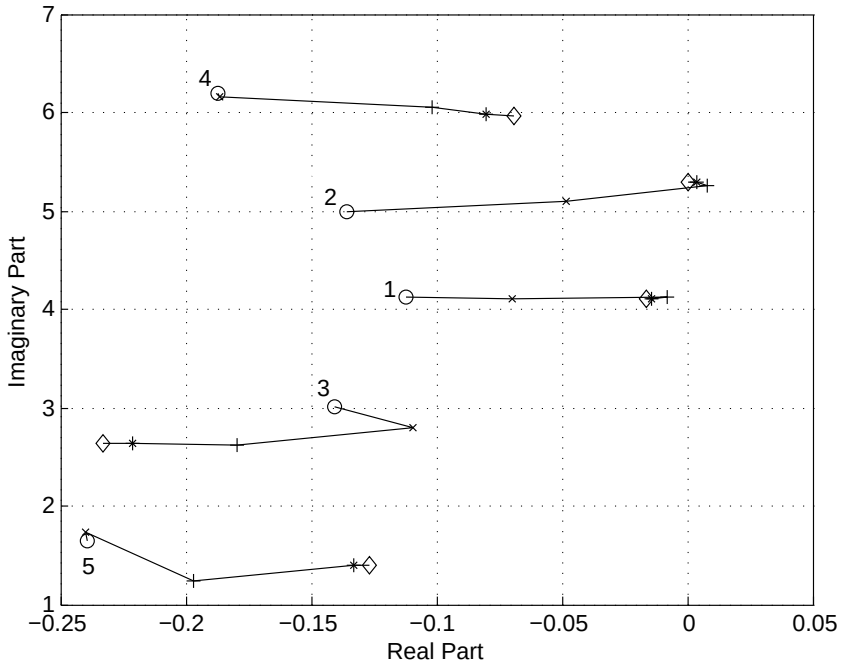

Figure 6.11 Eigenvalue Movements during the Iterative Process.

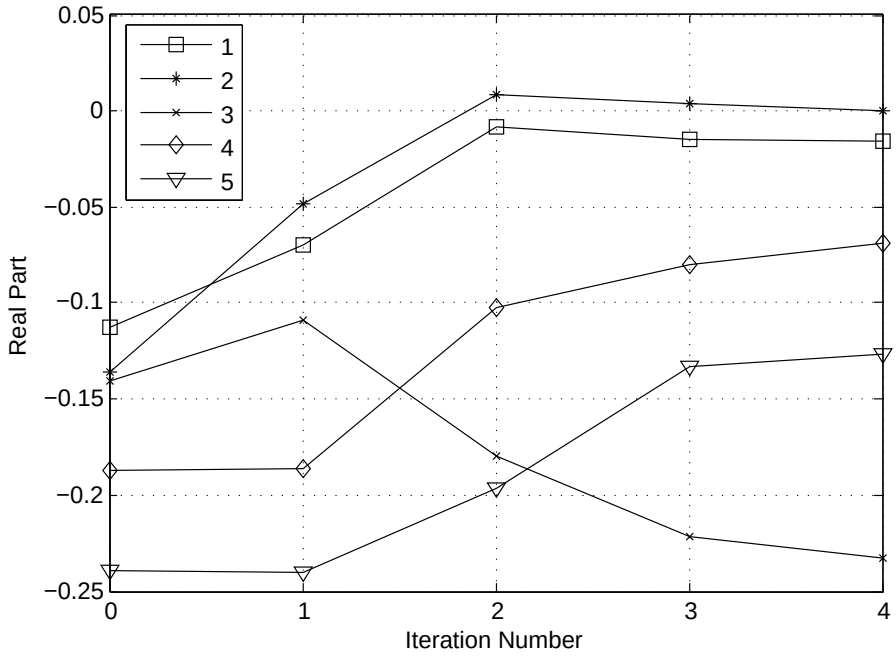

Figure 6.12 Eigenvalues Real Parts during the Iterative Process.

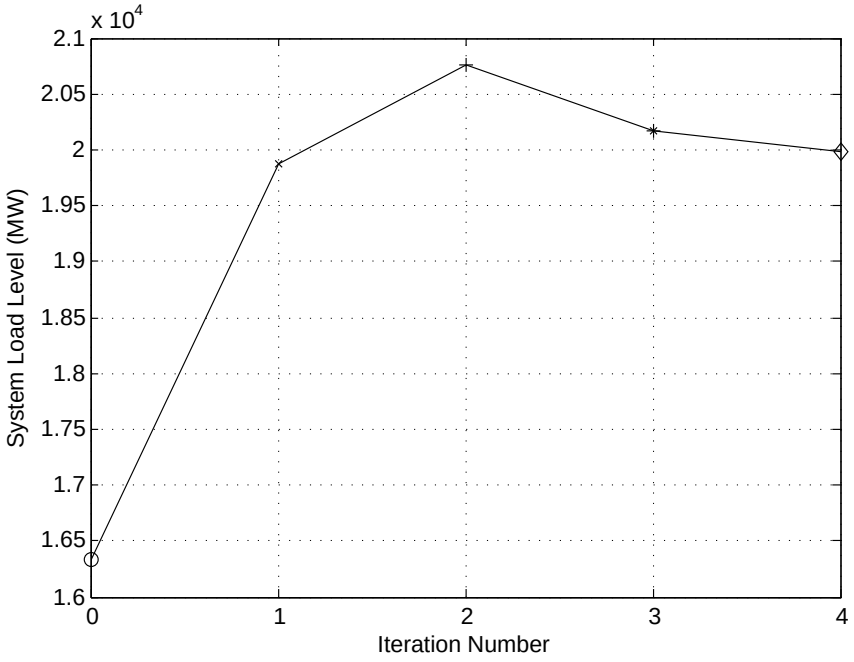

Figure 6.13 System Load Level Change with Uniform Load Increase.

symbols. It roughly shows the eigenvalues trajectory during the iterative process. Fig. 6.12 gives the real parts of the eigenvalues during the iterative process. The algorithm takes four iterations to converge to the oscillatory stability boundary point. The critical eigenvalue switches from λ_1 at base load to λ_2 at the second iteration. Fig. 6.13 shows the system load change. The final load level is 19.99 GW, which is 22.4% load increase compared with the base case.

Scenario II: The load scenario has been chosen with non-uniform changes in load at different buses. Specifically, among the total 64 load buses, only seven load buses are selected for load variation. The total load level of the selected load buses is 3.93 GW. To compensate for the change in load, the generation at each generator bus is increased uniformly by a certain factor.

Fig. 6.14 shows the eigenvalues trajectory during the iterative process. Fig. 6.15 shows the real parts of the eigenvalues during the iterative process. The algorithm takes four iterations to converge. Different from the first scenario, the critical eigenvalue λ_1 does not change during

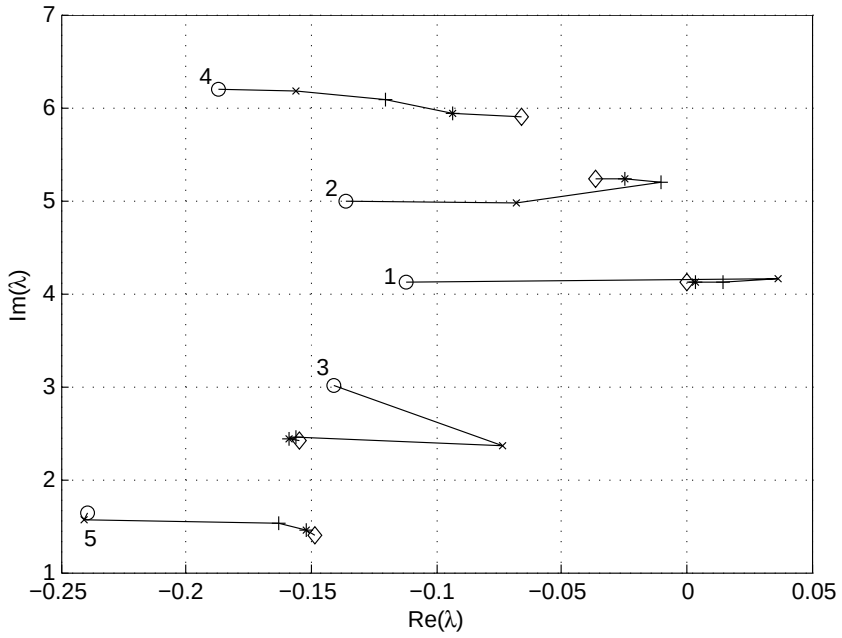

Figure 6.14 Eigenvalue Movements during the Iterative Process.

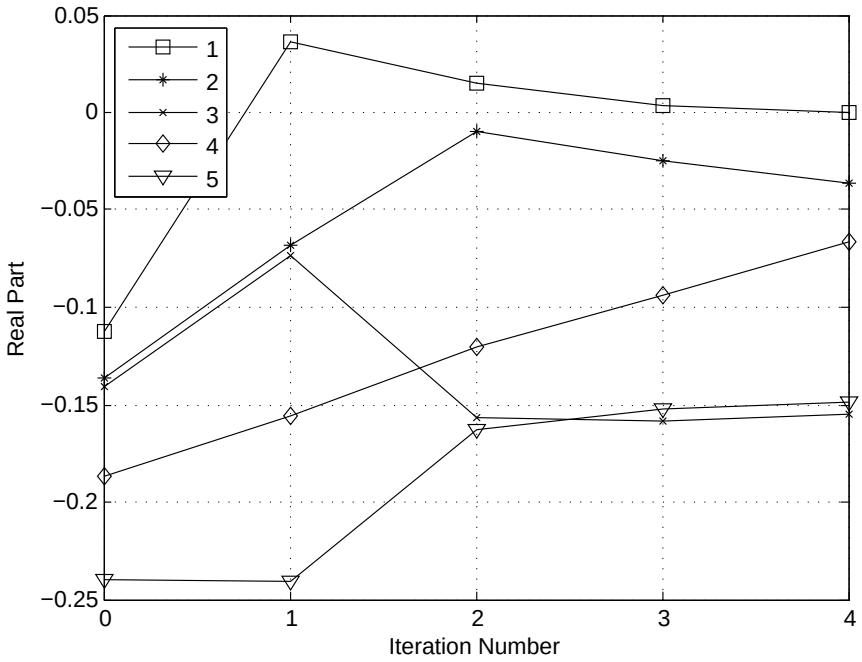

Figure 6.15 Eigenvalues Real Parts during the Iterative Process.

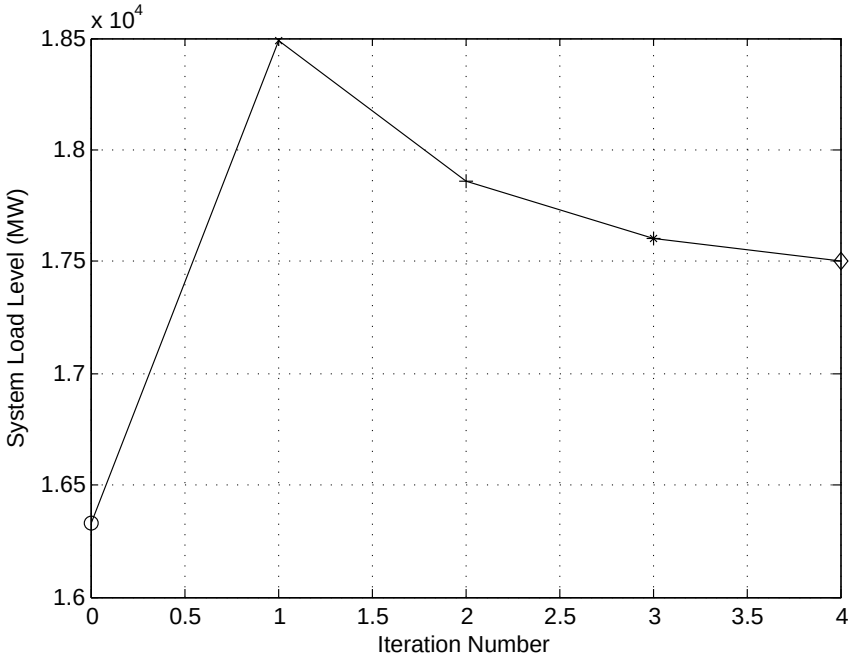

Figure 6.16 System Load Level Change with Nonuniform Load Increase.

the following iterations. Fig. 6.16 shows the system load change. The final load level is 17.50 GW, which is 7.2% total load increase compared with the base case. Specifically, the selected seven load buses have 29.8% load increase while other load buses remain the same level.

Table 6.5 IEEE 145-Bus System Simulation Performance

	Scenario I	Scenario II
Average Time of ICIS with Sensitivity (s)	3.076	3.018
Average Time of Repeated Eigenvalue Calculation (s)	4.742	4.705

The computation performance of the ICIS method and the repeated eigenvalue calculation in both scenarios is shown in Table 6.5. The ICIS method is still faster than the repeated calculation. Furthermore, it is observed from Tables 6.4 and 6.5 that with the increase in system size, the speedup becomes bigger. The ICIS method has the potential to be applied

to very large realistic system, since the computation cost of ICIS is only $\mathcal{O}(rn^2)$, whereas the conventional method takes $\mathcal{O}(n^3)$.

6.4 Conclusion

In this chapter, the eigenvalue sensitivity-based continuation of invariant subspaces is proposed to identify the oscillatory stability margin and the damping margin. The novelty of the work is to successively extract the eigenvalue sensitivities during the ICIS process which can be used for different applications of interest. The sensitivities are very useful in ranking eigenvalues and can also be applied to the design of power system controllers. The determination of the critical eigenvalue is efficiently implemented from the eigenvalue sensitivity information. The ICIS method accelerates the computations of both the eigenvalue and the eigenvalue sensitivity. It is used to trace a specific subset of eigenvalues of interest, and adjust the step size automatically using the eigenvalue sensitivity. With this method, we can identify both the oscillatory stability margin and the damping margin efficiently and accurately. The generalized Cayley transform and "semi-complex" Cayley transform are used to calculate a small subset of eigenvalues of interest for the ICIS initialization. The numerical results on the New England 39-bus system and IEEE 145-bus system are described to verify the effectiveness of the algorithm. Results have shown that the ICIS method is an accurate, fast, and robust method in eigenvalue calculation and margin identification.

CHAPTER 7. EQUILIBRIUM POINT TRACING AND EIGENVALUE ANALYSIS WITH THE PROPOSED METHOD

7.1 Introduction

In the previous chapters, we always assume that the matrices $A(p)$ in (3.3) are available analytically. In reality, the calculation of $A(p)$ includes two steps: calculate the equilibrium point for a given parameter p, and evaluate the Jacobian matrix $A(p)$ at the given value. For the second problem, there are different differentiation algorithms to efficiently obtain the derivatives of a DAE system, such as the automatic differentiation package (ADIFOR) [92]. For the first problem, the equilibrium point requires the calculation of the solution for the nonlinear system in (2.20), assuming the differential part equals to zero, i.e., $\dot{x} = 0$. The system has $(m + n)$ nonlinear equations with the same amount of unknowns (x, y) for any given p. Currently, there are three approaches to calculate the equilibrium points which are summarized as follows:

1. Integration method: This method uses certain integration method to integrate the DAE system (2.20) until the system reaches the steady state. By definition, this computation method produces the correct equilibrium point information. However, this is a very expensive method to compute since the time-domain simulation of power system is very costly. Another issue is that if the system is not stable at the equilibrium, then the time-domain simulation will not converge. The integration method will fail in this case.

2. Alternative iteration: This approach decomposes the nonlinear system to power flow equations and generator equations, and then applies alternative iteration to calculate the two parts separately until it converges. It is also called two-step procedure in [64].

The method has the advantage that existing commercial power flow software can be used. The algorithm can easily be implemented with the combination of existing commercial software code. The equations for each generator are decoupled and hence can be solved by a very low-order solution program. The disadvantage is that the number of iterations might be large depending on the selection of starting point. Consequently, the obtained equilibrium solution is very dependent on the assumed values for the PV buses and slack bus. The two-step approach has to be repeatedly performed by adjusting the assumed voltages and generators output based on a trial and error procedure. Furthermore, the iterative process might not converge under heavy load condition.

3. Simultaneous iteration: The method applies Newton's method or other methods to directly solve the full set of algebraic equations (3.1) obtained by setting the time derivatives of the dynamic model to zero. It simultaneously solves the system DAEs to obtain the equilibrium points. The assumptions of PV and slack buses are no longer needed.

In [64], the *equilibrium point tracing* (EQPT) approach is proposed to trace the equilibrium points as well as identify the voltage collapse point related to the saddle-node bifurcation. The saddle-node bifurcation is caused by the singularity of Jacobian matrix $A(p)$ in (3.3). Similar to CPF [62], the continuation method is applied to calculate system equilibrium manifold defined by (3.1). During the predictor-corrector procedure, the singularity of the augmented Jacobian matrix which includes $A(p)$ can be easily avoided by appropriately selecting the continuation parameter.

During the ICIS process, we apply the simultaneous iteration using Newton's method to calculate the equilibrium points with respect to parameter variation. This is particularly annoying when the value of parameter p is constantly changing as shown in Chapter 5. Furthermore, near the voltage collapse point where the Jacobian $A(p)$ becomes singular, Newton's method converges slowly or even does not converge because of the singularity problem. Noticing the continuation method can be applied to the calculation of both equilibrium points and invariant subspaces, in order to avoid such nested iterations and coordinate different step size controls for these two problems [36, 93], a continuation-based unified approach which com-

bines the equilibrium point tracing and critical eigenvalues tracing is proposed in this chapter. It is called simultaneous branch following in [36] which is the coupling of invariant subspace continuation and nonlinear equilibrium branch continuation. The detailed description of the algorithm is given in the following section.

7.2 Continuation-Based Equilibrium Point Tracing and Critical Eigenvalue Tracing

Considering both (3.1) and (4.5), the equation set for the new combined problem has the form

$$S(\Phi, \Omega, \Lambda, x, y, p) = \begin{bmatrix} F(x, y, p) \\ T(\Phi, \Omega, \Lambda, p) \end{bmatrix} = 0 \tag{7.1}$$

where

$$F(x, y, p) = \begin{bmatrix} f(x, y, p) \\ g(x, y, p) \end{bmatrix} = 0 \tag{7.2}$$

$$T(\Phi, \Omega, \Lambda, p) = \begin{bmatrix} f_x(p)\Phi(p) + f_y(p)\Omega(p) - \Phi(p)\Lambda(p) \\ g_x(p)\Phi(p) + g_y(p)\Omega(p) \\ \widehat{\Phi}^T\Phi(p) - I_r \end{bmatrix} = 0. \tag{7.3}$$

$T(\Phi, \Omega, \Lambda, p)$ in (7.3) is the same as (4.5), and $F(x, y, p)$ in (7.2) is the same as (3.1). In (7.1), there are totally $((m+n)(r+1)+r^2)$ equations and the same number of unknowns for $(\Phi, \Omega, \Lambda, x, y)$. The equation set can be solved by the continuation method along the parameter path. The predictor-corrector techniques are applied to (7.1). Notice that the first $(m+n)$ equations do not depend on (Φ, Ω, Λ), so (7.2) and (7.3) can be solved in sequence separately in both the predictor and corrector.

In the prediction stage, the tangent vector (dx, dy, dp) at p_0 is solved from

$$\begin{bmatrix} f_x(p_0) & f_y(p_0) & f_p(p_0) \\ g_x(p_0) & g_y(p_0) & g_p(p_0) \\ & e_k & \end{bmatrix} \begin{bmatrix} dx \\ dy \\ dp \end{bmatrix} = \begin{bmatrix} 0 \\ 0 \\ \pm 1 \end{bmatrix} \tag{7.4}$$

where e_k is a unit row vector with all of the elements equal to zero except for the kth one, which corresponds to the current continuation parameter. The sign on the right hand side indicates the direction of the predictor and $+1$ is used when the operating point is on the upper branch of the solution curve. Generally, the load parameter p is chosen as the continuation parameter, hence we have $k = m + n + 1$.

Assume $(H_0, L_0, \Delta_0) = (\dot{\Phi}(p), \dot{\Omega}(p), \dot{\Lambda}(p))$ which is the tangent to $(\Phi(p), \Omega(p), \Lambda(p))$ at p_0, it can be solved from

$$\begin{bmatrix} f_x(p_0)H_0 - H_0\Lambda_0 + f_y(p_0)L_0 - \Phi_0\Delta_0 \\ g_x(p_0)H_0 + g_y(p_0)L_0 \\ \widehat{\Phi}^T H_0 \end{bmatrix} = \begin{bmatrix} -\dot{f}_x(p_0)\Phi_0 - \dot{f}_y(p_0)\Omega_0 \\ -\dot{g}_x(p_0)\Phi_0 - \dot{g}_y(p_0)\Omega_0 \\ 0 \end{bmatrix}. \tag{7.5}$$

After all of the tangents have been found, the prediction can be made as

$$\begin{bmatrix} \bar{x}_1 \\ \bar{y}_1 \\ \bar{p}_1 \\ \Phi_1 \\ \Omega_1 \\ \Lambda_1 \end{bmatrix} = \begin{bmatrix} x_0 \\ y_0 \\ p_0 \\ \Phi_0 \\ \Omega_0 \\ \Lambda_0 \end{bmatrix} + s \begin{bmatrix} dx \\ dy \\ dp \\ dpH_0 \\ dpL_0 \\ dp\Delta_0 \end{bmatrix} \tag{7.6}$$

where s is an appropriate step size.

Once the prediction is made with the tangent, the following correction is performed to find the equilibrium point

$$\begin{bmatrix} f_x(\bar{p}_1) & f_y(\bar{p}_1) & f_p(\bar{p}_1) \\ g_x(\bar{p}_1) & g_y(\bar{p}_1) & g_p(\bar{p}_1) \\ & e_k & \end{bmatrix} \begin{bmatrix} \Delta x \\ \Delta y \\ \Delta p \end{bmatrix} = \begin{bmatrix} f(\bar{x}_1, \bar{y}_1, \bar{p}_1) \\ g(\bar{x}_1, \bar{y}_1, \bar{p}_1) \\ 0 \end{bmatrix} \tag{7.7}$$

$$\begin{bmatrix} x_1 \\ y_1 \\ p_1 \end{bmatrix} = \begin{bmatrix} \bar{x}_1 \\ \bar{y}_1 \\ \bar{p}_1 \end{bmatrix} + \begin{bmatrix} \Delta x \\ \Delta y \\ \Delta p \end{bmatrix}. \tag{7.8}$$

The Newton iteration process (7.7) and (7.8) will be repeated until it converges. The technique used in the corrector to calculate the equilibrium point is called local parameterization,

where the original set of equations is augmented by one equation specifying the value of one of the unknowns (usually load parameter p). Since f_p and g_p cannot be null vectors at the same time, the singularity of the augmented Jacobian matrix can be avoided by appropriately choosing the continuation parameter.

After the corrector for the equilibrium point calculation is converged, we use the solution (x_1, y_1, p_1) for the calculation of invariant subspaces in the corrector. The corrector step for the invariant subspace is

$$\begin{bmatrix} f_x(p_1)\Phi_{k+1} - \Phi_{k+1}\Lambda_k + f_y(p_1)\Omega_{k+1} - \Phi_k\Lambda_{k+1} \\ g_x(p_1)\Phi_{k+1} + g_y(p_1)\Omega_{k+1} \\ \Phi_0^T\Phi_{k+1} \end{bmatrix} = \begin{bmatrix} -\Phi_k\Lambda_k \\ 0 \\ I_r \end{bmatrix}. \tag{7.9}$$

It can be seen that the linear systems arising during the predictor and corrector steps of (7.1) can be reduced to solve

1. Three linear systems with a bordering of $D_{x,y}F$ as in (7.4) and (7.7);

2. Three linear systems with a bordering of $D_{\Phi,\Omega,\Lambda}T$ as in (7.5) and (7.9).

Both (7.5) and (7.9) will be solved by the bordered Bartels-Stewart algorithm as described in Chapter 4. As for (7.4) and (7.7), the traditional approach is to use the LU factorization to decompose the augmented Jacobian matrix, and then solve the linear system in two steps. This is easy if both the Jacobian $A(p)$ and the augmented Jacobian matrix are well conditioned. But as pointed out in [94], as the load increases close to the collapse point, $A(p)$ is a nearly singular matrix so that a naive block elimination strategy to solve (7.4) or (7.7) leads to big errors. Although this is often acceptable since (7.7) is solved only to compute the Newton corrections. But of course this does not lead to very robust algorithm. A particular method, called *block elimination mixed* (BEM) method, was developed by Govaerts [94] to overcome this problem. This method can also be used to solve the bordered systems when using the bordered Bartels-Stewart algorithm to solve (7.5) and (7.9) to improve the robustness and stability of the computation.

7.3 Bifurcation Analysis and Voltage Collapse

7.3.1 Critical Eigenvalue Tracing and Bifurcation Analysis

During the continuation process, we can choose any pre-defined set of critical eigenvalues to trace. The only thing we need to do is to initialize and update the invariant subspaces corresponding to the critical eigenvalues. Section 4.3 in Chapter 4 describes the initialization of rightmost and least damping ratio eigenvalues tracing. The tracing of least damping ratio eigenvalues gives the system damping change when parameter varies and furthermore, can be used to determine the damping margin for any given scenario. The rightmost eigenvalues provide the system stability change during the parameter variation. Hopf bifurcation is the most common bifurcation in power systems. It is related to the oscillatory stability margin. The oscillatory stability margin boundary corresponds to the point where HB happens. The bifurcation analysis can be performed from the rightmost eigenvalues tracing. The oscillatory stability margin can be determined from the rightmost eigenvalues.

It should be mentioned that the least damping ratio eigenvalues and the rightmost eigenvalues can be combined together and traced simultaneously.

7.3.2 Voltage Stability Margin Identification

The voltage collapse is caused either by saddle-node bifurcation when the system Jacobian becomes singular [64], or limit-induced bifurcation due to a generator hitting its field or armature current limit [95]. Instead of solving the equilibrium point separately by the two-step approach, we simultaneously solve the system DAEs to obtain the dynamic state variables x and the static algebraic variables y (bus voltage magnitudes and angles). The generator field and armature current limits can be explicitly considered in the framework. The continuation method is the bridge to link between the equilibrium points tracing and critical eigenvalues tracing.

During the continuation process, the critical point representing the voltage stability margin can be identified. This can be done easily because the critical point is the point at which maximum loading ($p_{\max}$) occurs before decreasing. Since parameter p is introduced to param-

eterize the system generation and load level, it increases monotonically. For this reason, the tangent vector component dp in (7.6) is positive before p reaches its maximum, zero at the critical point, and becomes negative once it passes the critical point. Thus, the sign of the dp component can be used to determine whether the critical point has been passed or not.

Furthermore, the rightmost real eigenvalues can be considered as an index to measure the distance to the voltage collapse point. The stability of an equilibrium point of the DAE system depends on the eigenvalues of the unreduced Jacobian $A(p)$. The system will experience a SNB as parameter p increases when $A(p)$ has a zero eigenvalue, i.e., $\det(A) = 0$. Assuming g_y is nonsingular, there is $\det(A) = \det(A_s)\det(g_y)$. The singularity of A_s implies singularity of A. Therefore, we may analyze eigenvalues of A_s to ascertain stability. References [75] and [96] provide an in-depth analysis of the relation between the singularity of g_y and the singularity of A. As the algebraic equation Jacobian g_y is close to singular, its determination becomes very small as it approaches the impasse surface, and consequently it will cause the determination of the reduced Jacobian A_s to become very large due to (3.5). As a result, one of the eigenvalues will tend to infinity. Similarly, on the other side of the impasse surface, the system has also an eigenvalue approaching infinity but with an opposite sign. Therefore, there is a change of system stability properties due to the singularity of the algebraic equation Jacobian. This bifurcation is called *singularity induced bifurcation* [97].

Reference [98] investigated the dynamic aspects of PV curve and pointed out that maximum loadability analysis must include dynamic analysis based on DAE model and not only load flow analysis. Therefore, by tracing the critical eigenvalue of A_s that will cause the singularity of the Jacobian, we cannot only adjust the step size during the continuation method to speed up the voltage stability margin identification, but also identify the cause of the voltage collapse through modal analysis on the critical eigenvalue.

Fig. 7.1 gives the flowchart for equilibrium point tracing and margin boundary identification using the proposed approach.

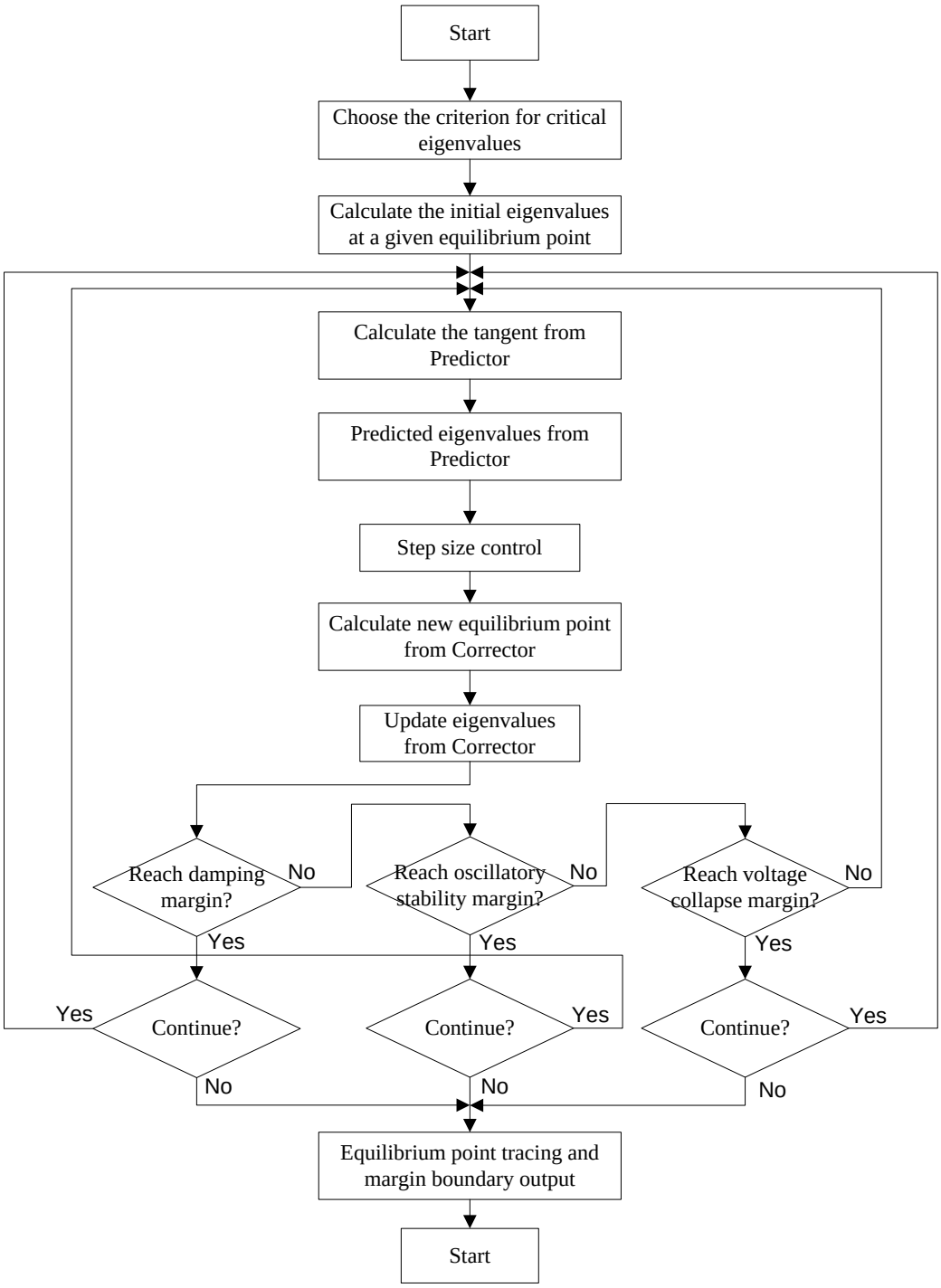

Figure 7.1 Flowchart for Equilibrium Point Tracing and Margin Boundary Identification.

7.3.3 Step Size Adjustment

In order to identify the bifurcation points such as the node-focus bifurcation, limit-induced bifurcation, the step size adjustment is needed. A simple and robust method to determine the bifurcation point is the *binary search* algorithm (also called the bisection search or half-interval search). The binary search is a simple and robust search algorithm which has been widely used in various areas. In [96] and [99], the binary search algorithm is applied to the secure operating limit determination for voltage security assessment. Similar approach is proposed in the thesis to identify the bifurcation-related dynamic security margin. For example, for the identification of NFB point, we are trying to identify the condition under which the critical eigenvalues change from complex to real. Hence, zero value in the imaginary part is the condition of passing the NFB point. The procedure can be described as follows (ϵ is the tolerance):

$p_{k+1} = p_k + s$;

calculate λ_{k+1};

if $Im(\lambda_{k+1}) \neq 0$

    go to next iteration;

else

    $right = p_{k+1}$;

    $left = p_k$;

    do while $(abs(right - left) > 2\epsilon)$;

        midpoint = (right+left)/2;

        calculate $\lambda(midpoint)$;

        if $Im(\lambda(midpoint)) = 0$

            $right = midpoint$;

        else

            $left = midpoint$;

        end if

    loop

end if

Similar process can be used to locate the SIB and NFB points, etc. The voltage stability margin boundary is identified by adjusting the step size according to the tangent vector and the critical eigenvalue information as described in the previous section.

7.4 Simulation Results

The continuation-based equilibrium point tracing and eigenvalue analysis is test on the New England system.

Fig. 7.2 shows the system power-voltage relationships as load changes. The load scenario is the same as described in Subsection 5.2.1. These curves are generally referred to as the PV curves or nose curves. They play a major role in helping understand the voltage stability. Fig. 7.2 shows the voltage magnitudes of six generator buses (buses 30, 33, 36, 37, and 39). The tracing process will stop after the equilibrium point passes the nose point and moves to the lower branch. Fig. 7.3 describes the critical eigenvalues movement. The arrows give the direction of eigenvalues movement as load increases. The symbols '+' and 'o' represent the starting and ending points of the eigenvalue trajectories. Figs. 7.4 and 7.5 show the real and imaginary parts of the critical eigenvalues, respectively. The initial load condition is 4300 MW, which is the same as the scenario in Subsection 6.3.1.1. As we know, the critical modes that will cross the imaginary first are $\lambda_{1,2} = -0.1942 \pm j4.1239$ at the base case. For simplicity, only these two eigenvalues are traced in order to determine the steady state stability of an operating point. The bifurcation points and margin boundaries will be captured as load increases. It should be pointed out that the critical eigenvalue identification by eigenvalue sensitivity as described in Chapter 6 can also by applied here to speed up the process.

We trace the movement of equilibrium point and critical eigenvalues $\lambda_{1,2}$ as load changes. At a loading of 6526 MW, this complex pair of eigenvalues cross over into the right half complex plane. From the eigenvalue sensitivity, we have $\partial \mathrm{Re}(\lambda_{1,2})/\partial p \neq 0$. Since there is no other eigenvalue with zero real part or on the right half plane, the system loses stability due to the occurrence of HB. When load increases to 8830 MW, the complex pair collide and break into two real eigenvalues. This indicates a NFB and is identified by the step size adjustment

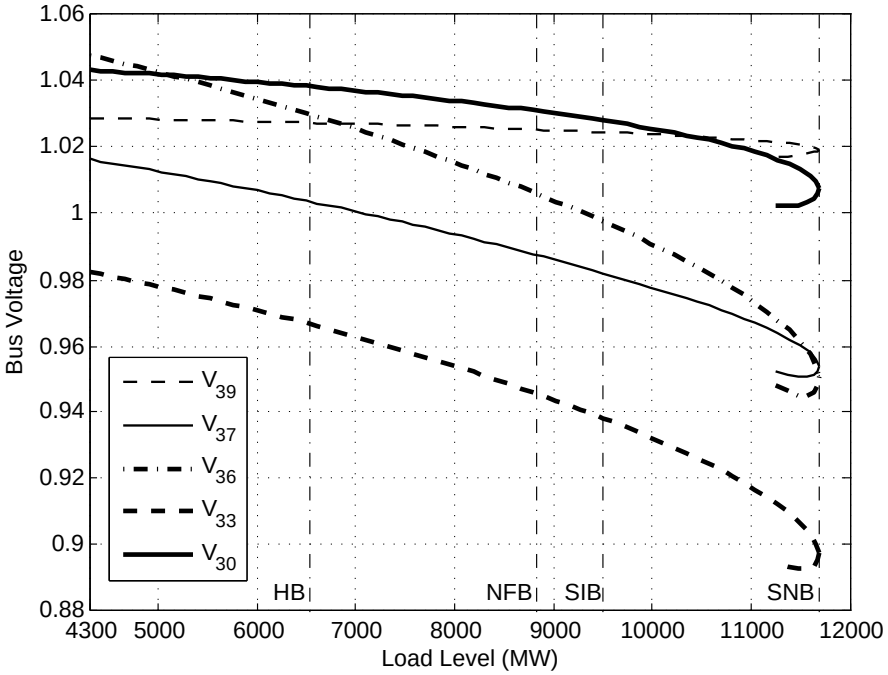

Figure 7.2 PV Curve for the New England System.

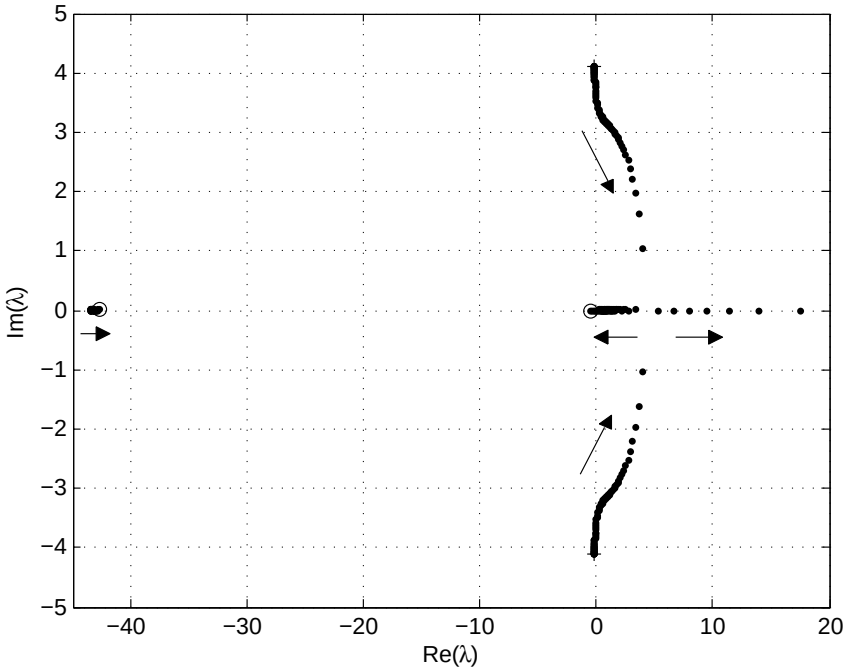

Figure 7.3 Critical Eigenvalues Movement in Complex Plane during Load Increase.

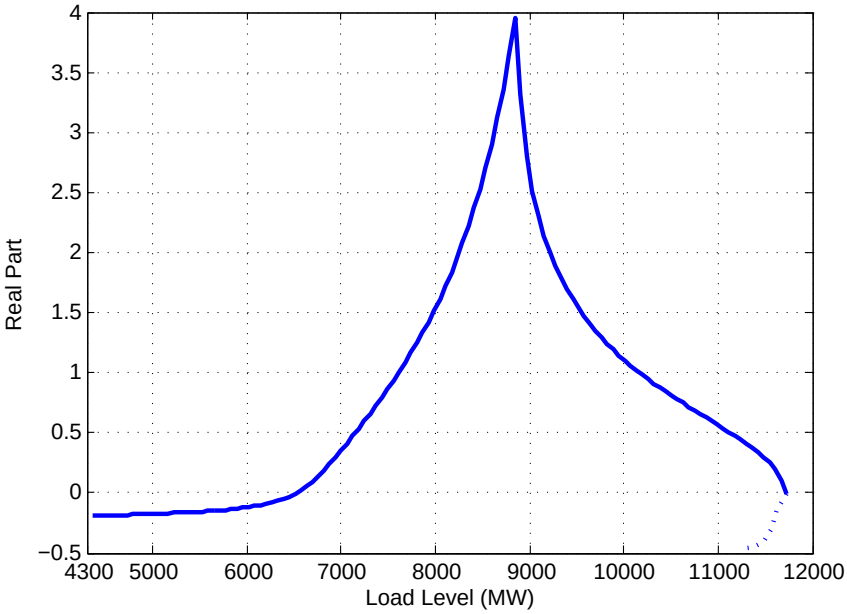

Figure 7.4 Real Parts of the Critical Eigenvalues.

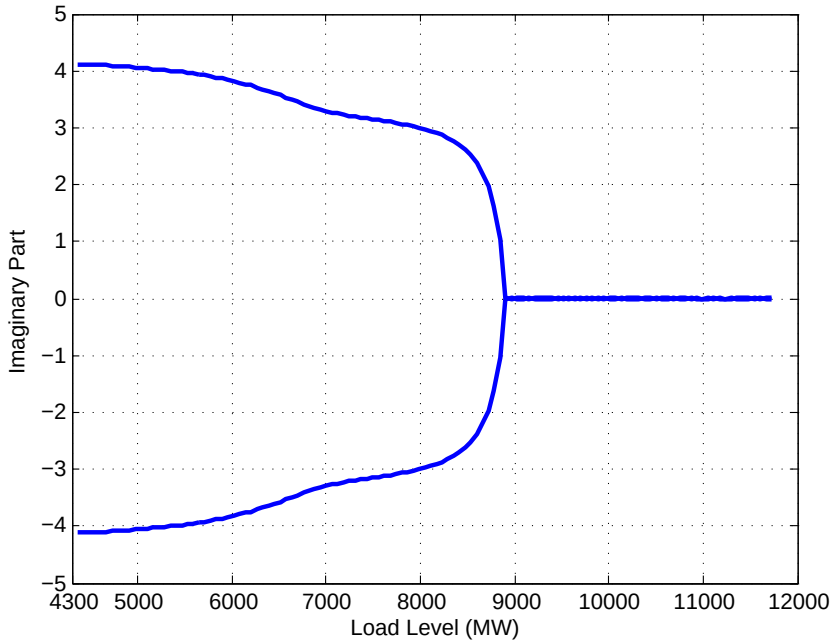

Figure 7.5 Imaginary Parts of the Critical Eigenvalues.

described before. As the load is increased further, one of these two eigenvalues moves further toward positive infinity, and at a loading of 9505 MW, it turns from positive infinity into negative infinity. It indicates a SIB point. At the same time, the other one moves toward the origin, and at 11688 MW loading level, the real eigenvalue becomes zero, which corresponds to the voltage stability margin boundary. The unstable operating region lies between 6526 MW and 11688 MW. With the increase in load from the base case, the system undergoes a sequence of bifurcations namely: HB → NFB → SIB → SNB. These bifurcation points are also shown in Fig. 7.2. All of them have been successfully captured by the proposed method.

7.5 Conclusion

This chapter proposes a continuation-based approach to combine the equilibrium point tracing and eigenvalue tracing for the bifurcation analysis of power systems. EQPT and ICIS are formulated and solved simultaneously in a unified framework using the continuation method. The singularity of the Jacobian at the voltage collapse point and the singularity of the algebraic equation Jacobian at SIB are avoided. Different step size controls can be coordinated in the algorithm to efficiently trace the equilibrium point and critical eigenvalues as well as identify the voltage stability margin.

Bifurcation analysis can be performed during the tracing process to identify various types of bifurcations, such as node-focus, saddle-node, Hopf, limit-induced, and singularity-induced, etc. The proposed approach is a useful tool to investigate the steady state as well as the dynamic behavior of power systems.

CHAPTER 8. CONTRIBUTIONS AND FUTURE WORK

8.1 Contributions

The contributions of the thesis are as follows:

- Proposed an improved continuation of invariant subspaces that has the following properties:
  - Successively extract the eigenvalue sensitivity during ICIS with proper re-initialization;
  - A formal mathematical proof is given to justify the eigenvalue sensitivity that is derived from ICIS. It is also verified by numerical results.
  - An efficient update of invariant subspace for ICIS is proposed.

  The ICIS has the following applications:
  - Track the movement of rightmost eigenvalues, least damping ratio eigenvalues, and a specified subset of eigenvalues;
  - Trace close and multiple eigenvalues to show the advantage of ICIS over conventional methods;
  - Systematic identification of interacting power system dynamic phenomena, such as low-frequency oscillations, subsynchronous resonance, model resonance, and node-focus bifurcation, etc.;
  - Proposed an eigenvalue sensitivity-based algorithm to efficiently identify the oscillatory stability margin and damping margin.
- The ICIS is integrated with the equilibrium point tracing for overall bifurcation analysis in power systems.

- Identification of voltage stability margin and other eigenvalue-related margins with the proposed method;
- A generalized approach for bifurcation analysis to identify various bifurcations in power systems, such as Hopf, saddle-node, node-focus, singularity-induced, etc.

- With these proposed approaches, we can get a novel comprehensive invariant subspace-based framework for power system equilibrium point calculation and small-signal stability analysis.

8.2 Future Work

1. Apply ICIS for SSR analysis on large power system such as a realistic CORPALS benchmark model in [45] to show the effectiveness of the algorithm in big systems.
2. Apply ICIS for the parameter setting of power system stability controller.
3. Apply the parallel computing and sparse matrix techniques in ICIS to further speed up the computation of critical eigenvalues.
4. Implement RPM for the decoupled time-domain simulation and equilibrium point calculation.

APPENDIX A. SCHEMATIC DIAGRAM OF THE NEW ENGLAND 39-BUS SYSTEM

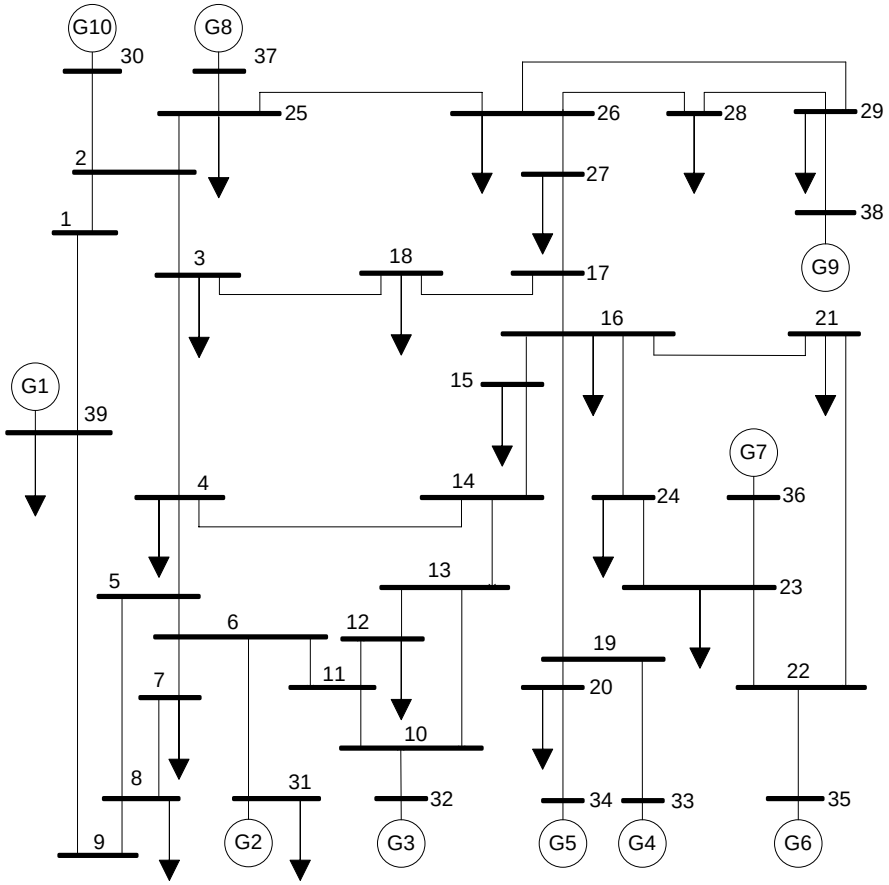

APPENDIX B. THE IEEE 145-BUS SYSTEM

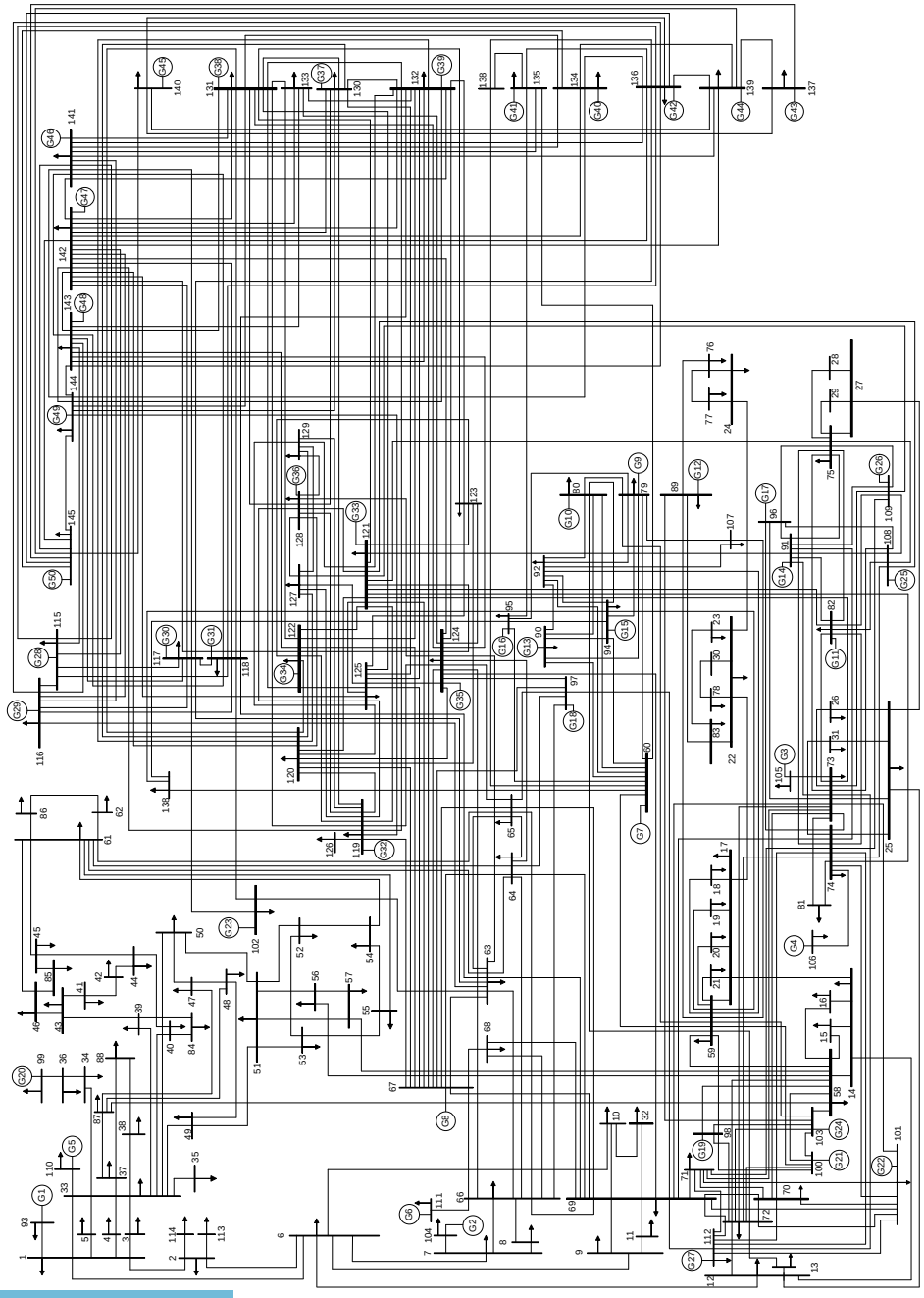

BIBLIOGRAPHY

[1] B. Lee and V. Ajjarapu, "A piecewise global small-disturbance voltage-stability analysis of structure-preserving power system models," *IEEE Trans. Power Syst.*, vol. 10, no. 4, pp. 1963–1971, Nov. 1995.

[2] K. Kim, H. Schättler, V. Venkatasubramanian, J. Zaborszky, and P. Hirsch, "Methods for calculating oscillations in large power systems," *IEEE Trans. Power Syst.*, vol. 12, no. 4, pp. 1639–1648, Nov. 1997.

[3] J. Hauer, D. Trudnowski, G. Rogers, B. Mittelstadt, W. Litzenberger, and J. Johnson, "Keeping an eye on power system dynamics," *IEEE Computer Applications in Power*, vol. 10, no. 4, pp. 50–54, Oct. 1997.

[4] D. N. Kosterev, C. W. Taylor, and W. A. Mittelstadt, "Model validation for the August 10, 1996 WSCC system outage," *IEEE Trans. Power Syst.*, vol. 14, no. 3, pp. 967–979, Aug. 1999.

[5] J. F. Hauer and J. R. Hunt, "Extending the realism of planning models for the Western North American power system," In *Proc. V Symposium of Specialists in Electric Operation and Expansion Planning (V SEPOEP)*, May 1996.

[6] L. Wang, M. Klein, S. Yirga, and P. Kundur, "Dynamic reduction of large power systems for stability studies," *IEEE Trans. Power Syst.*, vol. 12, no. 2, pp. 889–895, May 1997.

[7] J. F. Hauer, M. J. Beshir, and W. A. Mittelstadt, "Dynamic performance validation in the western power system," *APEx 2000*. [Online]. Available: http://certs.lbl.gov/pdf/apex2000.pdf.

[8] D. Chaniotis and M. A. Pai, "Model reduction in power systems using Krylov subspace methods," *IEEE Trans. Power Syst.*, vol. 20, no. 2, pp. 888–894, May 2005.

[9] D. Yang and V. Ajjarapu, "A decoupled time-domain simulation method via invariant subspace partition for power system analysis," *IEEE Trans. Power Syst.*, vol. 21, no. 1, pp. 11–18, Feb. 2006.

[10] P. Kundur, J. Paserba, V. Ajjarapu, G. Andersson, A. Bose, C. Cañizares, N. Hatziargyriou, D. Hill, A. Stankovic, C. Taylor, T. Van Cutsem, and V. Vittal, "Definition and classification of power system stability IEEE/CIGRE joint task force on stability terms and definitions," *IEEE Trans. Power Syst.*, vol. 19, no. 2, pp. 1387–1401, May 2004.

[11] M. J. Gibbard, N. Martins, J. J. Sanchez-Gasca, N. Uchida, V. Vittal, and L. Wang, "Recent applications of linear analysis techniques," *IEEE Trans. Power Syst.*, vol. 16, no. 1, pp. 154–162, Feb 2001.

[12] G. H. Golub and H. A. van der Vorst, "Eigenvalue computation in the 20th century," in *J. Comput. and Appl. Math.*, vol. 123, no. 1–2, pp. 35–65, Nov. 2000.

[13] G. Angelidis and A. Semlyen, "Efficient calculation of critical eigenvalue clusters in the small signal stability analysis of large power systems," *IEEE Trans. Power Syst.*, vol. 10, no. 1, pp. 427–432, Feb. 1995.

[14] G. Angelidis and A. Semlyen, "Improved methodologies for the calculation of critical eigenvalues in small signal stability analysis," *IEEE Trans. Power Syst.*, vol. 11, no. 3, pp. 1209–1217, Aug. 1996.

[15] L. T. G. Lima, L. H. Bezerra, C. Tomei, and N. Martins, "New methods for fast small-signal stability assessment of large scale power systems," *IEEE Trans. Power Syst.*, vol. 10, no. 4, pp. 1979–1985, Nov. 1995.

[16] V. Ajjarapu and B. Lee, "Bifurcation theory and its application to nonlinear dynamical phenomena in an electrical power system," *IEEE Trans. Power Syst.*, vol. 7, no. 1, pp. 424–431, Feb. 1992.

[17] A. van der Sluis and H. A. van der Vorst, "The convergence behavior of Ritz values in the presence of close eigenvalues," *Linear Algebra Appl.*, vol. 88/89, pp. 651–694, Apr. 1987.

[18] R. T. Byerly, R. J. Bennon, and D. E. Sherman, "Eigenvalue analysis of synchronizing power flow oscillations in large electric power systems," *IEEE Trans. Power Appar. Syst.*, vol. PAS-101, no. 1, pp. 235–243, Jan. 1982.

[19] L. Wang and A. Semlyn, "Application of sparse eigenvalue techniques to the small signal stability analysis of large power systems," *IEEE Trans. Power Syst.*, vol. 5, no. 2, pp. 635–642, Nov. 1990.

[20] D. M. Lam, H. Yee, and B. Campbell, "An efficient improvement of the AESOPS algorithm for power system eigenvalue calculation," *IEEE Trans. Power Syst.*, vol. 9, no. 4, pp. 1880–1885, Nov. 1994.

[21] I. J. Pérez-Arriage, G. C. Verghese, and F. C. Schweppe, "Selective modal analysis with applications to electric power systems, Part I: Heuristic introduction," *IEEE Trans. Power Appar. Syst.*, vol. 101, no. 9, pp. 3117–3125, Sep. 1982.

[22] P. Kundur, G. J. Rogers, D. Y. Wong, L. Wang, and M. G. Lauby, "A comprehensive computer program package for small signal stability analysis of power systems," *IEEE Trans. Power Syst.*, vol. 5, no. 4, pp. 1076–1083, Nov. 1990.

[23] N. Uchida and T. Nagao, "A new eigen-analysis method of steady-state stability studies for large power systems: S matrix method," *IEEE Trans. Power Syst.*, vol. 3, no. 2, pp. 706–714, May 1988.

[24] A. Semlyen and L. Wang, "Sequential computation of the complete eigensystem for the study zone in small signal stability analysis of large power systems," *IEEE Trans. Power Syst.*, vol. 3, no. 2, pp. 715–725, May 1988.

[25] J. M. Campagnolo, N. Martins, and D. M. Falcão, "An efficient and robust eigenvalue method for small-signal stability assessment in parallel computers," *IEEE Trans. Power Syst.*, vol. 10, no. 1, pp. 506–511, Feb. 1995.

[26] C. A. Cañizares, N. Mithulananthan, F. Milano, and J. Reeve, "Linear performance indices to predict oscillatory stability problems in power systems," *IEEE Trans. Power Syst.*, vol. 19, no. 2, pp. 1104–1114, May 2004.

[27] I. Dobson, J. Zhang, S. Greene, H. Engdahl, and P. W. Sauer, "Is strong modal resonance a precursor to power system oscillations?" *IEEE Trans. Circuits Syst.*, vol. 48, no. 3, pp. 340–349, Mar. 2001.

[28] I. Dobson and E. Barocio, "Perturbations of weakly resonant power system eletromechanical modes," *IEEE Trans. Power Syst.*, vol. 20, no. 1, pp. 330–337, Feb. 2005.

[29] K. R. Padiyar and H. V. SaiKumar, "Investigation on strong resonance in multimachine power systems with STATCOM supplementary modulation controller," *IEEE Trans. Power Syst.*, vol. 21, no. 2, pp. 754–762, May 2006.

[30] D. J. Stadnicki and J. E. Van Ness, "Invariant subspace method for eigenvalue computation," *IEEE Trans. Power Syst.*, vol. 8, no. 2, pp. 572–580, May 1993.

[31] Z. Du, W. Liu, and W. Fang, "Calculation of rightmost eigenvalues in power systems using the Jacobi-Davidson method," *IEEE Trans. Power Syst.*, vol. 21, no. 1, pp. 234–239, Feb. 2006.

[32] Z. Du, C. Li, and Y. Cui, "Computing critical eigenvalues of power systems using inexact two-sided Jacobi-Davidson," *IEEE Trans. Power Syst.*, 2011, to appear.

[33] L. Dieci and M. J. Friedman, "Continuation of invariant subspaces," *Numer. Linear Algebra Appl.*, vol. 8, pp. 317–327, 2001.

[34] D. Bindel, J. Demmel, and M. Friedman, "Continuation of invariant subspaces for large bifurcation problems," in *Proc. of the SIAM Conf. Applied Linear Algebra*, pp. 1–25, 2003.

[35] J. Bosec, "Continuation of invariant subspaces in bifurcation problems," Ph.D. dissertation, Univ. of Marburg, 2002.

[36] W. J. Beyn, W. Kless, and V. Thümmler, "Continuation of low-dimensional invariant subspaces in dynamical systems of large dimension," in *Ergodic Theory, Analysis, and Efficient Simulation of Dynamical Systems*, B. Fiedler, Ed. New York: Springer, 2001, pp. 47–72.

[37] O. Liberda and V. Janovský, "Indication of a stability loss in the continuation of invariant subspaces," *Math. Comput. Sim.*, vol. 61, pp. 517–524, Jan. 2003.

[38] D. Yang and V. Ajjarapu, "Critical eigenvalues tracing for power system analysis via continuation of invariant subspaces and projected Arnoldi method," *IEEE Trans. Power Syst.*, vol. 21, no. 1, pp. 324–332, Feb. 2007.

[39] X. Wen and V. Ajjarapu, "Application of a novel eigenvalue trajectory tracing method to identify both oscillatory stability margin and damping margin," *IEEE Trans. Power Syst.*, vol. 21, no. 2, pp. 817–824, May 2006.

[40] G. H. Golub and C. F. Van Loan, *Matrix Computations,* 3rd ed. Baltimore, MD: The Johns Hopkins Univ. Press, 1996.

[41] K.-W. E. Chu, "On multiple eigenvalues of matrices depending on several parameters," *SIAM J. Numer. Anal.*, vol. 27, pp. 1368–1385, Oct. 1990.

[42] K. R. Padiyar, *Analysis of Subsynchronous Resonance in Power Systems.* Norwell, MA: Kluwer, 1998.

[43] Yao-Nan Yu, *Electric Power System Dynamics.* New York: Academic Press, 1983.

[44] G. Rogers, *Power System Oscillations.* Norwell, MA: Kluwer, 2000.

[45] P. M. Anderson, B. L. Agrawal, and J. E. Van Ness, *Subsynchronous Resonance in Power Systems.* New York: IEEE Press, 1989.

[46] L. Rouco and F. L. Pagola, "An eigenvalue sensitivity approach to location and controller design of controllable series capacitors for damping power system oscillations," *IEEE Trans. Power Syst.*, vol. 12, no. 4, pp. 1660–1666, Nov. 1997.

[47] C. Y. Chung, K. W. Wang, C. T. Tse, and R. Niu, "Power-system stabilizer (PSS) design by probabilistic sensitivity indexes (PSIs)," *IEEE Trans. Power Syst.*, vol. 17, no. 3, pp. 688–693, Aug. 2002.

[48] M. A. Choudhry, A. S. Emarah, K. A. Ellithy, and G. D. Galanos, "Stability Analysis of a modulated AC/DC system using the eigenvalue sensitivity approach," *IEEE Trans. Power Syst.*, vol. 1, no. 2, pp. 128–136, May 1986.

[49] H.-K. Nam, Y.-K. Kim, K.-S. Shim, and K. Y. Lee, "A new eigen-sensitivity theory of augmented matrix and its applications to power system stability analysis," *IEEE Trans. Power Syst.*, vol. 15, no. 1, pp. 363–369, Feb. 2000.

[50] J. E. Van Ness, J. M. Boyle, and F. P. Imad, "Sensitivities of large, multiple-loop control systems," *IEEE Trans. Autom. Control*, vol. 10, no. 3, pp. 308–315, Jul. 1965.

[51] E. E. Souza Lima and L. F. de Jesus Fernandes, "Assessing eigenvalue sensitivities," *IEEE Trans. Power Syst.*, vol. 15, no. 1, pp. 299–306, Feb. 2000.

[52] P. J. Nolan, N. K. Sinha, and R. T. H. Alden, "Eigenvalue sensitivities of power systems including network and shaft dynamics," *IEEE Trans. Power Appar. Syst.*, vol. 95, no. 4, pp. 1318–1324, Jul. 1976.

[53] T. Smed, "Feasible eigenvalue sensitivity for large power systems," *IEEE Trans. Power Syst.*, vol. 8, no. 2, pp. 555–563, May 1993.

[54] K. W. Wang, C. Y. Chung, C. T. Tse, and K. M. Tsang, "Multimachine eigenvalue sensitivities of power system parameters," *IEEE Trans. Power Syst.*, vol. 15, no. 2, pp. 741–747, May 2000.

[55] J. Rommes and N. Martins, "Computing large-scale system eigenvalues most sensitive to parameter changes, with applications to power system small-signal stability," *IEEE Trans. Power Syst.*, vol. 23, no. 2, pp. 434–442, May 2008.

[56] N. Amjady and M. Esmaili, "Application of a new sensitivity analysis framework for voltage contingency ranking," *IEEE Trans. Power Syst.*, vol. 20, no. 2, pp. 973–983, May 2005.

[57] Y. V. Makarov, D. J. Hill, and Z.-Y. Dong, "Computation of bifurcation boundaries for power systems: a new Δ-plane method," *IEEE Trans. Circuits Syst. I, Fundam. Theory Appl.*, vol. 47, no. 4, pp. 536–544, Apr. 2000.

[58] A. Özcan and H. Schättler, "A computational method for the calculation of the feasibility boundary and clustering in differential-algebraic systems," *IEEE Trans. Circuits Syst. I, Regular Papers*, vol. 52, no. 9, pp. 1940–1952, Sep. 2005.

[59] C. Y. Chung, K. W. Wang, C. T. Tse, X. Y. Bian, and A. K. David, "Probabilistic eigenvalue sensitivity analysis and PSS design in multimachine systems," *IEEE Trans. Power Syst.*, vol. 18, no. 4, pp. 1439–1445, Nov. 2003.

[60] C.-W. Liu and J. S. Thorp, "New methods for computing power system dynamic response for real-time transient stability prediction," *IEEE Trans. Circuits Syst. I, Fundam. Theory Appl.*, vol. 47, no. 3, pp. 324–337, Mar. 2000.

[61] G. M. Shroff and H. B. Keller, "Stabilization of unstable procedures: The recursive projection method," *SIAM J. Numer. Anal.*, vol. 30, pp. 1099–1120, Aug. 1993.

[62] V. Ajjarapu and C. Christy, "The continuation power flow: A tool for steady state voltage stability analysis," *IEEE Trans. Power Syst.*, vol. 7, no. 1, pp. 416–423, Feb. 1992.

[63] V. Ajjarapu, P. L. Lau, and S. Battula, "An optimal reactive power planning strategy against voltage collapse," *IEEE Trans. Power Syst.*, vol. 9, no. 2, pp. 906–917, May 1994.

[64] Z. Feng, V. Ajjarapu, and B. Long, "Identification of voltage collapse through direct equilibrium tracing," *IEEE Trans. Power Syst.*, vol. 15, no. 1, pp. 342–349, Feb. 2000.

[65] Q. Wang, H. Song, and V. Ajjarapu, "Continuation-based quasi-steady-state analysis," *IEEE Trans. Power Syst.*, vol. 21, no. 1, pp. 171–179, Feb. 2006.

[66] V. Ajjarapu, *Computational Techniques for Voltage Stability Assessment and Control.* New York: Springer, 2006.

[67] C. Luo and V. Ajjarapu, "Modified algorithm to trace critical eigenvalues of power system with sensitivities via continuation of invariant subspaces," *Bulk Power System Dynamics and Control - VII*, Charleston, SC, Aug. 2007.

[68] C. Luo and V. Ajjarapu, "Identification of interacting power system dynamic phenomena via continuation of invariant subspaces," *The 16th Power Systems Computation Conference*, Glasgow, Scotland, July 14–18, 2008.

[69] C. Luo and V. Ajjarapu, "Fast identification of oscillatory stability margin and damping margin using continuation of invariant subspaces with sensitivity," *The 40th North American Power Symposium*, Calgary, Canada, Sep. 28–30, 2008.

[70] C. Luo and V. Ajjarapu, "Invariant subspace based eigenvalue tracing for power system small-signal stability analysis," in *Proceedings of the IEEE Power and Energy Society General Meeting*, Calgary, Canada, Jul. 26–30, 2009.

[71] C. Luo and V. Ajjarapu, "A new method of eigenvalue sensitivity calculation using continuation of invariant subspaces," *IEEE Trans. Power Syst.*, vol. 26, no. 1, pp. 479–480, Feb. 2011.

[72] C. Luo and V. Ajjarapu, "Sensitivity-based efficient identification of oscillatory stability margin and damping margin using continuation of invariant subspaces," *IEEE Trans. Power Syst.*, 2011, to appear.

[73] M. Fan, V. Ajjarapu, C. Wang, D. Wang, and C. Luo, "RPM-based approach to extract power system steady state and small signal stability information from the time-domain simulation," *IEEE Trans. Power Syst.*, vol. 26, no. 1, pp. 261–269, Feb. 2011.

[74] V. Janovsky and O. Liberda, "Continuation of invariant subspaces via the recursive projection method," *Appl. Math.*, vol. 48, pp. 241–255, 2003.

[75] P. W. Sauer and M. A. Pai, "Power system steady-stability and the load-flow Jacobian," *IEEE Trans. Power Syst.*, vol. 5, no. 4, pp. 1374–1383, Nov. 1990.

[76] N. Martins, "Efficient eigenvalue and frequency response methods applied to power system small-signal stability studies," *IEEE Trans. Power Syst.*, vol. 1, no. 1, pp. 217–224, Feb. 1986.

[77] L. E. Jones, *On Zero Dynamics and Robust Control of Large AC and DC Power Systems,* Doctoral thesis, Royal Institute of Technology (KTH), Dept. of Electric Power Engineering, Stockholm, Sweden, 1999.

[78] P. Kundur, *Power System Stability and Control.* New York: McGraw-Hill, 1994.

[79] E. E. S. Lima, "A sensitivity analysis of eigenstructures," *IEEE Trans. Power Syst.*, vol. 12, no. 3, pp. 1393–1399, Aug. 1997.

[80] T. J. Garratt, G. Moore, and A. Spence, "A generalised Cayley transform for the numerical detection of Hopf bifurcations in large systems," in *Contributions in numerical mathematics*, River Edge, NJ: World Sci. Ser. Appl. Anal., vol. 2, World Sci. Publ., pp. 177–195, 1993.

[81] K. Meerbergen, A. Spence, and D. Roose, "Shift-invert and Cayley transforms for the detection of eigenvalues with largest real part of nonsymmetric matrices," *BIT Numer. Math.*, vol. 34, pp. 409–423, 1994.

[82] Z. Bai and G. W. Stewart, "Algorithm 776: SRRIT: A Fortran subroutine to calculate the dominant invariant subspace of a nonsymmetric matrix," *ACM Trans. Math. Softw.*, vol. 23, no. 4, pp. 494–513, Dec. 1997.

[83] R. H. Bartels and G. W. Stewart, "Solution of the matrix equation $AX + XB = C$," *Comm. ACM*, vol. 15, pp. 820–826, 1972.

[84] J. J. Dongarra, C. B. Moler, and J. H. Wilkinson, "Improving the accuracy of computed eigenvalues and eigenvectors," *SIAM J. Numer. Anal.*, vol. 20, no. 1, pp. 23–45, Feb. 1983.

[85] J. L. Sancha and I. J. Pérez-Arriage, "Selective modal analysis of power system oscillatory instability," *IEEE Trans. Power Syst.*, vol. 3, no. 2, pp. 429–438, May 1988.

[86] IEEE Committee, "First benchmark model for computer simulation of subsynchronous resonance," *IEEE Trans. Power Appar. Syst.*, vol. 96, no. 5, pp. 1565–1572, Sep./Oct. 1977.

[87] J. Machowskiand, J. W. Bialek, and J. R. Bumby, *Power System Dynamics: Stability and Control.* 2nd ed. Chichester, United Kingdom: Wiley, 2008.

[88] S. P. Teeuwsen, I. Erlich, M. A. El-Sharkawi, and U. Bachmann, "Genetic algorithm and decision tree-based oscillatory stability assessment," *IEEE Trans. Power Syst.*, vol. 21, no. 2, pp. 746–753, May 2006.

[89] Y. V. Makarov, Z. Y. Dong, and D. J. Hill, "A general method for small signal stability analysis," *IEEE Trans. Power Syst.*, vol. 13, no. 3, pp. 979–985, Aug. 1998.

[90] S. Gomes, N. Martins, and C. Portela, "Computing small-signal stability boundaries for large-scale power systems," *IEEE Trans. Power Syst.*, vol. 18, no. 2, pp. 747–752, May 2003.

[91] V. Vittal, "Transient stability test systems for direct stability methods," *IEEE Trans. Power Syst.*, vol. 7, no. 1, pp. 37–43, Feb. 1992.

[92] A. Ibsais and V. Ajjarapu, "The role of automatic differentiation in power system analysis," *IEEE Trans. Power Syst.*, vol. 12, no. 2, pp. 592–597, May 1997.

[93] E. Doedel and L. S. Tuckerman, *Numerical Methods for Bifurcation Problems and Large-Scale Dynamical Systems.* vol. 119 of IMA Volumes in Mathematics and its Applications, New York: Springer, 2000.

[94] W. Govaerts, *Numerical Methods for Bifurcations of Dynamical Equilibria.* Philadelphia, PA: SIAM, 2000.

[95] I. Dobson and L. Lu, "Voltage collapse precipitated by the immediate change in stability when generator reactive power limits are encountered," *IEEE Trans. Circuits Syst.*, vol. 39, no. 9, pp. 762–766, Sep. 1992.

[96] T. Van Cutsem and C. Vournas, *Voltage Stability of Electric Power Systems.* Norwell, MA: Kluwer, 1998.

[97] V. Venkatasubramanian, H. Schättler, V. Venkatasubramanian, and J. Zaborszky, "Local bifurcations and feasibility regions in differential-algebraic systems," *IEEE Trans. Autom. Control.*, vol. 40, no. 12, pp. 1992–2013, Dec. 1995.

[98] C. Rajagopalan, B. Lesieutre, P. W. Sauer, and M. A. Pai, "Dynamic aspects of voltage/power characteristics," *IEEE Trans. Power Syst.*, vol. 7, no. 3, pp. 990–1000, Aug. 1992.

[99] F. Capitanescu and T. Van Cutsem, "Preventive control of voltage security margins: a multicontingency sensitivity-based approach," *IEEE Trans. Power Syst.*, vol. 17, no. 2, pp. 358–364, May 2002.